

# Shoring up the foundations of image analysis

Sir Michael Brady FRS FREng FMedSci  
Professor of Oncological Imaging  
Department of Oncology  
University of Oxford



# The weakest link



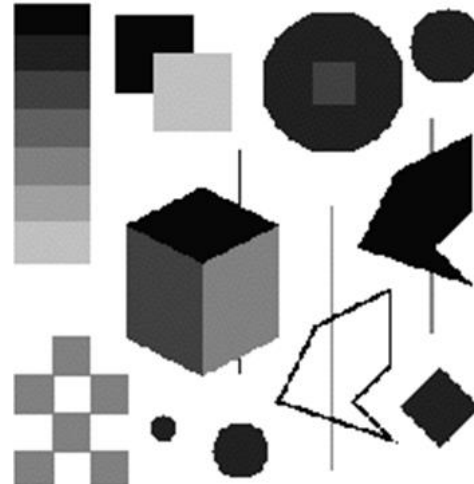
- Fun stuff: deformable registration, motion estimation, segmentation
- Mathematical heroics
- Let someone else worry about signal & image analysis, physics, all that jazz

Message of this talk: there is intelligent life in the basement, and it makes a difference!

# Overview

- Features
  - local phase, phase congruency
  - MR/US registration, cell segmentation, vascular segmentation, ...
- Texture
  - Fractal dimension on Riesz transform
  - Staging liver disease
- Uncertainty
  - Histograms & Shannon – NP Windows
  - Entropy, mutual information
- Shape
  - Integral invariants and eccentricity transform
  - Mammography segmentation and deformable registration
- ... and a postscript

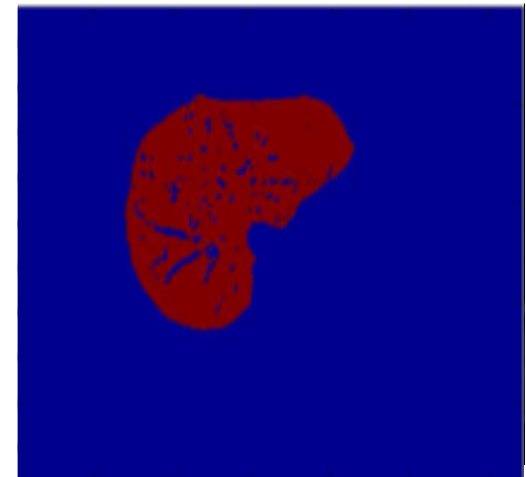
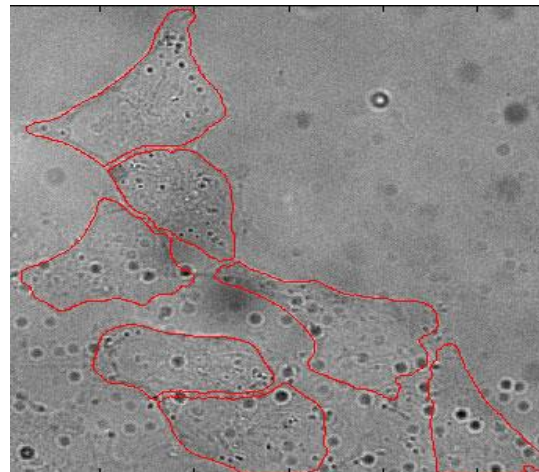
# The feature zoo



Steps of varying contrast  
Thin lines  
Localised “blob”s  
Corners of varying angle  
...

- There is more to images than steps
- They are relatively rare in medical images
- ..but most feature detectors are specialised for steps

Task: segment these HeLa cells, and identify the nuclei



Task: separate the vascular & bile structures from fibrosis

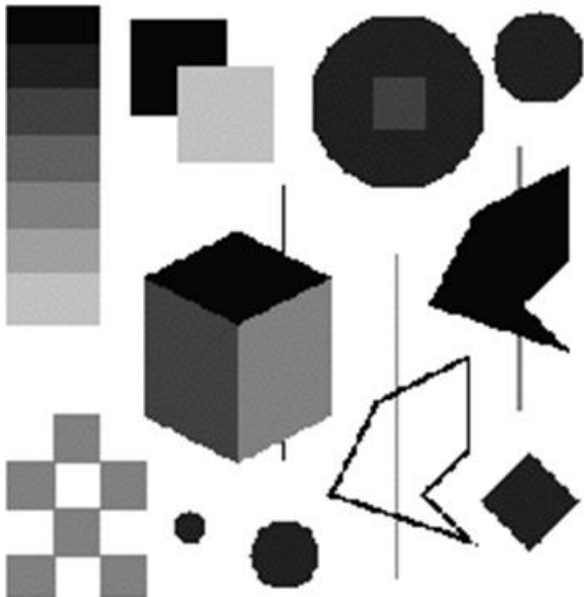
## ... which begs the questions

- Is there a *mathematical* definition of a feature, to replace this phenomenological view?
  - Most proposals have concentrated on  $|\nabla^n|$  ...
  - There have been formal definitions available for over 30 years
  - The (medical) image analysis has largely ignored them
- Does “texture” form part of being a feature, or is it something that is derivative, as a collection of features?
  - David Marr argued that “texture” can be defined as first-order statistical distributions over “zero crossings” of the Laplacian of a Gaussian (isotropic) filter
  - Bela Julesz argued for the primacy of texture, with “texton” receptors, that are learned.

# A case study: the Canny edge detector\*

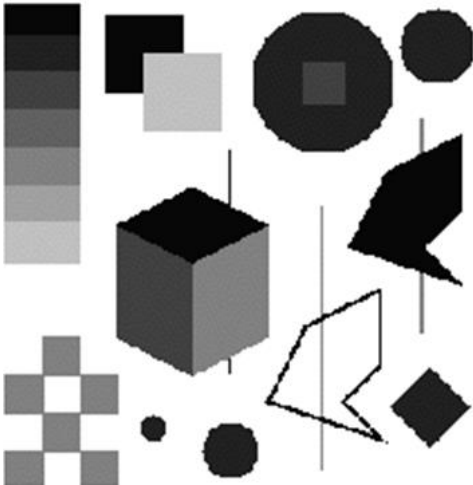
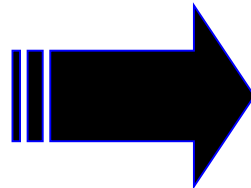


- Blur the image with a Gaussian
- Estimate  $d/dx$ ,  $d/dy$  with finite differences
- Estimate the local gradient direction
- Perform non-maximum suppression
- Perform hysteresis thresholding
- Combine over scales: fine to coarse

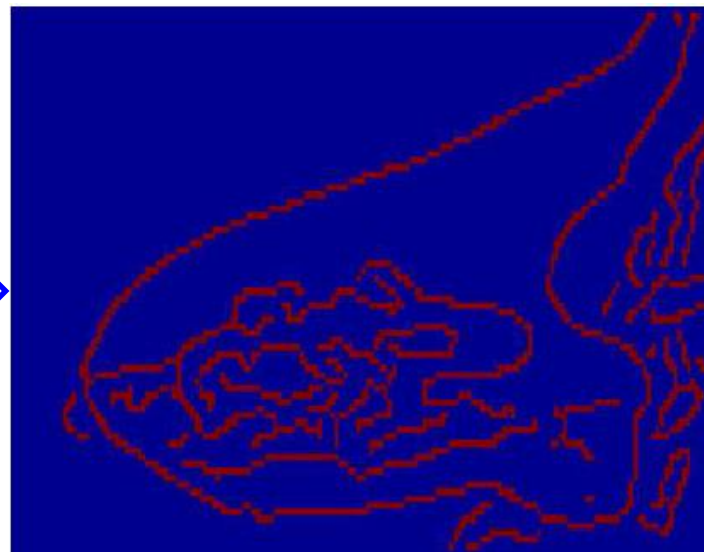
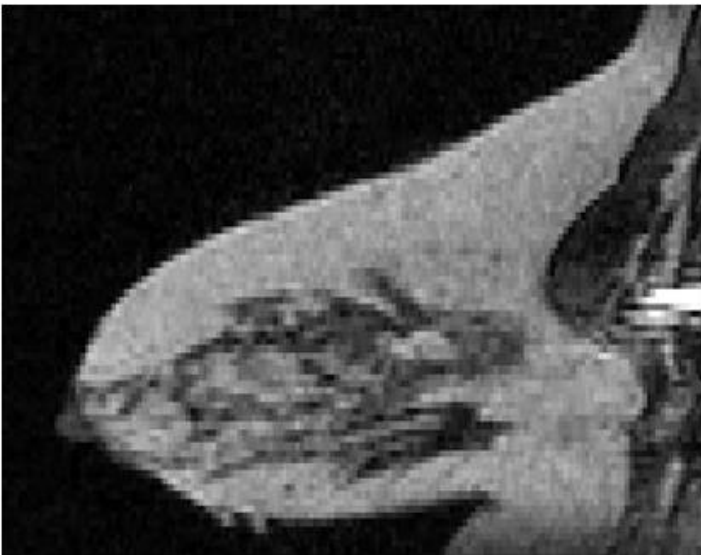


\*33 yrs ago

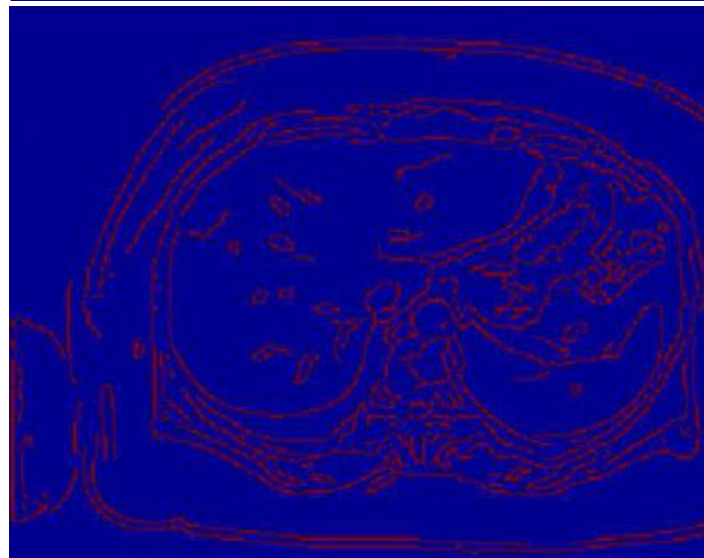
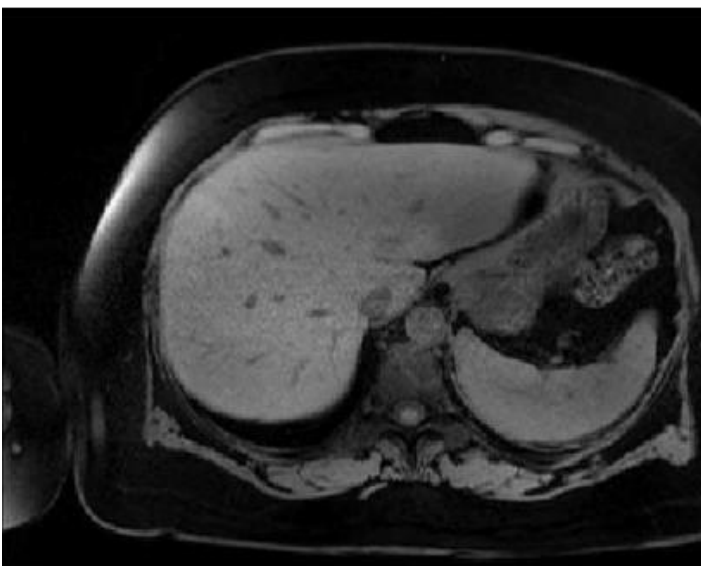
# Two examples of Canny



Breast MRI  
Task:  
segment the  
breast (✓)  
and the ductal  
structures (X)



Liver MRI  
Task:  
segment the  
pancreas,  
ductal and  
bile  
structures (X)





# Canny assessment

- Most widely used edge detector for last 20 years
- Works well on steps, not on other features
- On steps, response determined by contrast – because it uses intensity gradient
- Performs poorly on texture
- ... surely, we can do better?

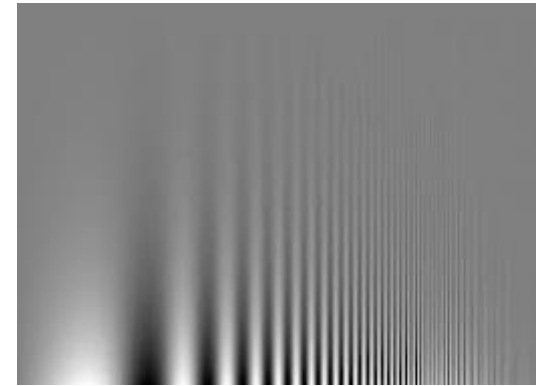
# Other proposals

- Marr's *primal sketch*
  - Pre-determined zoo of features + feature fusion
  - Never worked
- Anisotropic diffusion
  - Still predominantly steps
  - ... and energy of gradient
  - Total variation
- Wavelet transform
  - Decimated (Mallat): not shift invariant
  - Complex (Kingsbury): fundamentally 1D signals

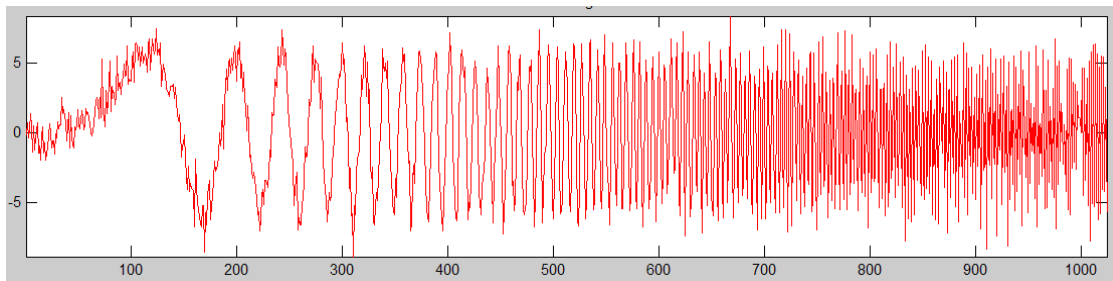
# An alternative approach: local phase

Features and texture are characterised by their high frequencies in Fourier transform, discussed in psychophysics literature since 1920s

Contrast sensitivity to gratings, and application to texture, Campbell & Robson, 1968

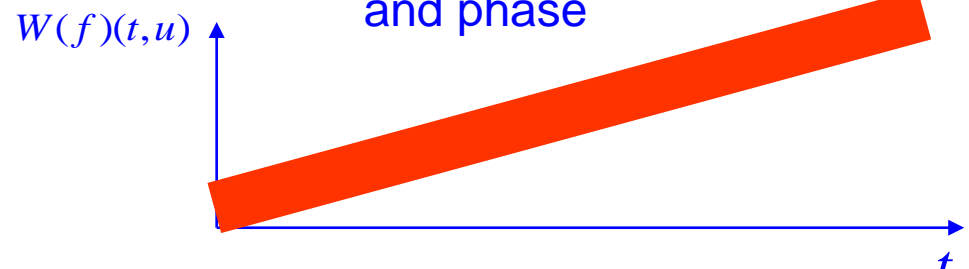
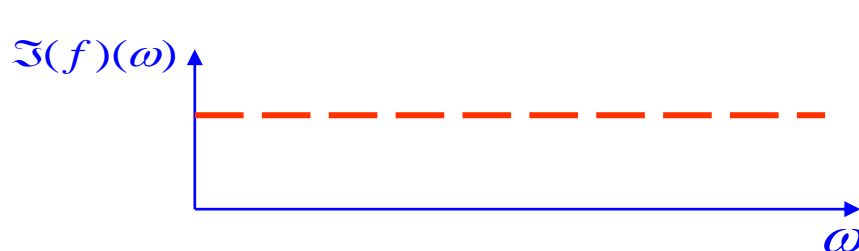


Windowed\* FT (Gabor, 1950)



Chirp signal

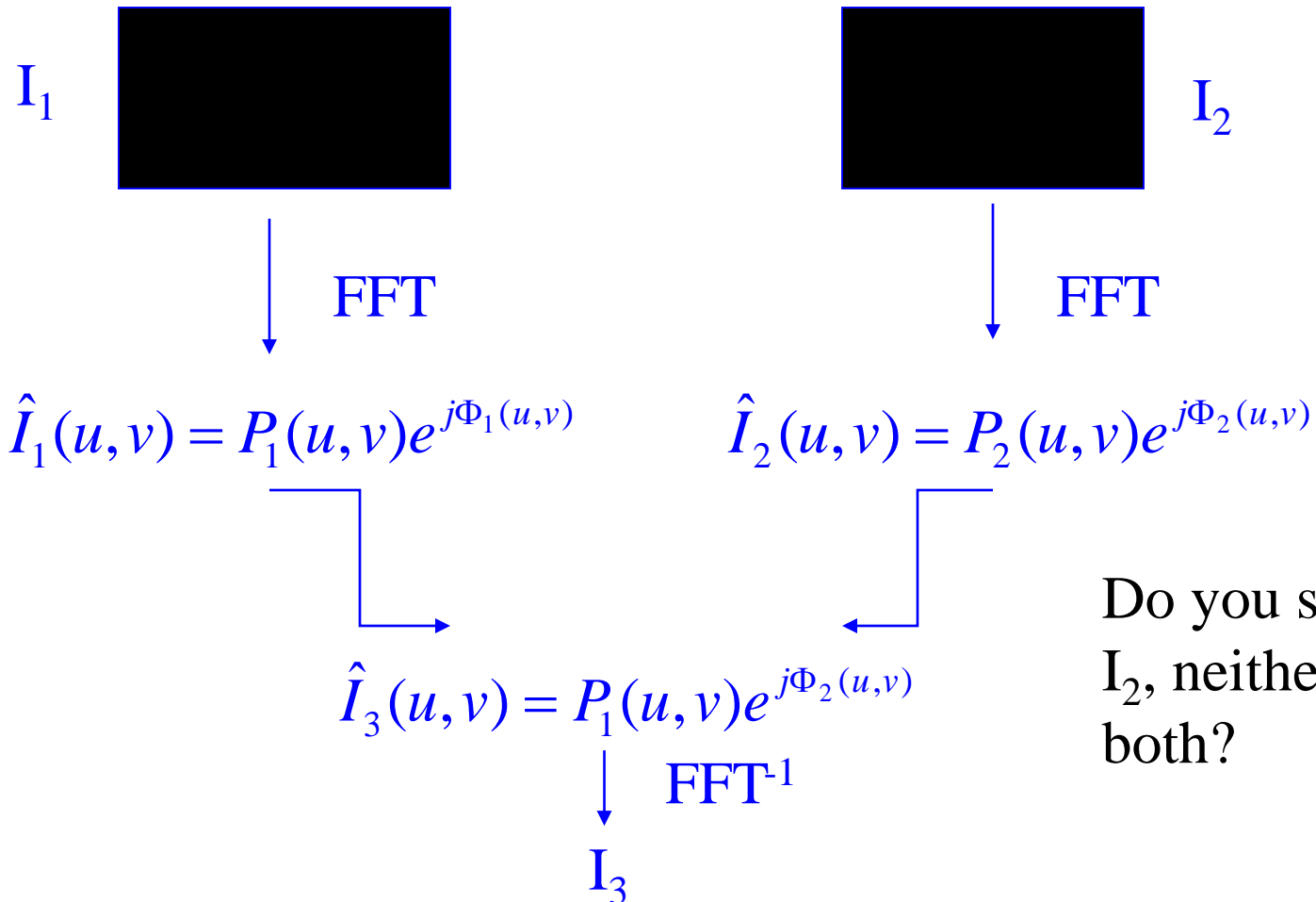
**Local** frequency  
and phase

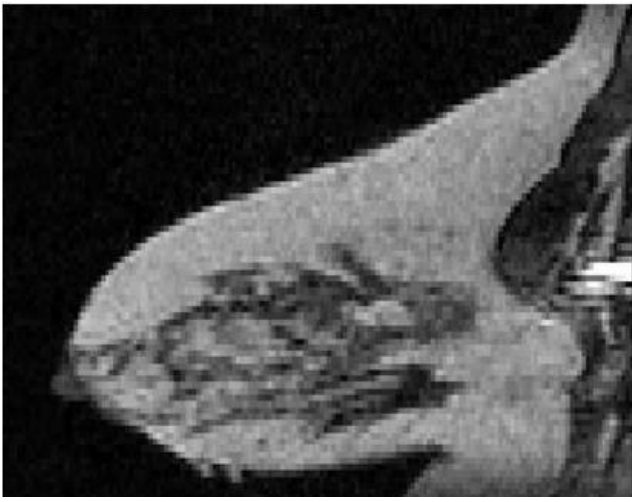


# The importance of phase

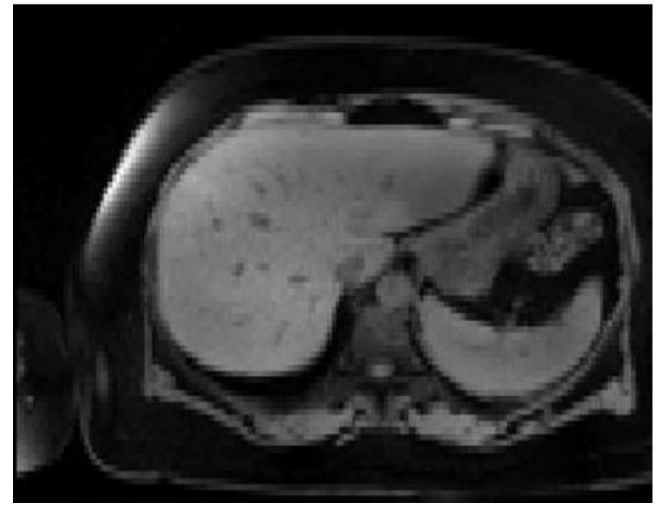
## Oppenheim's demonstration

The Fourier Transform of a signal is complex valued: generates frequency & phase





Breast MRI



Liver MRI



Breast energy; liver phase

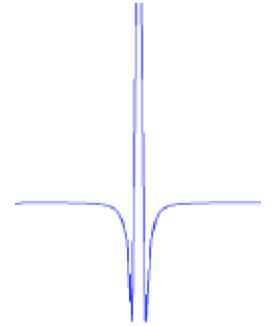


Breast phase; liver energy

# Local phase ... of a signal

Bandpass to tame noise, say  $b(t)$

Typically,  $b(t)$  is an even filter, so we call it  $b_e(t)$



The Hilbert Transform applied to  $b_e(t)$  gives an odd filter  $b_o(t)$

Then the local energy is  $\sqrt{(f * b_e)^2 + (f * b_o)^2}$  and

the local phase is  $\tan^{-1}\left(\frac{(f * b_o)}{(f * b_e)}\right)$

We can do this for "almost any" even bandpass filter  $b_e(t)$

# Hilbert transform

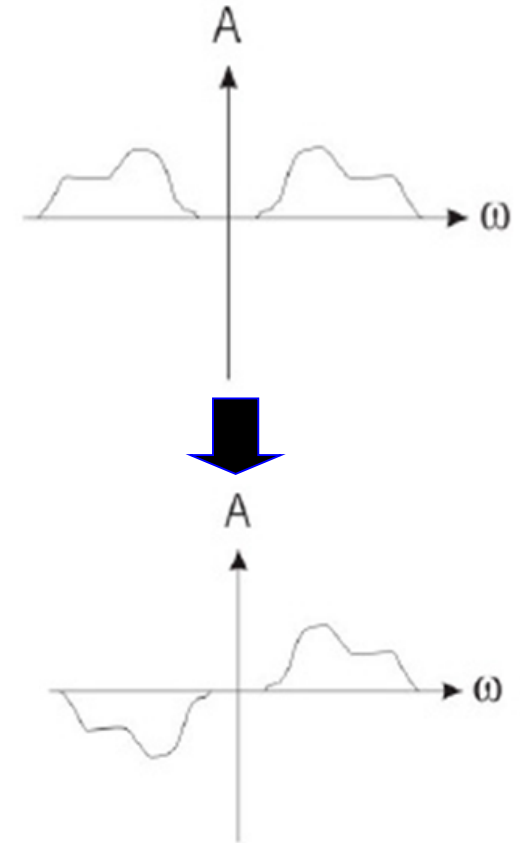
The *Hilbert Transform*\*  $f_H(t)$  of a function  $f(t)$  is defined by:

$$f_H(t) = \frac{1}{\pi} \left( f(t) * \left( \frac{1}{t} \right) \right)$$

Since the Fourier transform of  $\frac{1}{t}$  is the Heaviside step function  $\text{sgn}(u)$

We have:  $\hat{f}_H(u) = f(u) \cdot \text{sgn}(u)$

Fourier transform  $f(u)$



Fourier transform of Hilbert transform  $\hat{f}_H(u)$

# FT of 1/t

The Fourier Transform of  $\frac{1}{t}$  is  $-j \operatorname{sgn}(u)$

Denote the FT of  $\hat{f}(u) = \hat{f}_r(u) + j\hat{f}_i(u)$

$$\begin{aligned} \text{so that } \hat{f}_H(u) &= -j \operatorname{sgn}(u) \left( \hat{f}_r(u) + j\hat{f}_i(u) \right) \\ &= \operatorname{sgn}(u) \left( \hat{f}_i(u) - j\hat{f}_r(u) \right) \end{aligned}$$

and so

$$\begin{aligned} \left( \hat{f}_H \right)_r &= \hat{f}_i \\ \left( \hat{f}_H \right)_i &= -\hat{f}_r \end{aligned}$$

.. We can view this in a slightly different way ....



# Hilbert transform rotates by $\pi/2$ in the Fourier domain

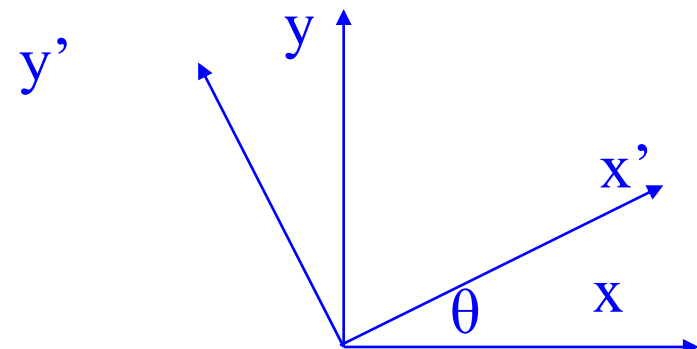
Let  $\hat{f}(u) = \hat{f}_r(u) + j\hat{f}_i(u)$ , then

$$\left(\hat{f}_H\right)_i = \hat{f}_r$$

$$\left(\hat{f}_H\right)_r = -\hat{f}_i$$

---

Recall rotation in the plane:



$$\begin{bmatrix} x' \\ y' \end{bmatrix} = \begin{bmatrix} \cos \theta & \sin \theta \\ -\sin \theta & \cos \theta \end{bmatrix} \begin{bmatrix} x \\ y \end{bmatrix}$$

In this case,  $\theta = -\pi/2$  .... and for such a rotation we say that the filters are in quadrature (e.g. sin, cos)

# Analytical Signal & Hilbert Transform

Mathematically, the local properties (amplitude, phase) of a signal  $f(t)$  are defined using the *Analytic Signal*  $f_A(t)$ :

$$f_A(t) = f(t) - jf_H(t)$$

where  $f_H(t)$  is the Hilbert Transform of  $f(t)$

We recall that in the Fourier domain, the Hilbert transform  $\hat{f}_H(u)$

has the same magnitude as  $f(u)$  but is rotated by  $\frac{\pi}{2}$ . This enables us to

define

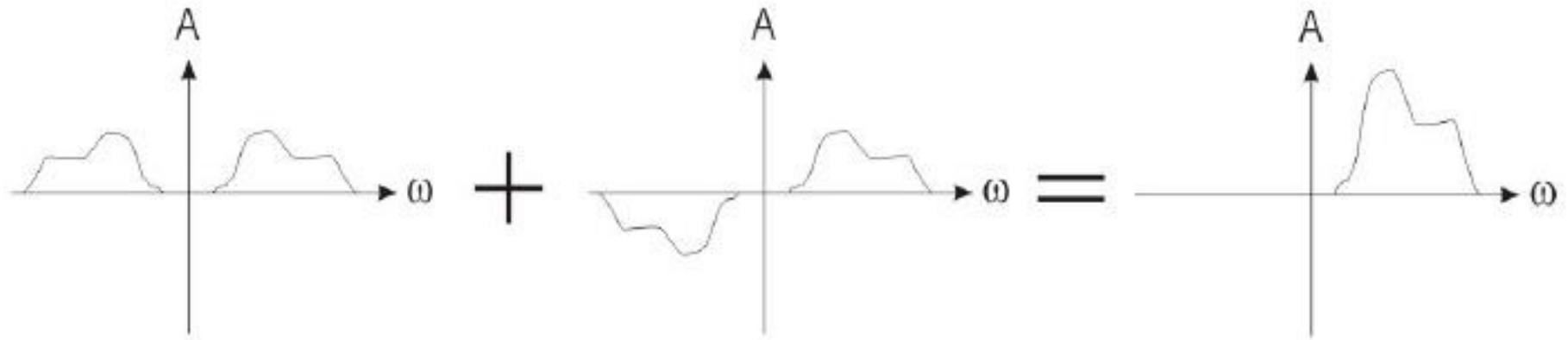
local energy  $A(t) = \sqrt{f^2(t) + f_H^2(t)}$

local phase  $\tan \phi(t) = \frac{f(t)}{f_H(t)}$

Quadrature filter pair

**Frequency throws away  
key information**

# Analytic signal



Original signal FT of  
f

Hilbert transform  
of f

Analytic signal for  
f

No residual “negative frequencies...”

... well, that's signals sorted, now let's look at  
images

# Local phase *congruency*

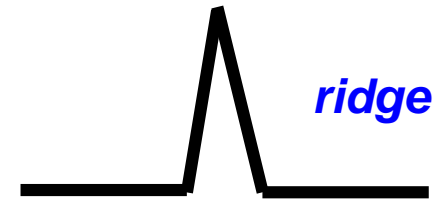
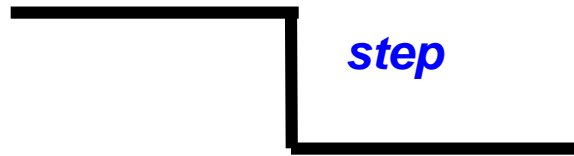
Phase, at any *single* scale is largely meaningless



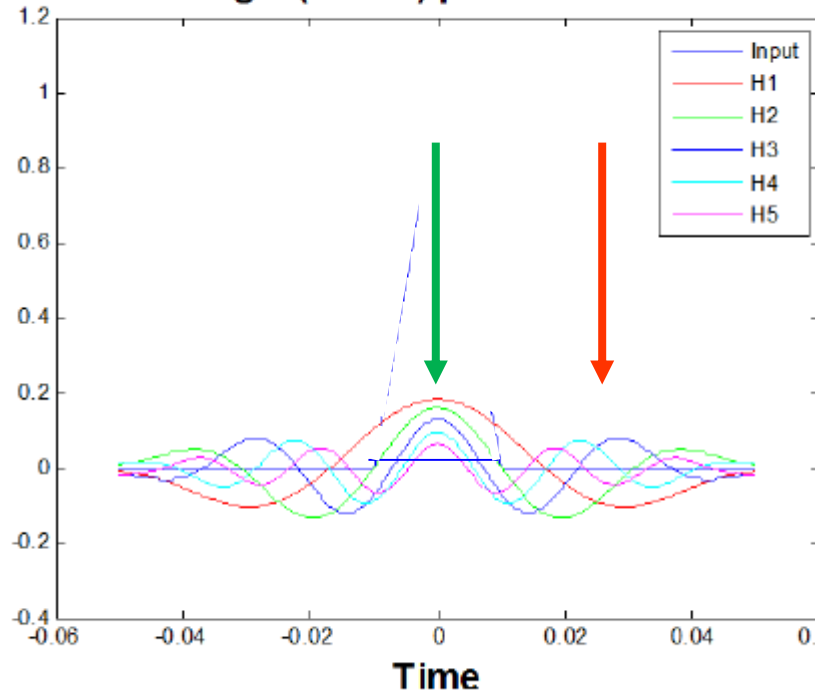
Maria Concetta Morrone

Robyn Owens

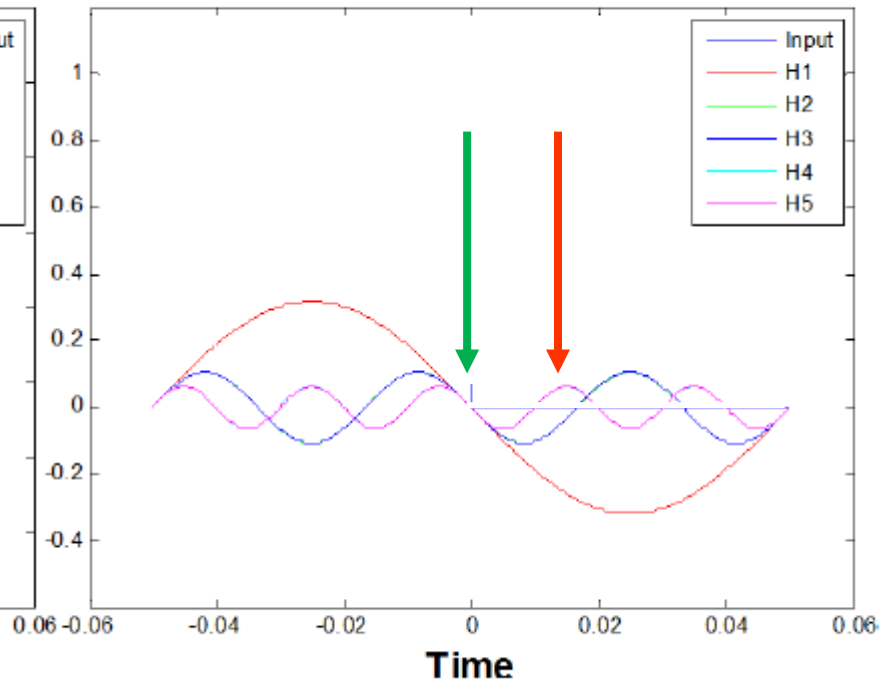
Idealised features



Triangle (EVEN) pulse harmonics

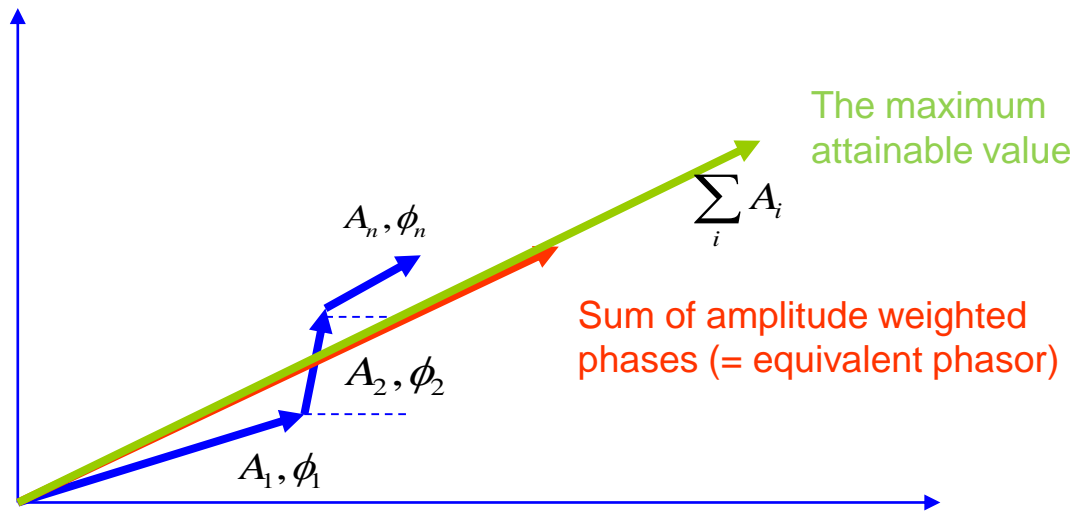


Rectangle (ODD) pulse harmonics



A feature is *defined* as a point in an image (or signal) where the phases line up

# Kovesi's implementation of phase congruency

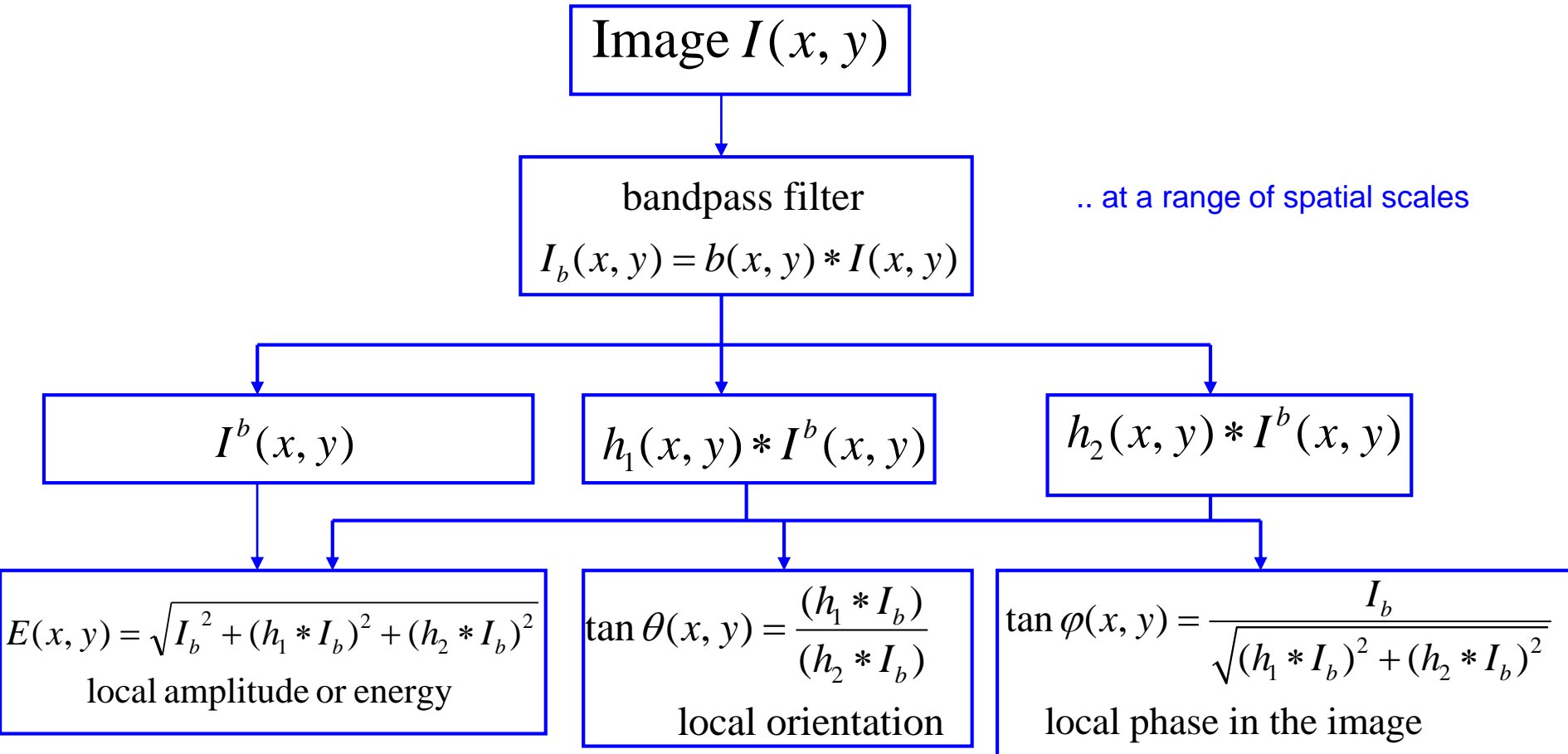


Define: 
$$PC(t) = \frac{W(t)}{\varepsilon + \sum_n A_n(t)},$$
 (typically  $\varepsilon = 0.01$ )

Two problems:

- The Hilbert Transform, and so Kovesi's implementation, only defined for 1D signals
- How do add phases and avoid phase wrap-around?

# the monogenic signal

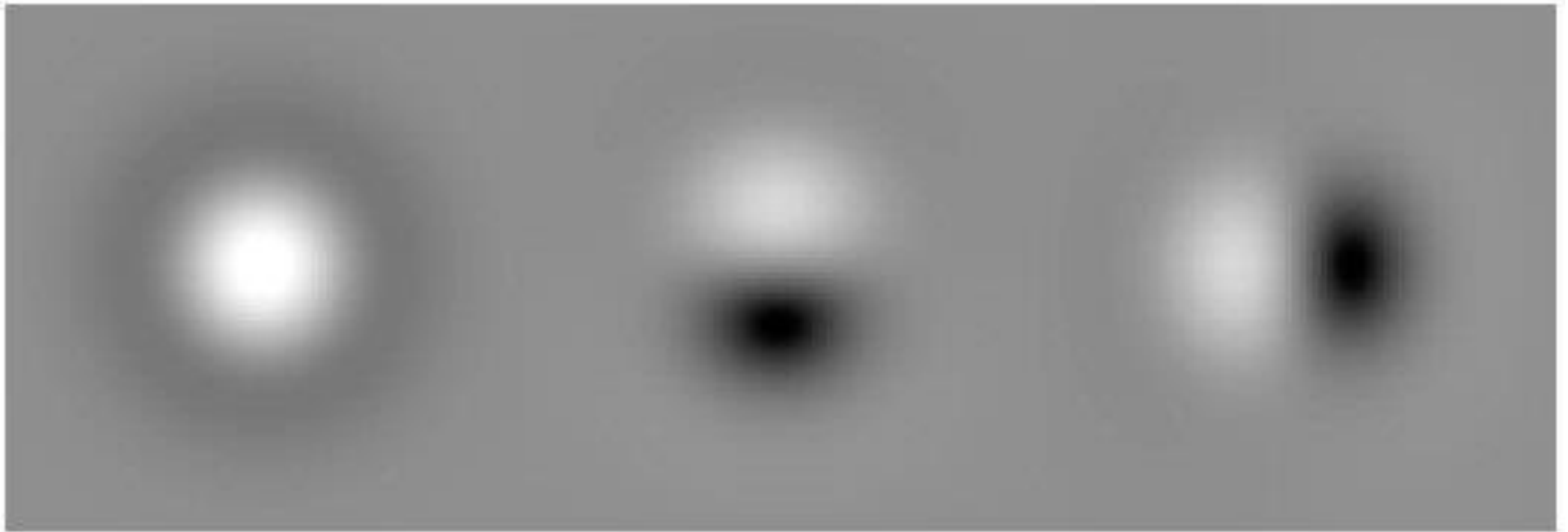


The convolution kernels  $h_1, h_2$  are shown on the next slide (Reisz transform).

The bandpass filters  $\{b_i; i = 1..n\}$  is the ONLY choice to be made  
aside from how to combine the results of the different scales

Note that  $h_j * b_i$  can be computed in advance, further speeding computation

# Monogenic triple of filters



Bandpass filter  $b$

$h_1 * b$

$h_2 * b$

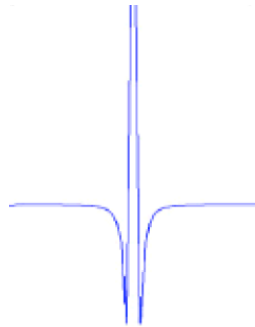
This is even

odd

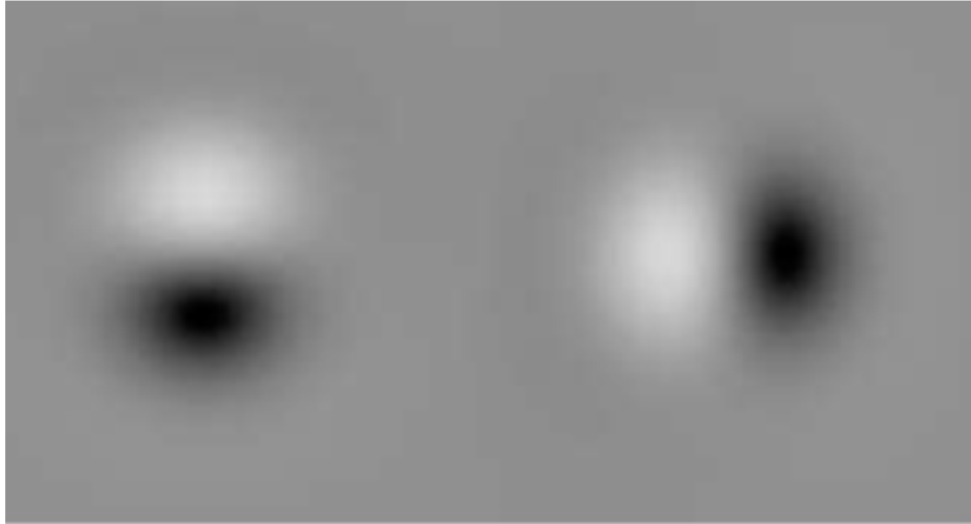
odd & quadrature pair to  $h_1 * b$

$h_1, h_2$  provide the quadrature required for local phase estimation

A key choice is the bandpass filter. Choices include difference of Gaussians, Gabor, log Gabor. Mellor and Brady have developed a family of rotationally-symmetric, scale-robust, linear bandpass filters (PAMI 2008)



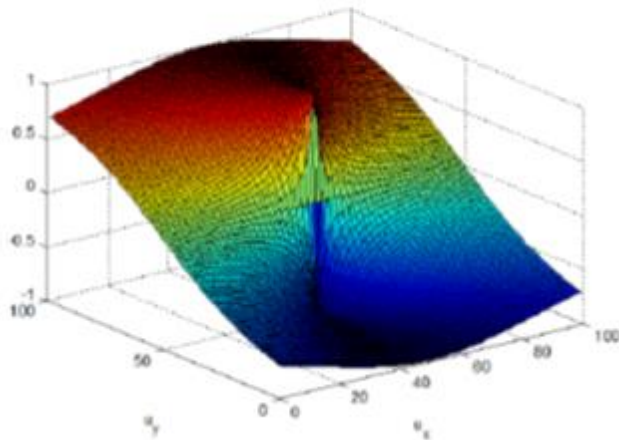
# Riesz filters



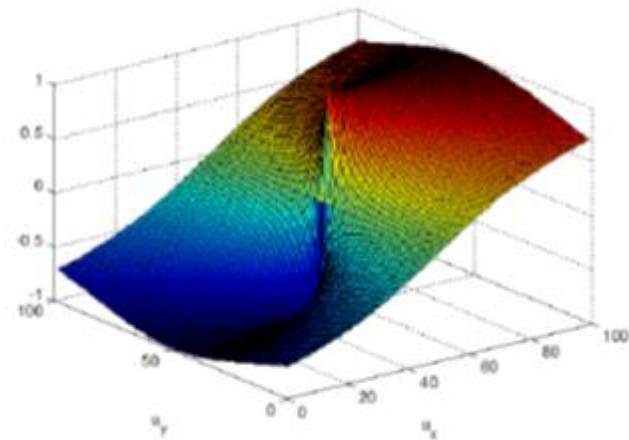
$h_1 * b$

$h_2 * b$

Riesz filter:  $V_1(u)$

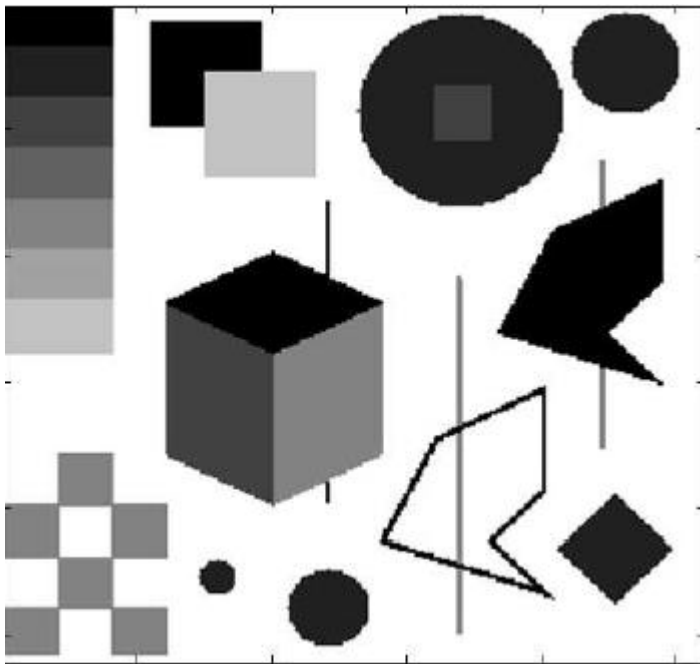


Riesz filter:  $V_2(u)$

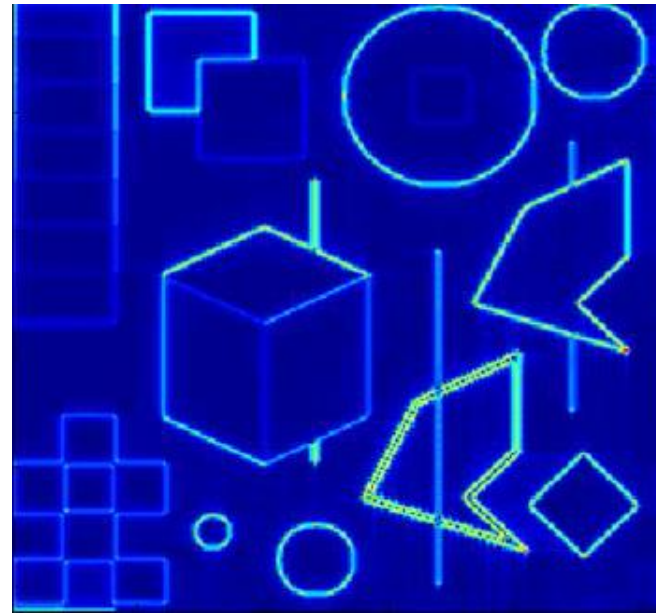
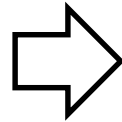




# Local energy, local phase

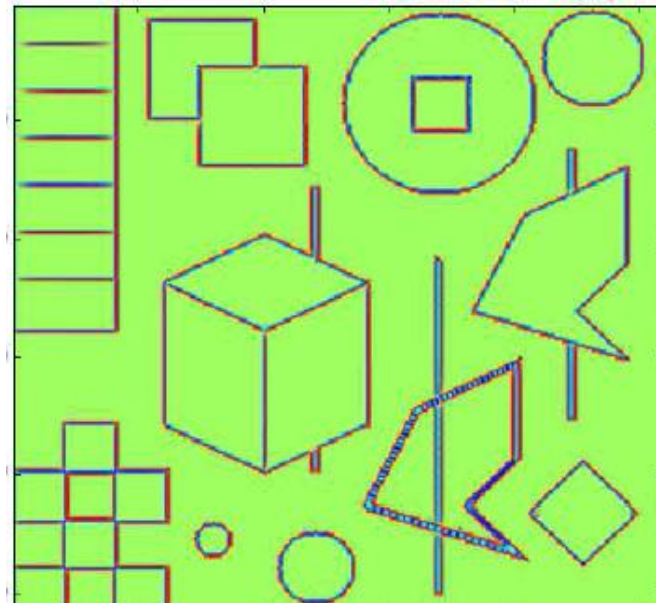


Bandpass filter is Mellor-Brady



Local energy

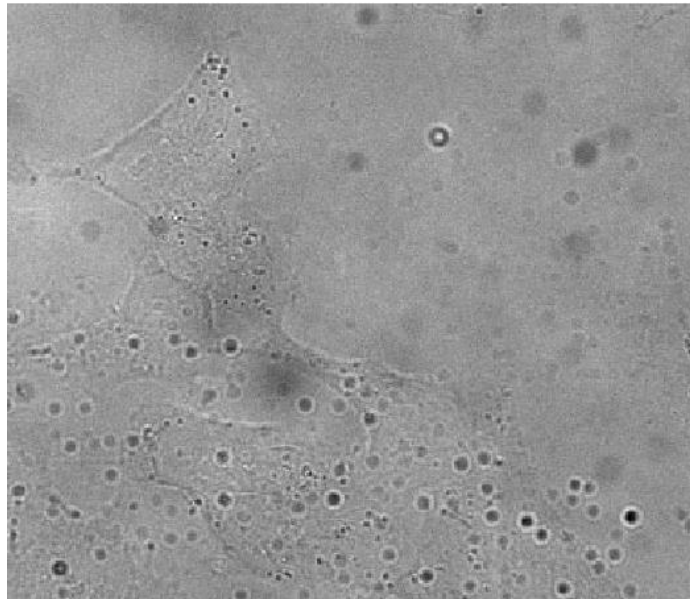
Note  
contrast  
variance



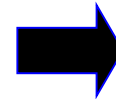
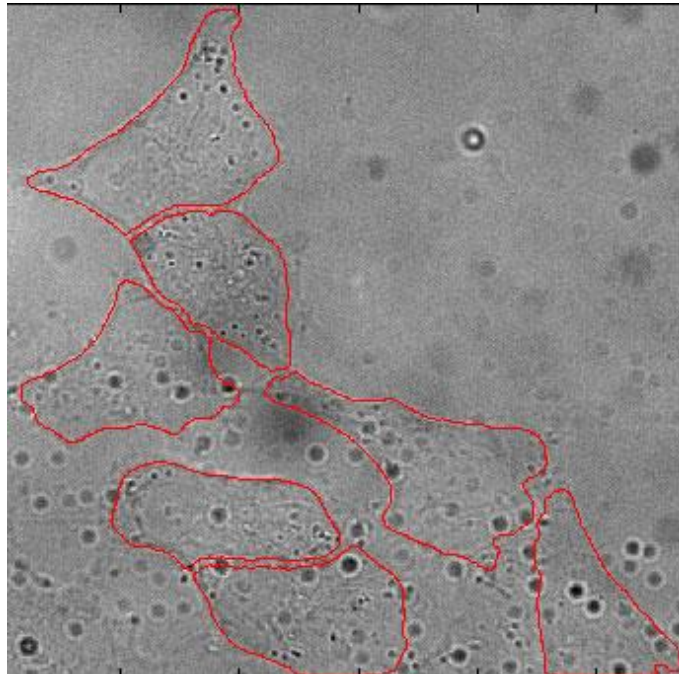
Local phase

Negligible  
contrast  
variance

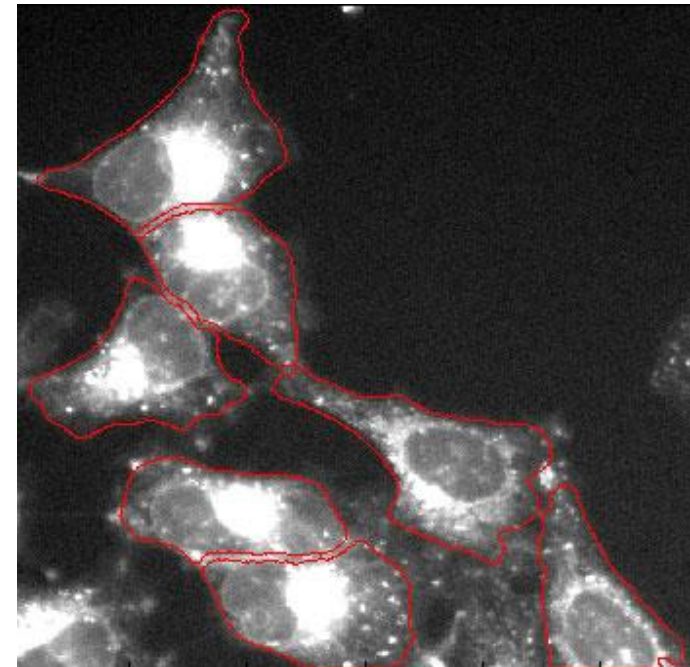
Brightfield confocal  
microscope image  
of clusters of  
touching HeLa\*  
cells



Segmented cells  
from monogenic  
signal features  
integrated into a  
level set  
segmentation  
algorithm

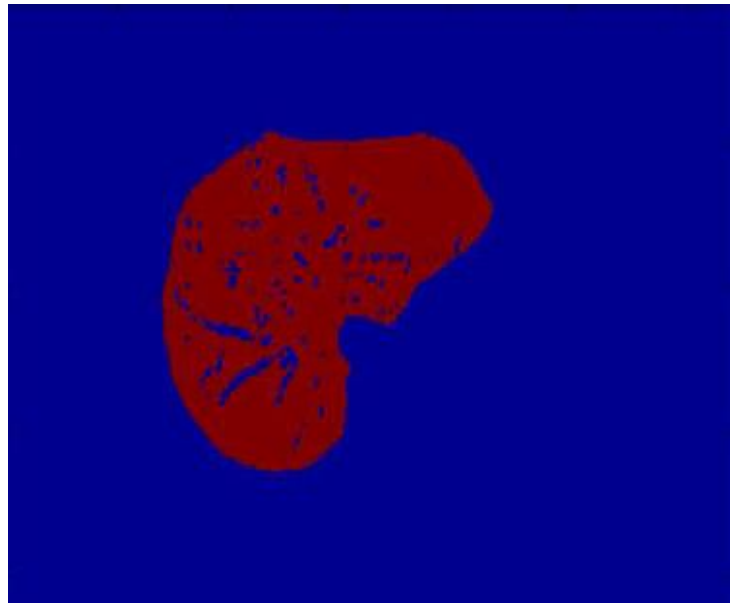
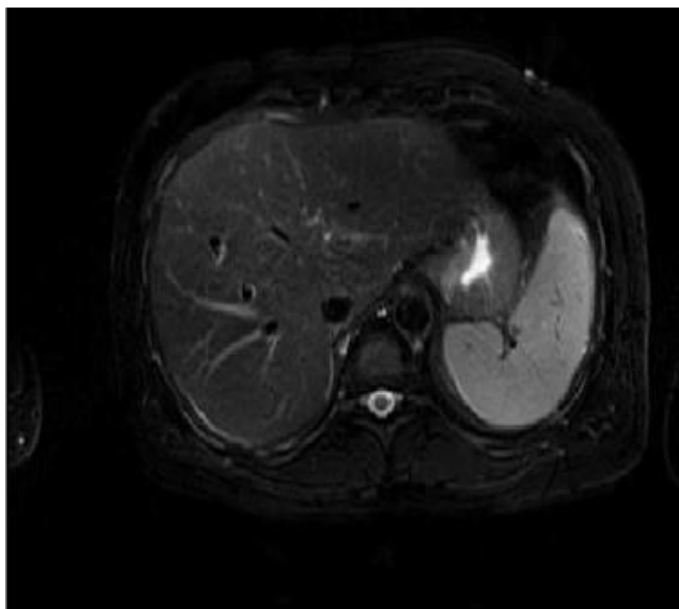
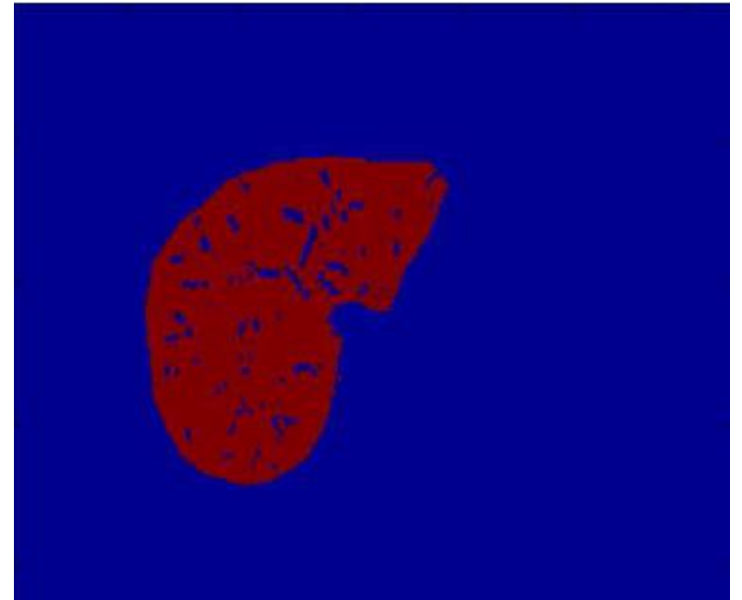
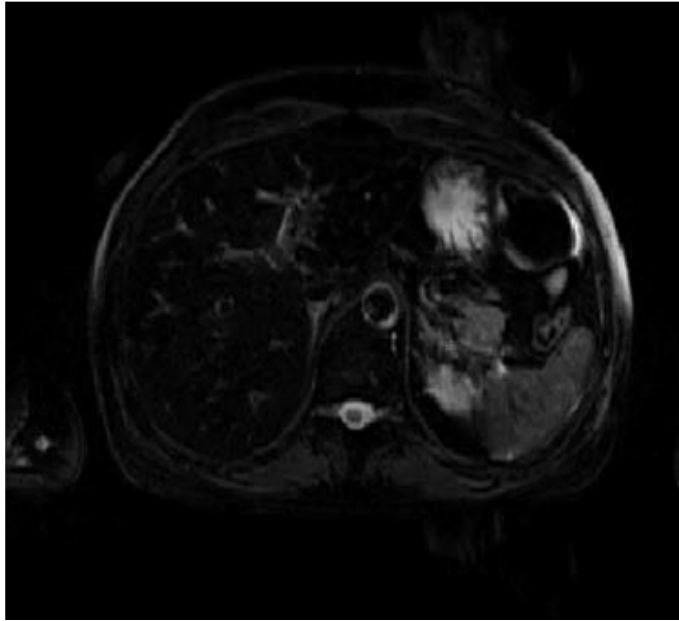


Segmentation superimposed on  
a Zn-ATSM fluorescent image



\*HeLa is an immortal cell line, first  
taken from Henrietta Lacks, who  
died of cervical cancer in 1951

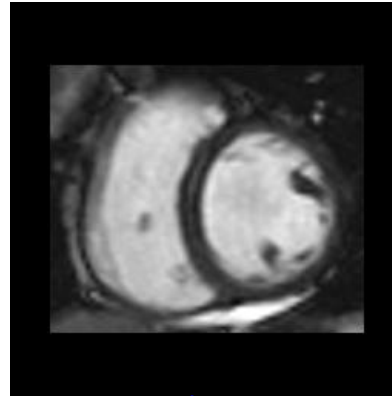
# Vascular segmentation in non-alcoholic steahepatitis



$T_2^*$   
weighted  
images

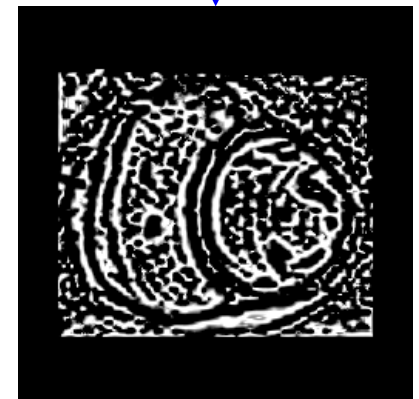
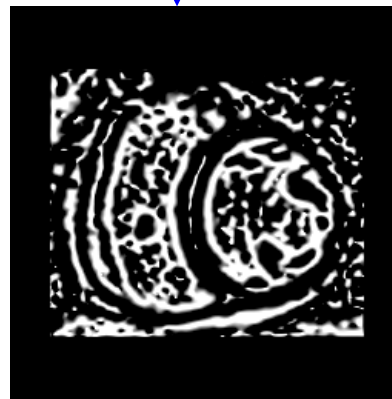
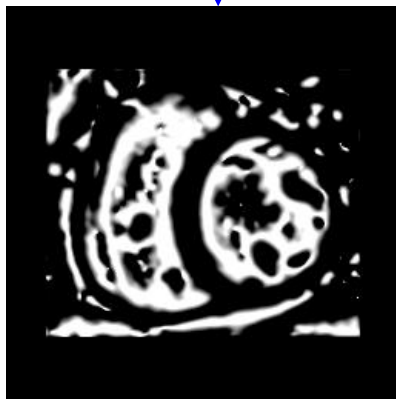
# MRI analysis using DOG\* (bandpass) filter

MRI image of a slice of the heart



$$DOG(u) = \exp\left(-\frac{\sigma_1^2 u^2}{2}\right) - \exp\left(-\frac{\sigma_2^2 u^2}{2}\right)$$

$$\frac{\sigma_1}{\sigma_2} = \gamma, \text{ in this case: } \gamma < 0.1$$

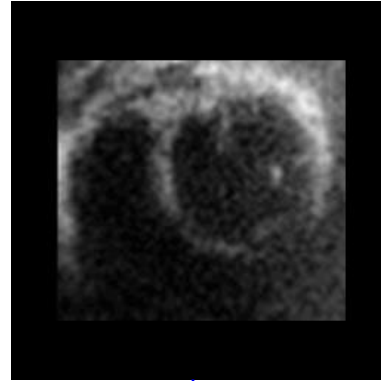


The images are phase estimated using monogenic signal

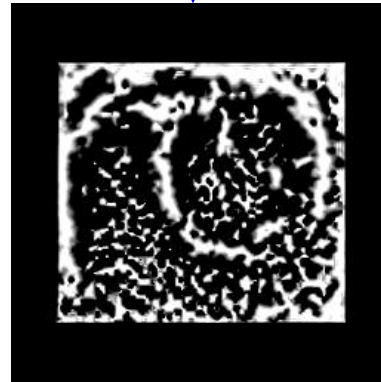
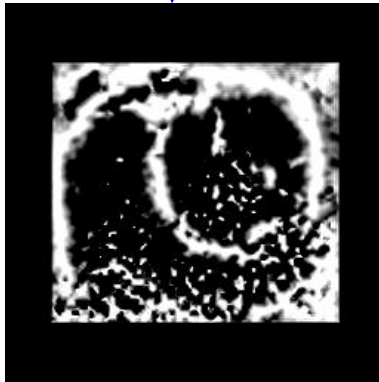
\* Difference of Gaussians

# 3D ultrasound phase estimation using DOG filter

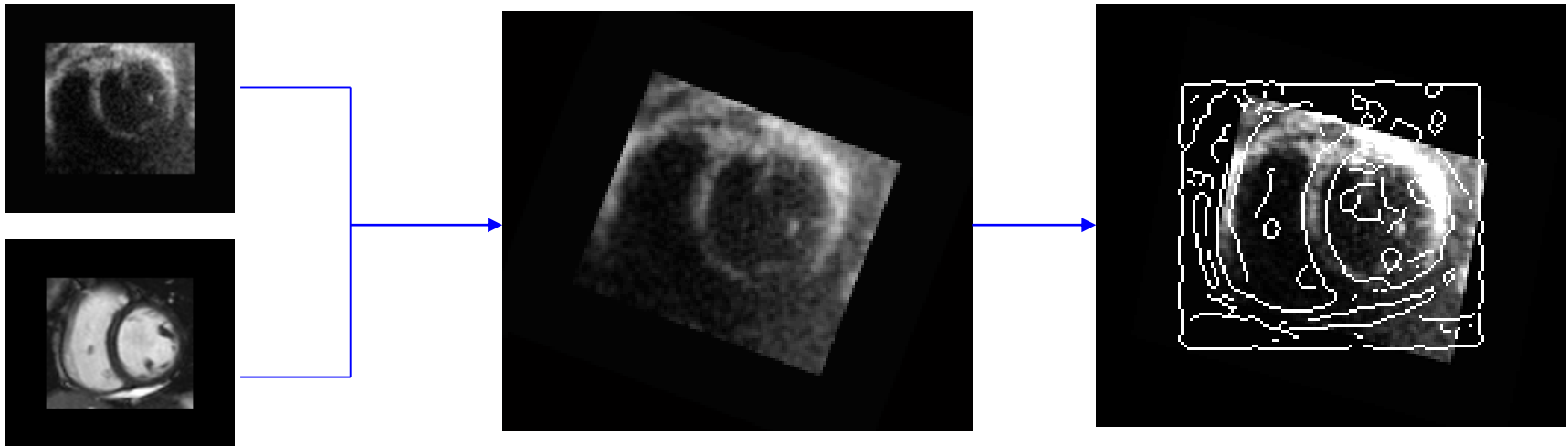
Slice of 3D  
ultrasound of the  
heart



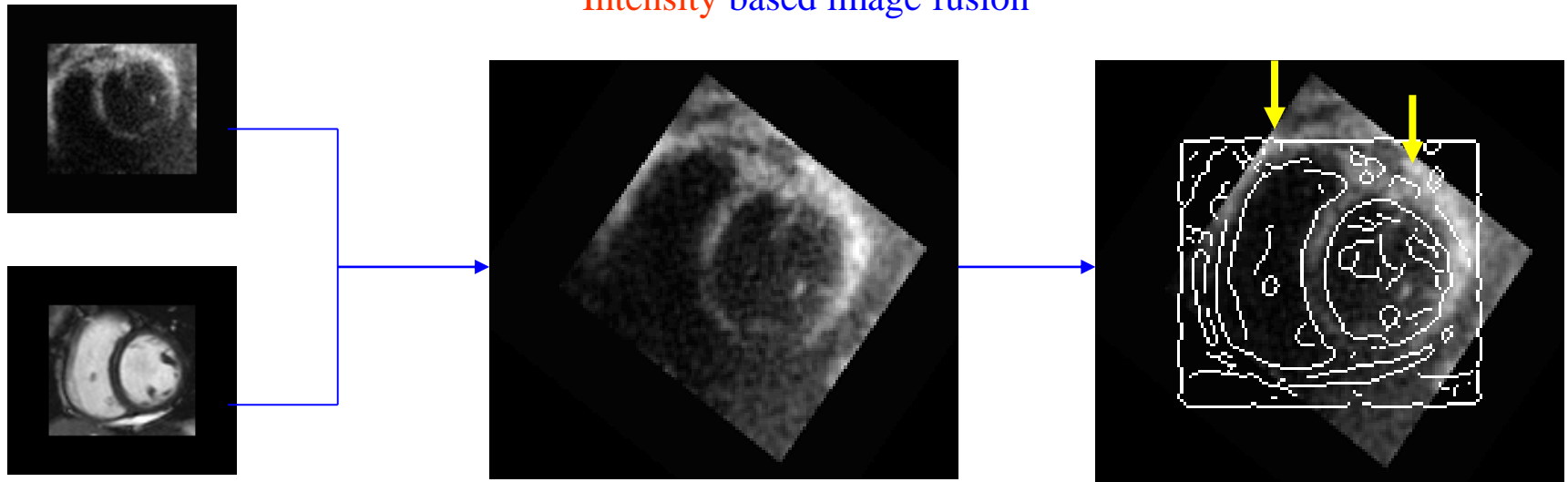
$\gamma < 0.1$ , filter spans 3.5 octaves



# MRI-ultrasound image fusion



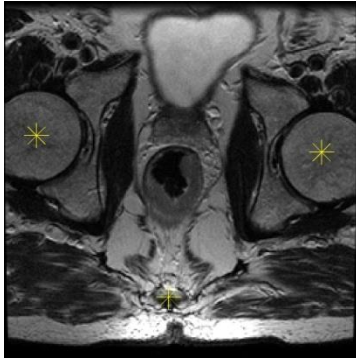
Intensity based image fusion



Phase-based image fusion based on the monogenic signal

# Similarity from (local) phase mutual information

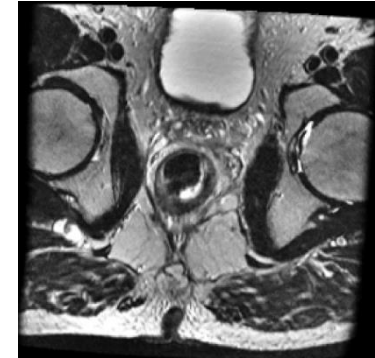
Pre-Treatment Image with Manually Identified control points



Local Phase (Pre)



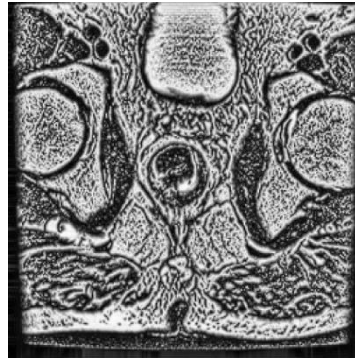
Warped Post-Treatment Image



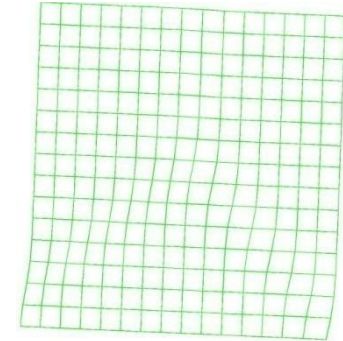
Post-Treatment Image with Manually Identified control points



Local Phase (Post)



Grid

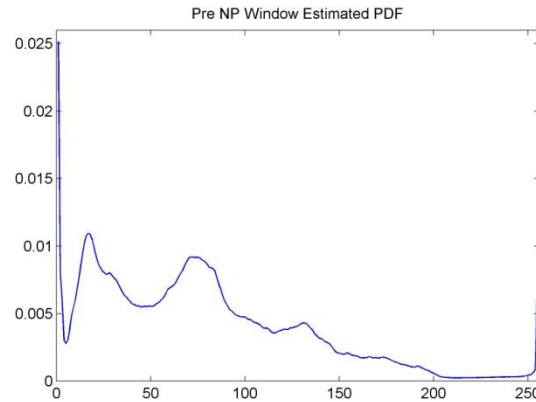


# Intensity PDF vs Phase PDF

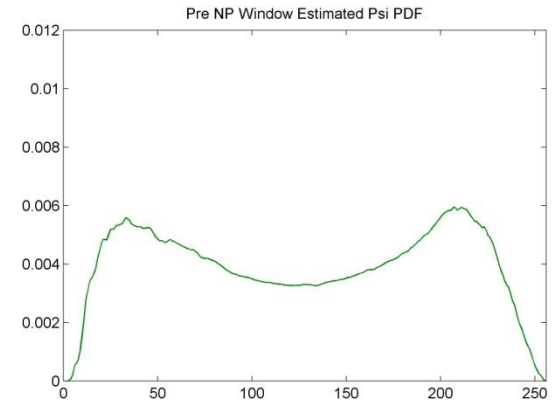
Pre-Treatment



Intensity PDF: pre

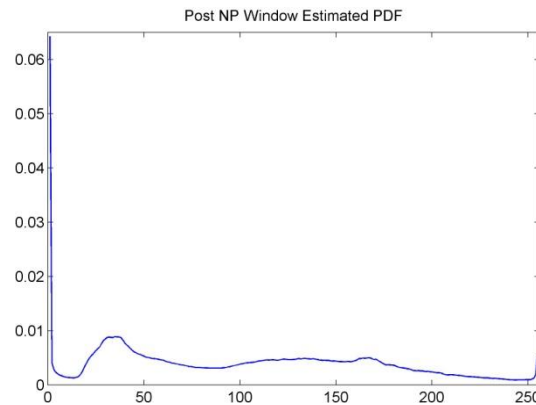


Local Phase PDF: pre

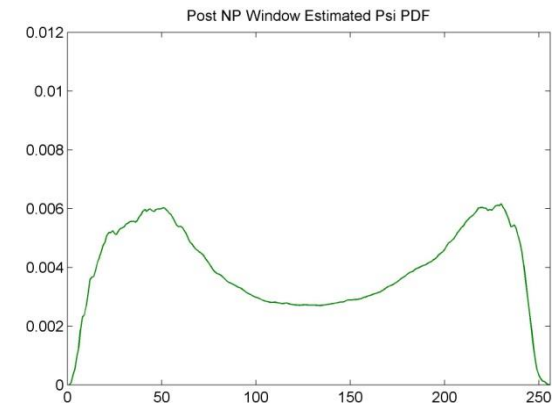


Post-Treatment

Intensity PDF: post



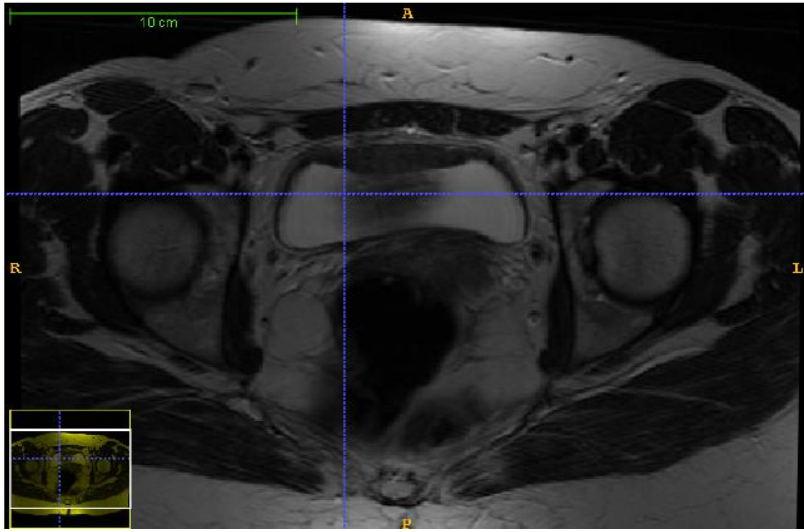
Local Phase PDF: post



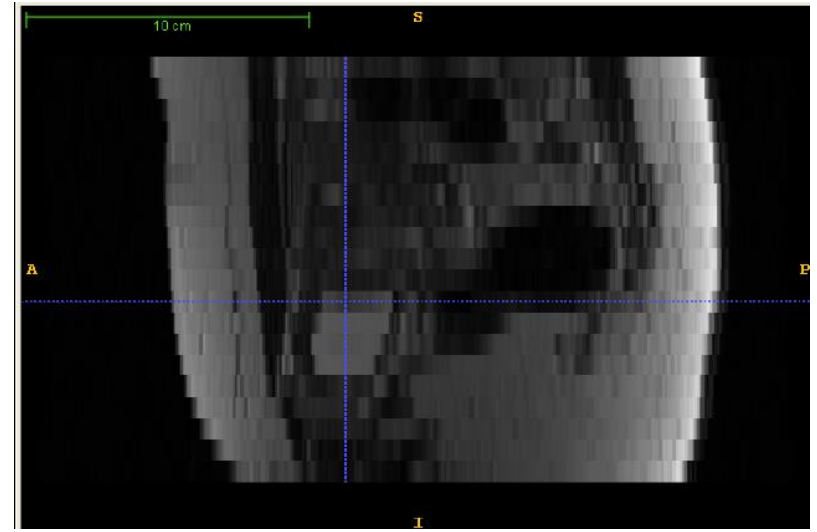
In both cases, intensity and local phase, we estimate PDF using NP windows



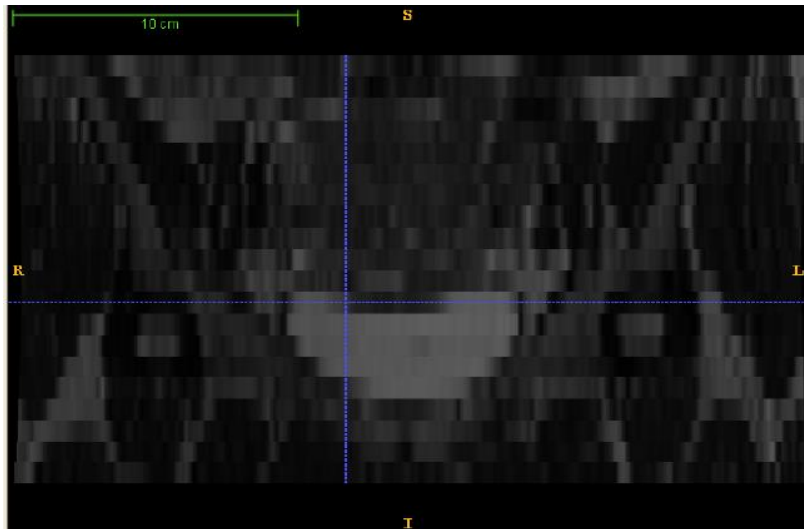
# Resampling MR images from Riesz components



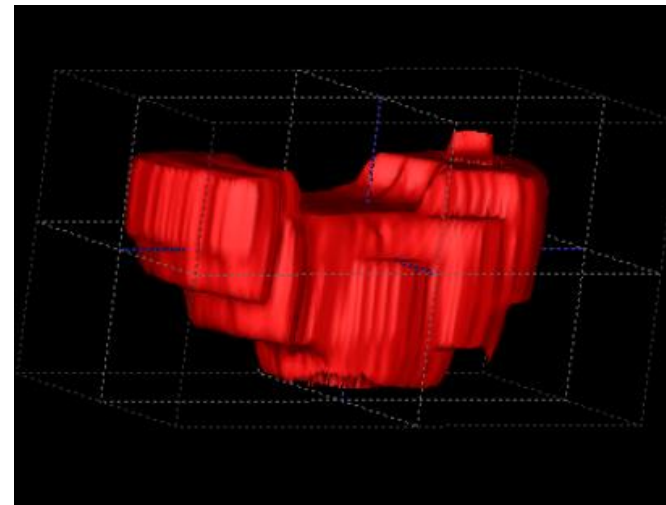
Axial view



Sagittal view

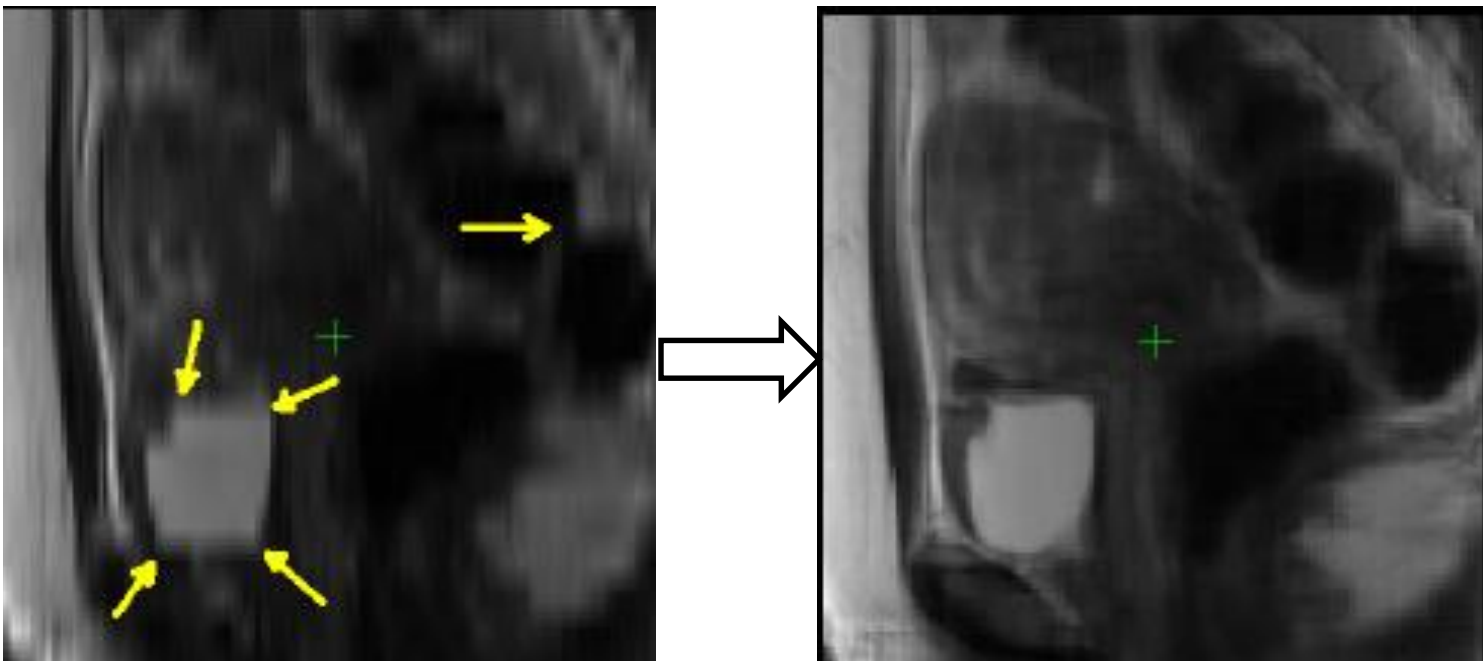
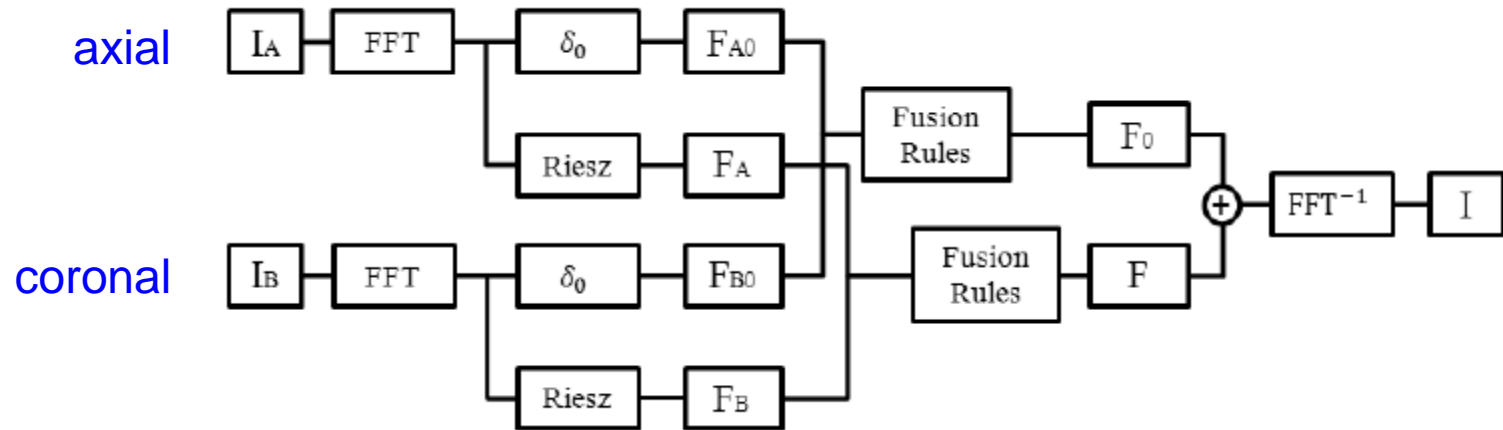


Coronal view



3D  
segmentation  
of the bladder

Often, we have images in all 3 directions...



# For “congruence”, how do you combine local phases?

The big problem is *phase wrapping*:  $(\pi+\alpha)+(\pi-\beta)=(\alpha-\beta)$

This impacts on every method (such as Kovesi's) for weighted sums of phases over scale (amplitude weighted, Riesz weighted, ...)

Let  $\mathbf{a} = |\mathbf{a}|\cos\theta_a + j|\mathbf{a}|\sin\theta_a$  and  $\mathbf{b} = |\mathbf{b}|\cos\theta_b + j|\mathbf{b}|\sin\theta_b$

We want :  $(\theta_a + \theta_b) / 2$

Is there an intelligent way to address this problem? YES: ***geometric algebra***

Build from the basis using geometric products:

$$\{1, \mathbf{e}_1, \mathbf{e}_2, \mathbf{e}_3, \mathbf{e}_{12}, \mathbf{e}_{13}, \mathbf{e}_{23}, \mathbf{e}_{123}\}$$

For two vectors  $\mathbf{a}, \mathbf{b}$  of "grade" 1,

$$\mathbf{ab} = \mathbf{a} \cdot \mathbf{b} + \mathbf{a} \wedge \mathbf{b}$$

$$\mathbf{ab} = |\mathbf{a}||\mathbf{b}|\cos(\theta_a + \theta_b) + \mathbf{e}_1 |\mathbf{a}||\mathbf{b}|\sin(\theta_a + \theta_b)$$

...nearly!

# A phase wrapping algorithm

First, De Moivre's theorem:  $\cos \theta + j \sin \theta = \left( \cos \{n\theta\} + j \sin \{n\theta\} \right)^{1/n}$

So take square root of the geometric product **ab** to get  $(\theta_a + \theta_b) / 2$

Suppose we write the monogenic signals as

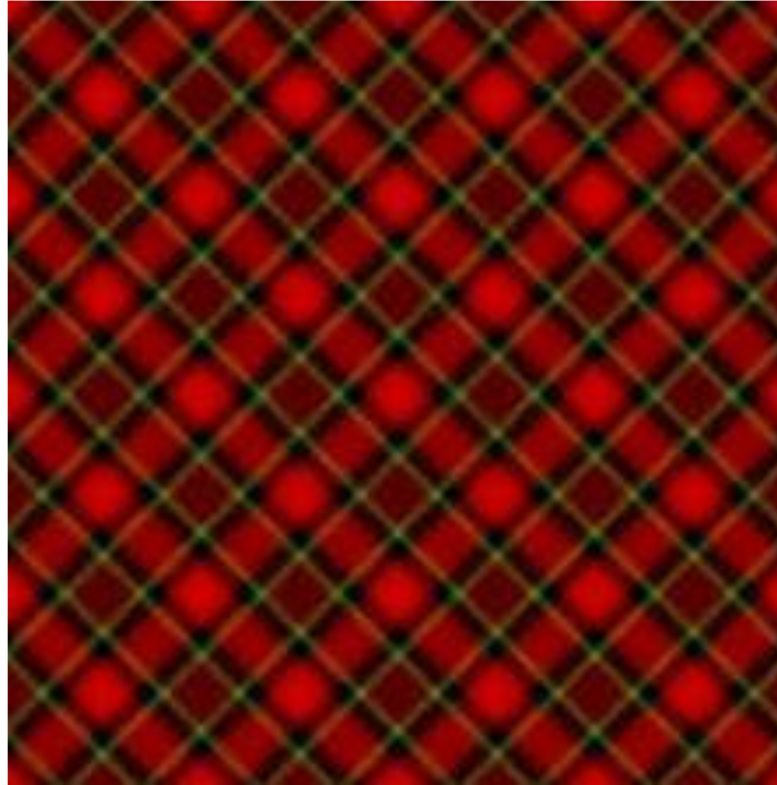
$\{\mathbf{m}_k : k = 1, \dots, n\}$  each  $\mathbf{m}_k$  is a 3-vector

Then:

$$LP_{mean} = \arg \left( \sqrt[n]{\prod_{k=1}^n \mathbf{m}_k} \right)$$

- This does not require the monogenic signals to have the same amplitudes (they rarely do)
- Normalisation is not necessary
- The number of operations required to implement this is  $4(n-1)$  – fast!!

# A regular texture



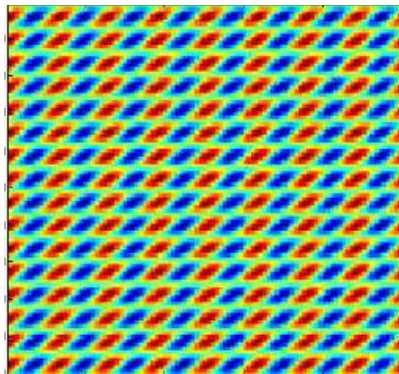
# Monogenic assumes a single orientation at each image location

Suppose that  $f_u, f_v$  are the Riesz components at any given image location.

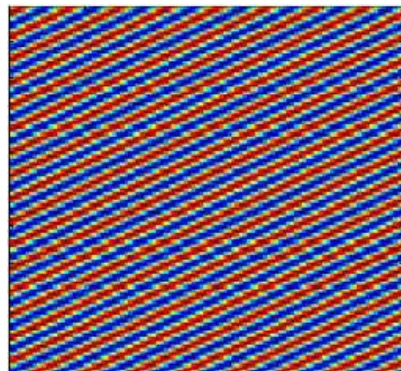
The local orientation in the monogenic signal is given by  $\tan \theta = (f_v / f_u)$

This defines a single orientation, and intrinsically loses information

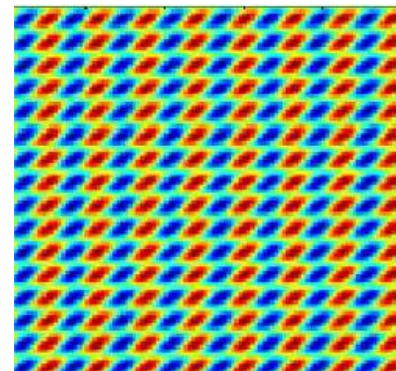
In textures, we often have multiple orientations at each point



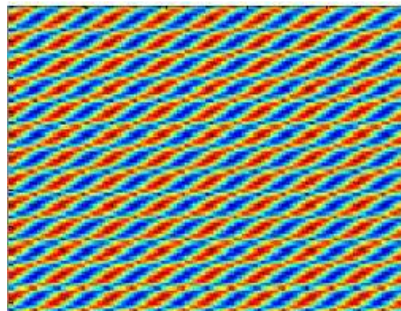
A simple texture: the sum of two sinusoids



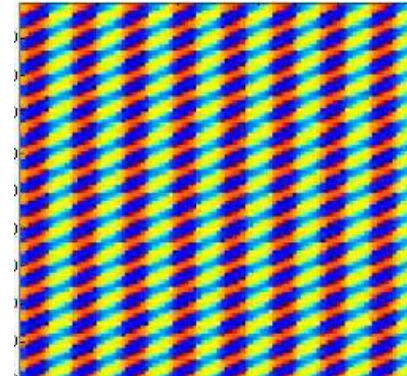
$f_u$



$f_v$



Local phase



Local orientation

**For texture analysis, use Riesz components**

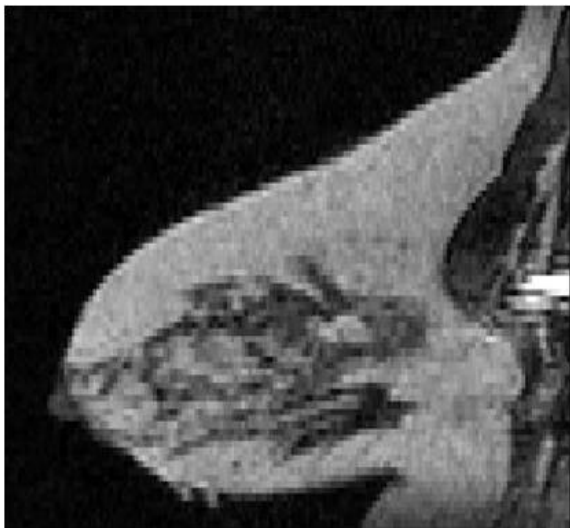
# Riesz component weighting for phase congruency

Let the Riesz components be denoted:  $R_1(s_k), R_2(s_k)$ , scale  $s_k$

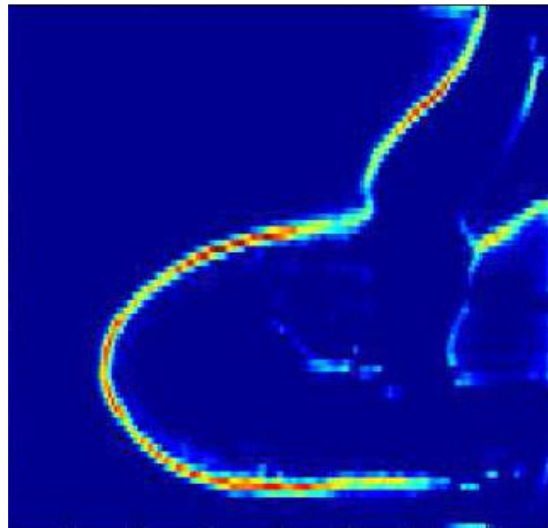
The Riesz weighted phase measure is:

$$LP_{\text{Riesz}}(\mathbf{x}) = \frac{\sum_{s_k=1}^n \left( \max_{s_k} |R_1(s_k)(\mathbf{x})| + \max_{s_k} |R_2(s_k)(\mathbf{x})| \right) \cdot \phi(\mathbf{x}, s_k)}{\sum_{s_k=1}^n \left( \max_{s_k} |R_1(s_k)(\mathbf{x})| + \max_{s_k} |R_2(s_k)(\mathbf{x})| \right)}$$

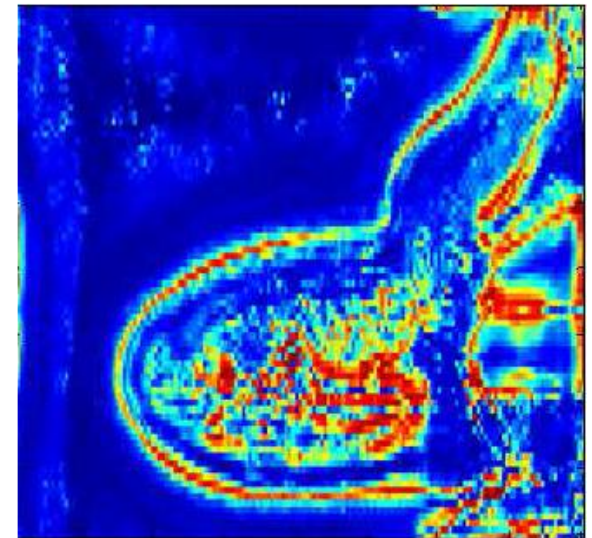
Breast MRI



Kovesi PC



Riesz-weighted PC



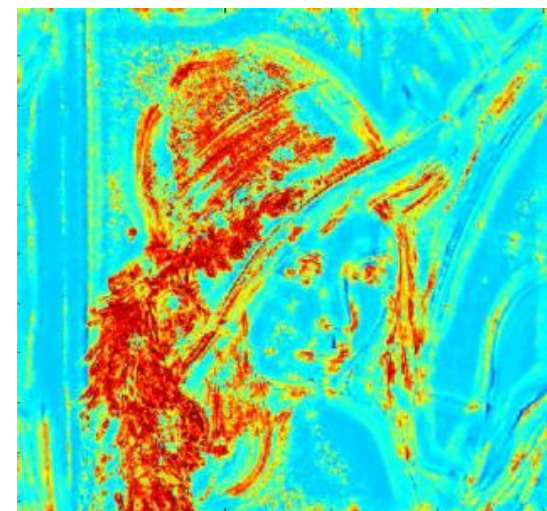
# Riesz components for texture



Kovesi's energy weighted PC



Riesz weighted PC



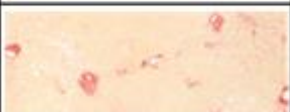






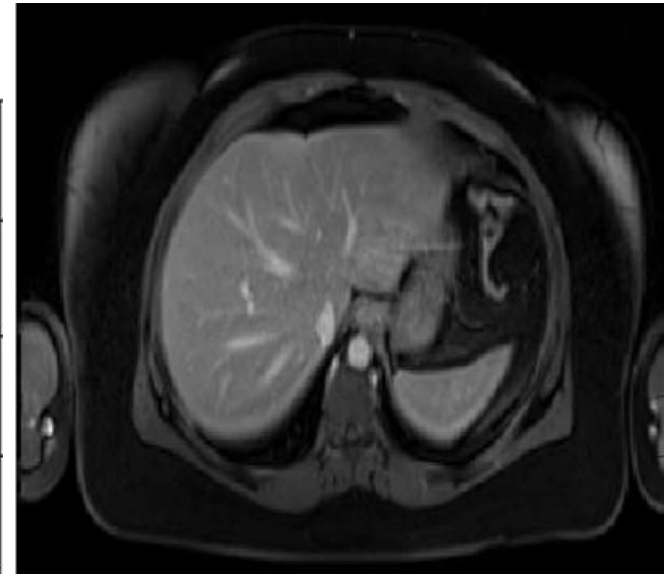
Riesz - Energy

the difference is most pronounced in the texture that is of interest



# Staging liver disease: primary sclerosing cholangitis

| Appearance   | Ishak stage:<br>Categorical description  | Ishak stage:<br>Categorical assignment |
|--|--|--|
|    | No fibrosis (normal)   | 0                                      |
|    | Fibrous expansion of some portal areas +/- short fibrous septa   | mild<br>1                              |
|    | Fibrous expansion of most portal areas +/- short fibrous septa   |  |
|    | Fibrous expansion of most portal areas with occasional portal to portal (P-P) bridging                             | severe<br>3                            |
|    | Fibrous expansion of portal areas with marked bridging (portal to portal (P-P) as well as portal to central (P-C)) |  |
|   | Marked bridging (P-P and/or P-C), with occasional nodules (incomplete cirrhosis)                                   | very severe<br>5                       |
|  | Cirrhosis, probable or definite  |  |

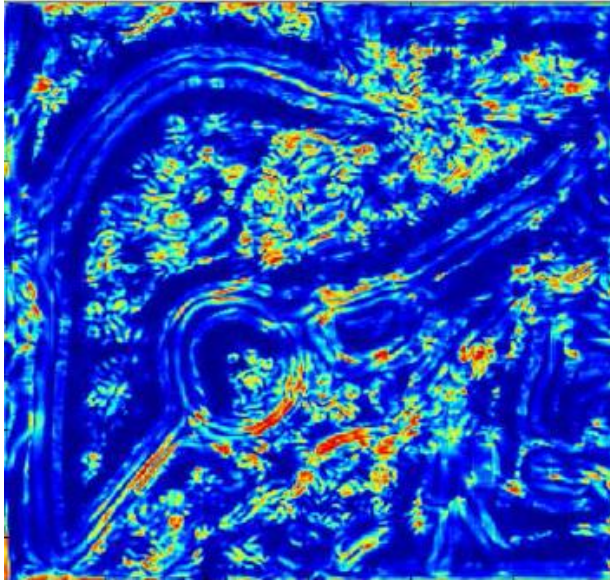


Ishak grade 0: healthy

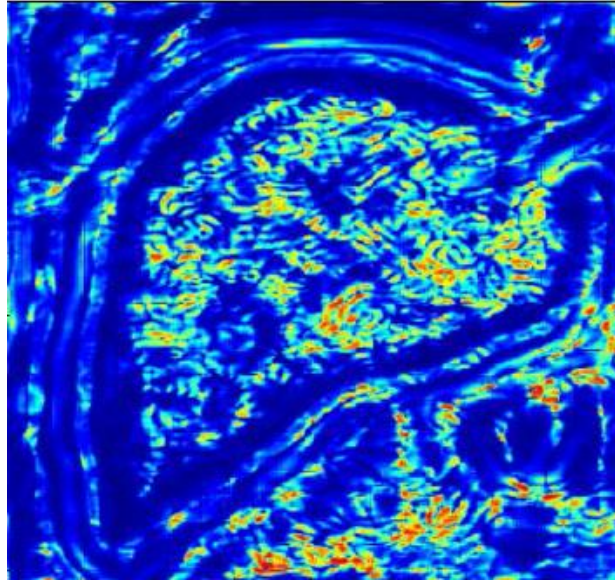


Ishak grade 4: severe disease

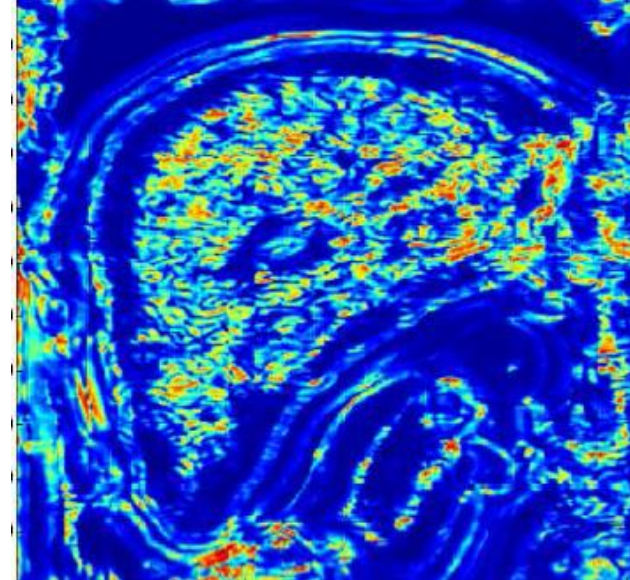
# Ishak grades



Grade 2

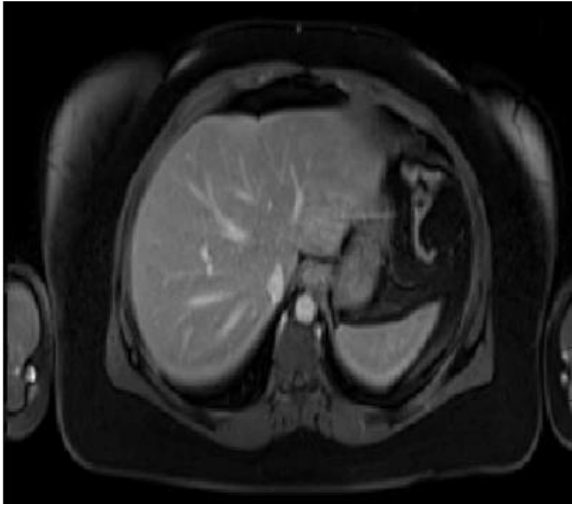


Grade 3

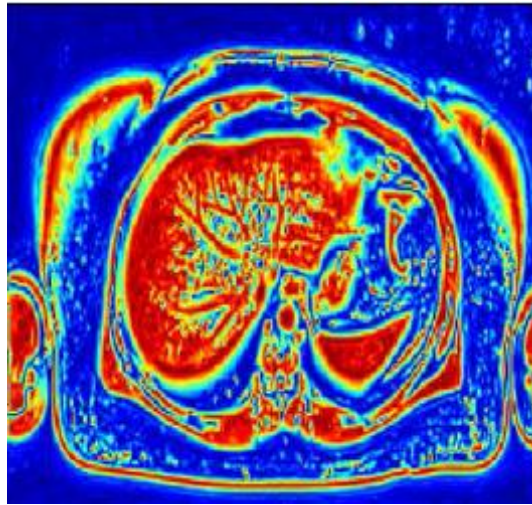


Grade 4

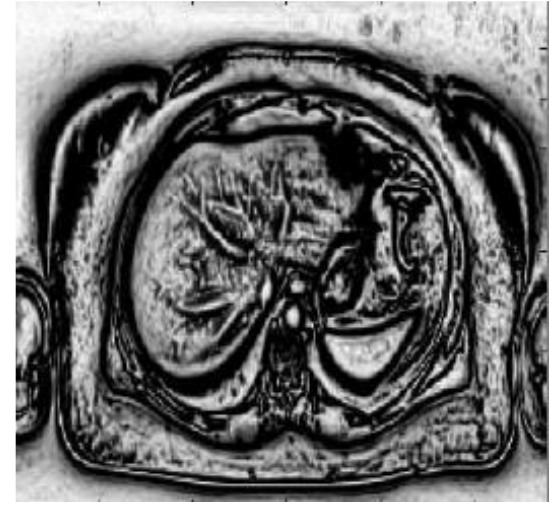
# Towards automated Ishak scoring



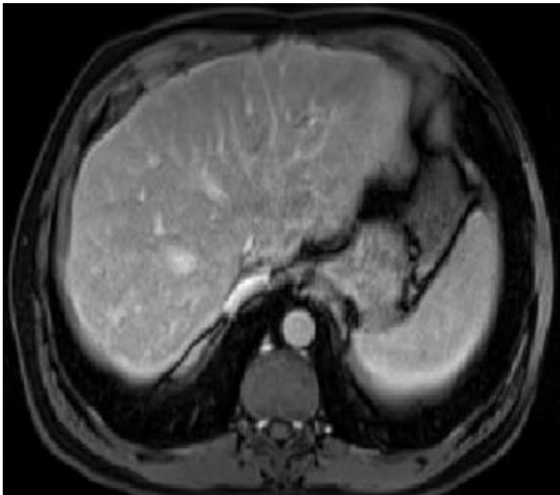
Ishak 0: healthy



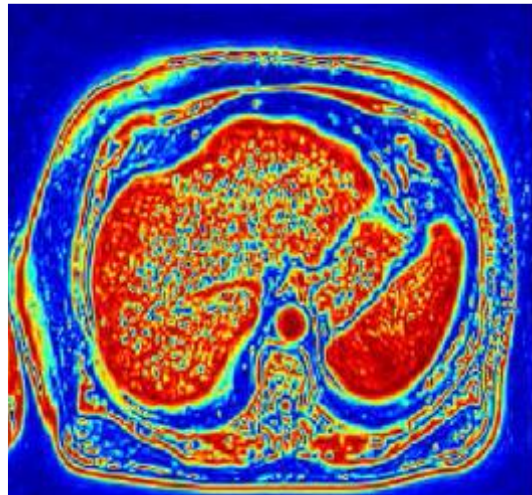
phase



Feature asymmetry



Ishak 4: severe disease

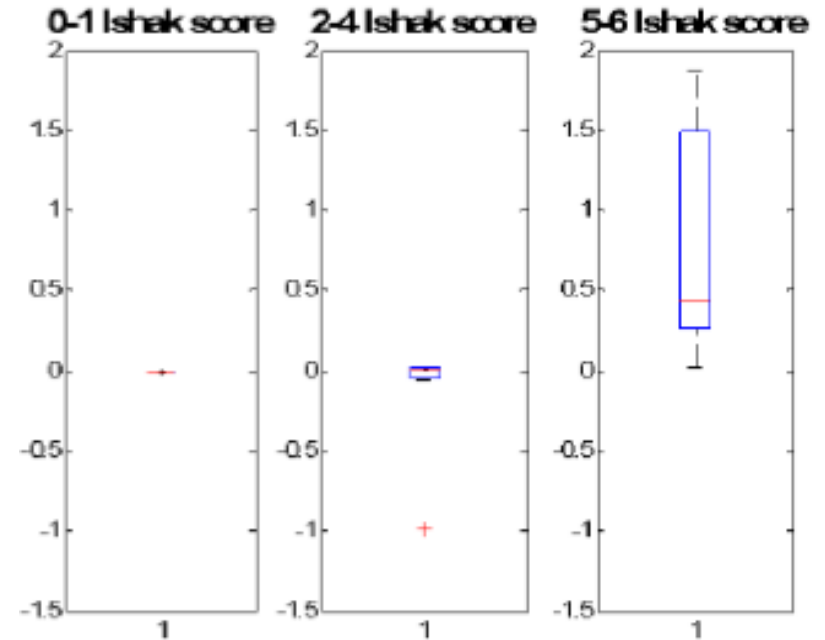
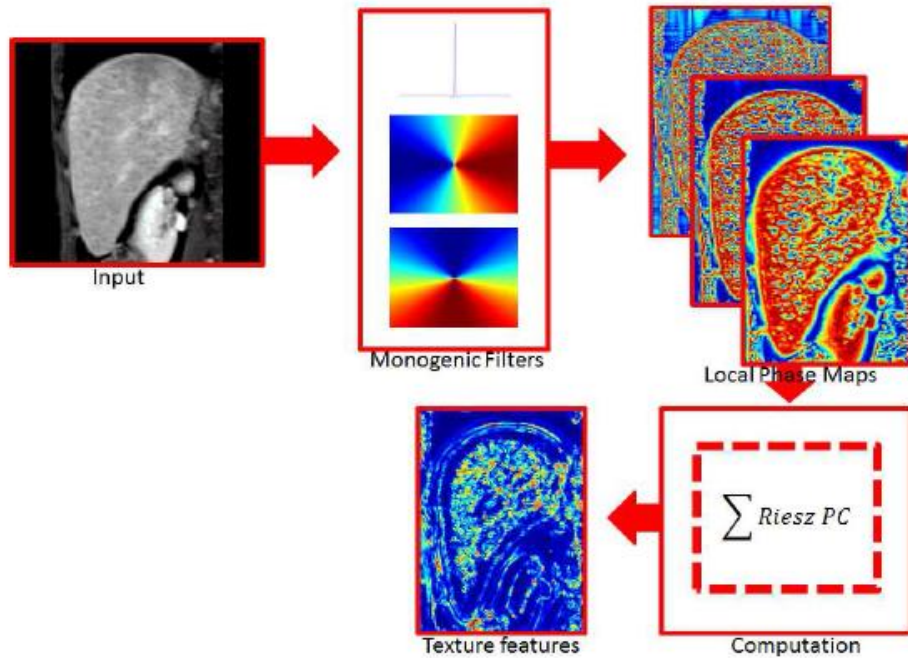


phase



Feature asymmetry

# Liver texture analysis



Correlation with pathology,  $r = 0.967$

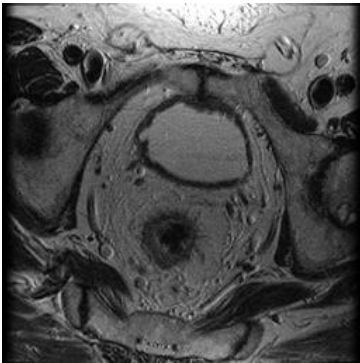
The texture features we have experimented with to date include:

- Fractal dimension ✓
- Entropy X
- Clumpedness X
- Laws filters ✓

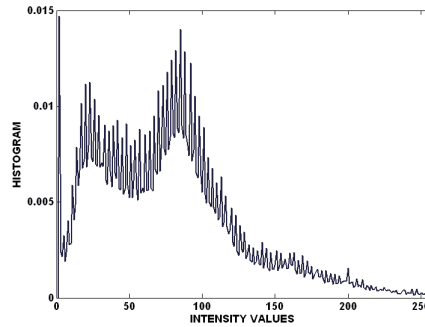
# Uncertainty is ubiquitous in signal/image analysis

## Comparison of various PDF estimates

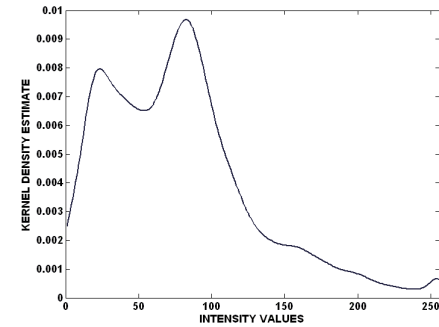
Test image



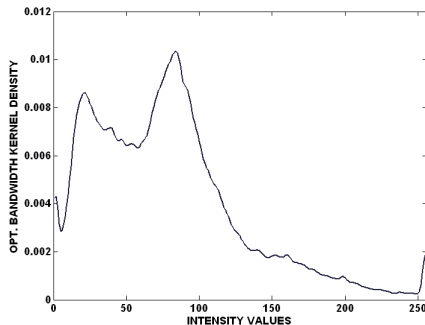
Histogram



Kernel estimator

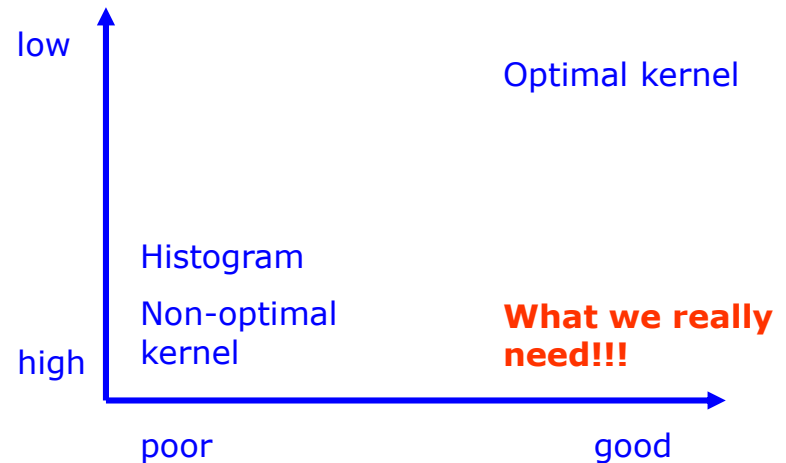


Kernel estimator  
With optimal bandwidth



T= 180 seconds,  
Bandwidth = 1.79

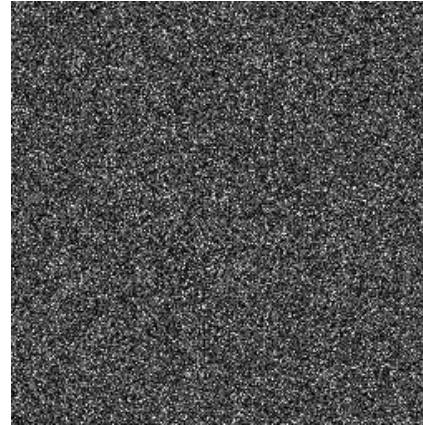
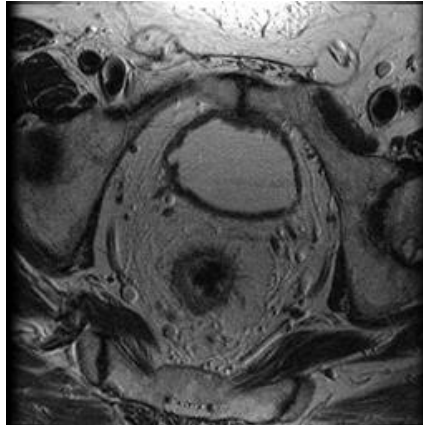
Computational  
efficiency



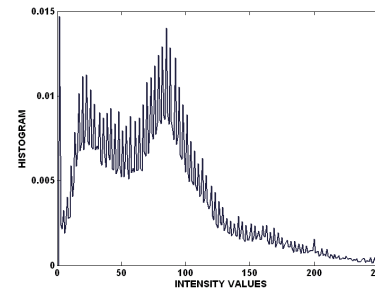
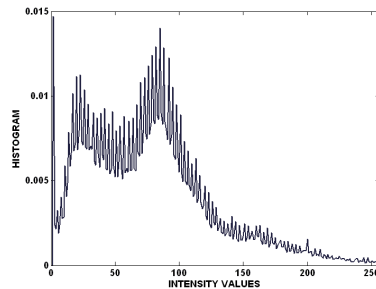
Accurate estimate

# What's the root of the problem?

Two images that seem to be dissimilar...

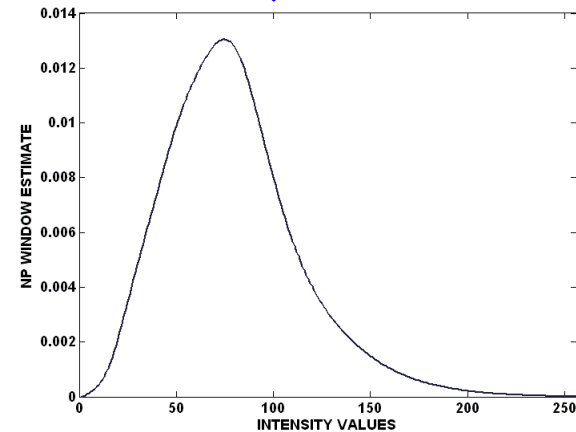
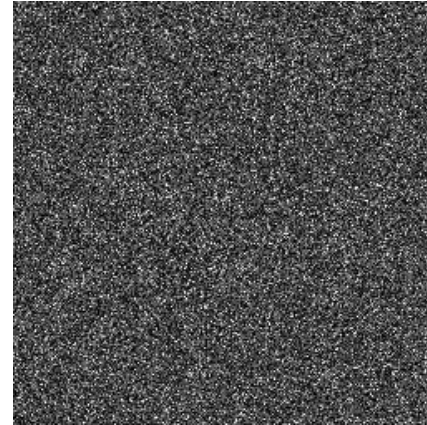
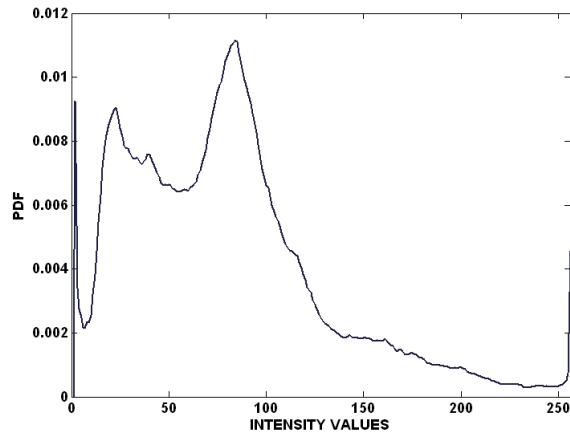
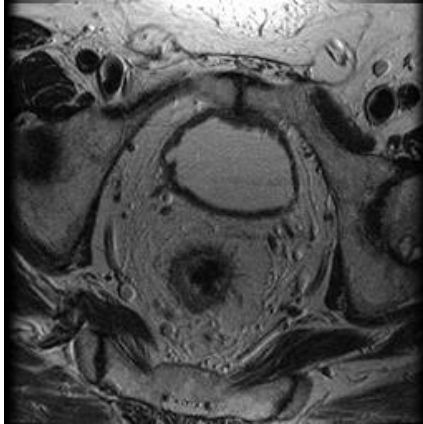


Their histograms are identical ... and so are their kernel density estimators!



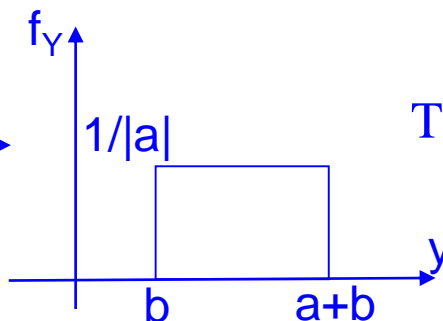
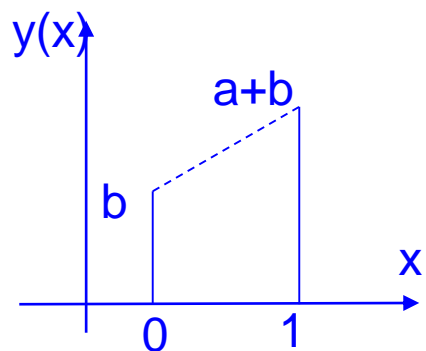
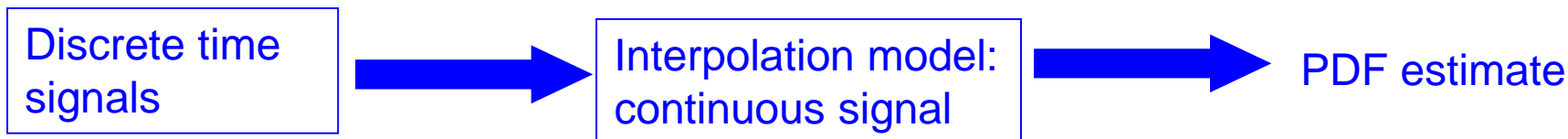
- Estimators based on population statistics *ignore* the order of samples in a signal or image
- Order is important in a signal!! And, signals are critically band-limited
- Choosing a suitable interpolation scheme, we can form a *continuous* version of the signal/image, and, from this, derive a superior PDF estimate ...quickly!!

..if you do take sample order into account



Now they are clearly distinguished! Here the PDFs are derived using NP Windows.

# NP windows



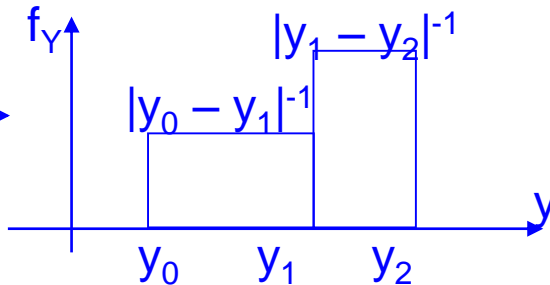
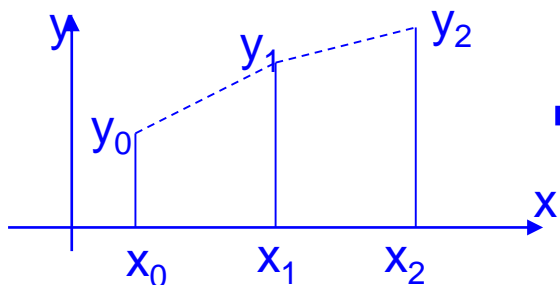
a portion of a signal:

$$y(x) = ax + b, 0 \leq x \leq 1$$

The transformation formula:

$$f_Y(y) = \frac{1}{\left| \frac{dy}{dx} \right|} f_X(x) = \frac{1}{a}, b \leq y \leq a+b$$

Linear interpolation  $\rightarrow$  uniform distribution. Other interpolation is possible, of course



Calculate PDF of each piecewise linear section, using the Transformation Formula, and superpose them

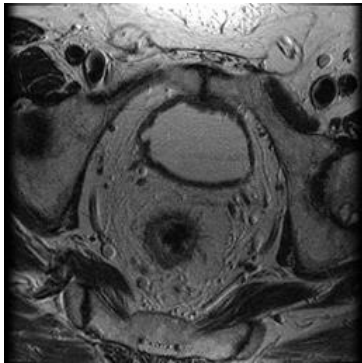
This extends readily to 2D, 3D, ....

From signal to PDF

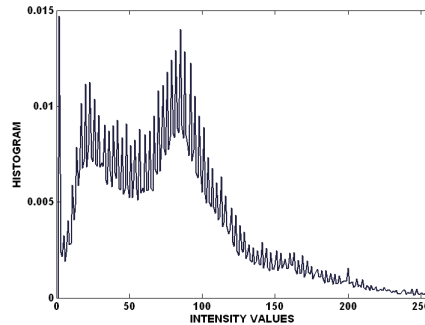


# Comparison of various PDF estimates

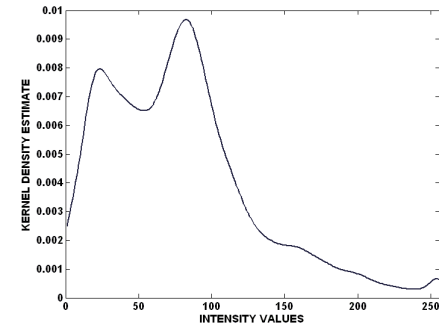
Test image



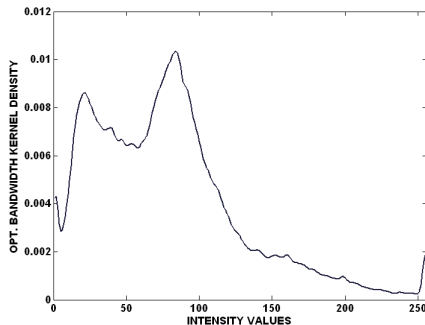
Histogram



Kernel estimator

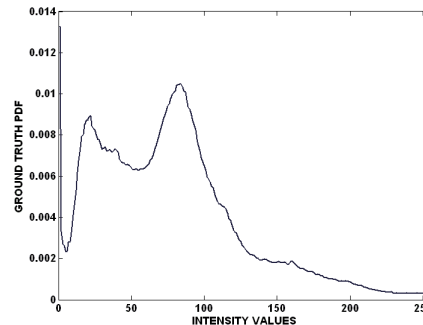


Kernel estimator  
With optimal bandwidth



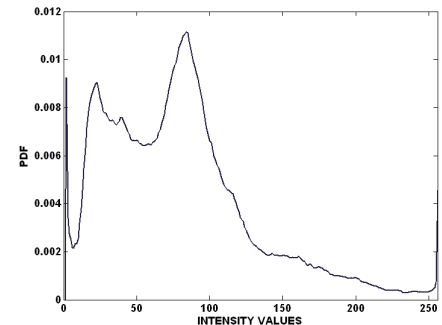
**T= 180 seconds,**  
**Bandwidth = 1.79**

Ground Truth



Histogram of highly upsampled version  
of the test image

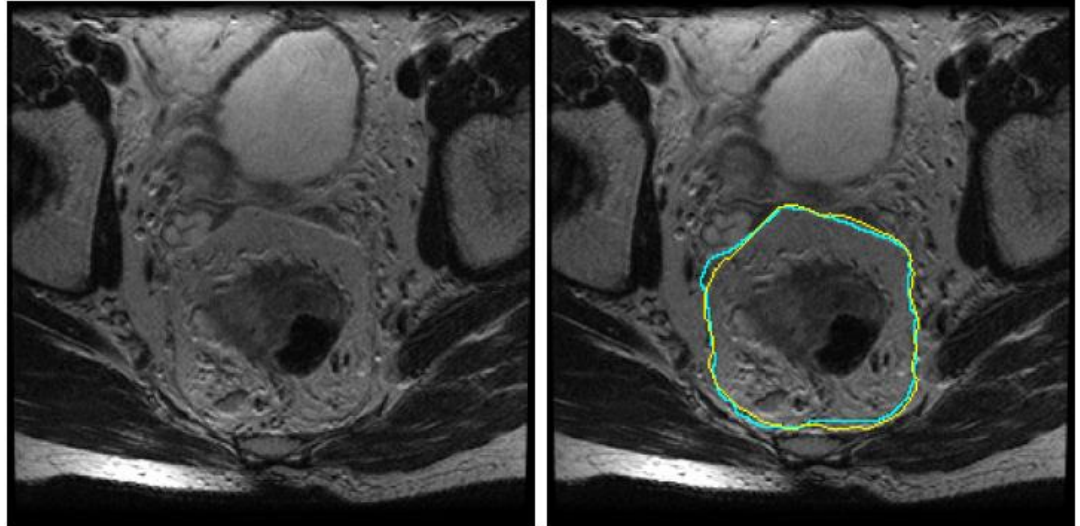
NP windows



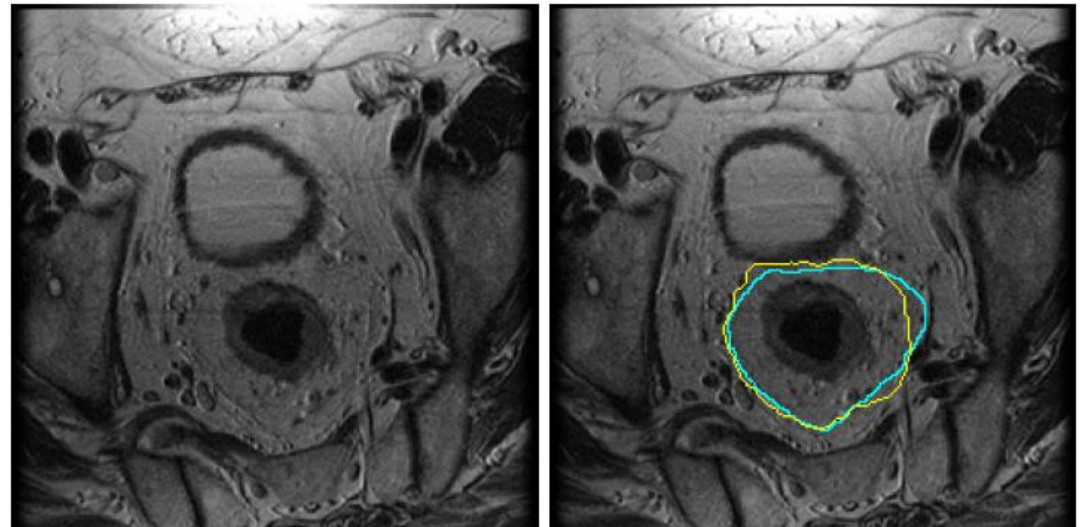
**T=30 milliseconds**

# Mesorectal fascia segmentation

Cyan coloured contour:  
Hand-drawn by clinical  
expert



Yellow coloured contour:  
Our algorithm

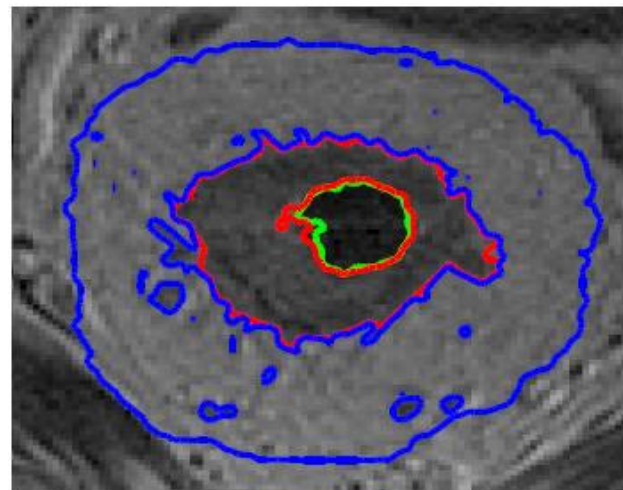
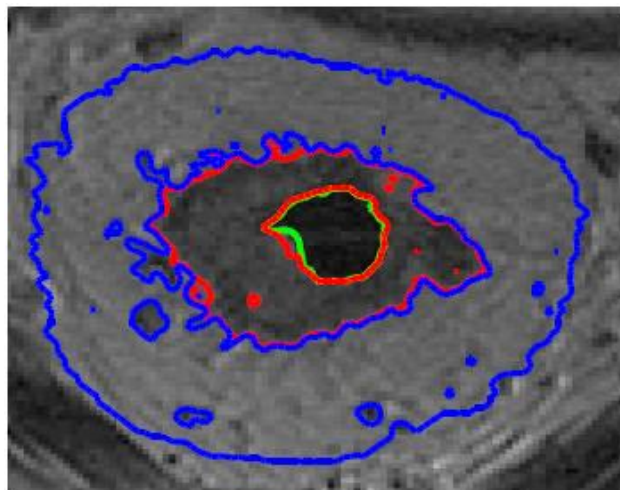
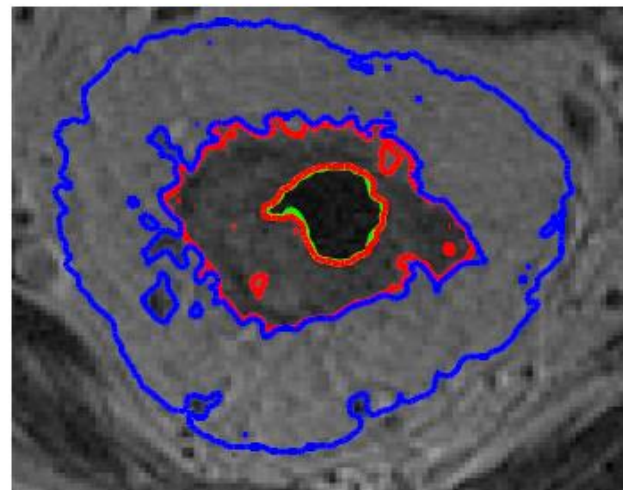
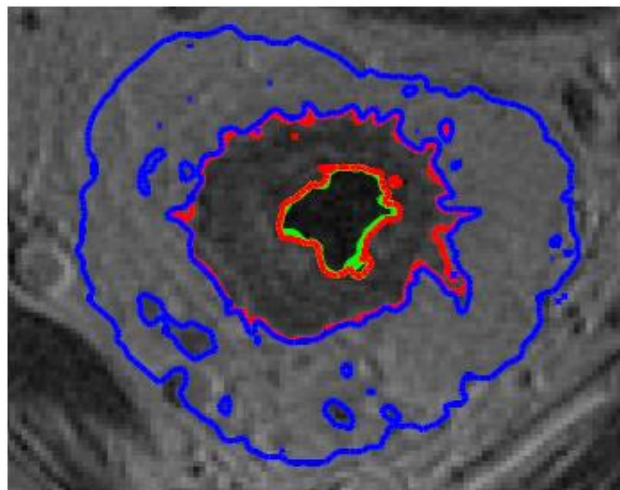


# Tissue class segmentation

Green: lumen

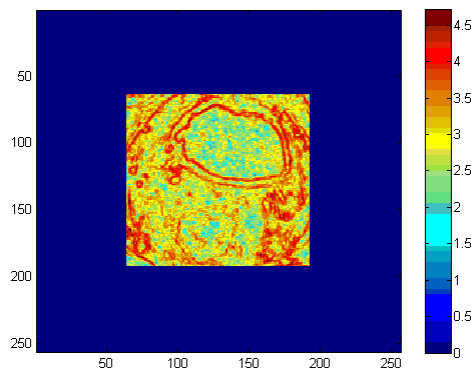
Red: rectum/  
tumour

Blue: mesorectum



# Does *NP Windows* really make a difference to the calculation of entropy?

*NPW* on 3X3 window



*NPW* on 5X5 window

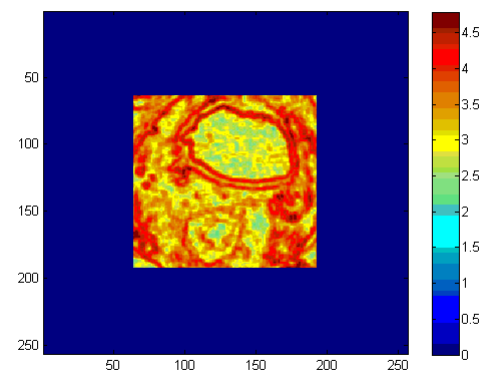
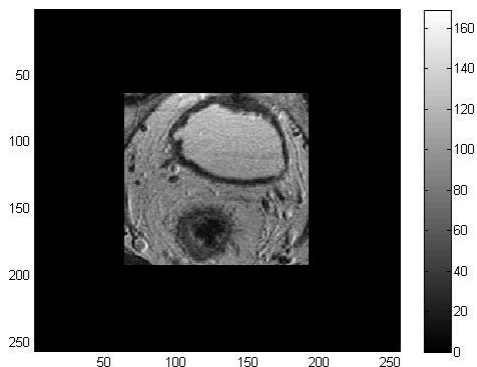
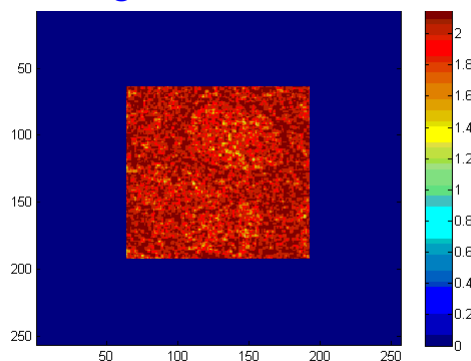


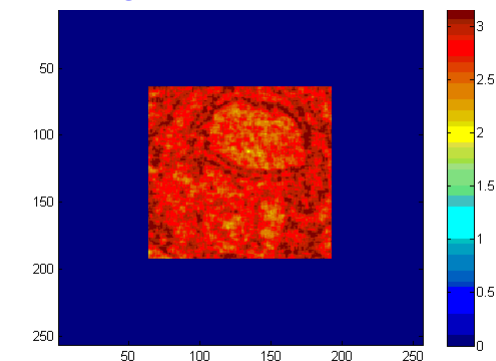
Image fragment



Histogram on 3X3 window



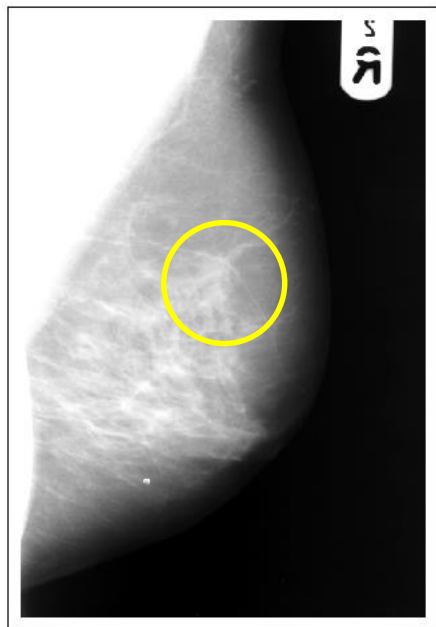
Histogram on 5X5 window



Unlike kernel density estimators, there is no bandwidth parameter to optimise .. In fact, there are no parameters to set!! Typical compute time = 35ms for a 128X128 image

# Matching shapes

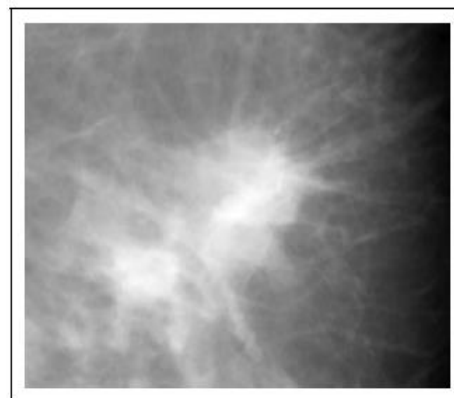
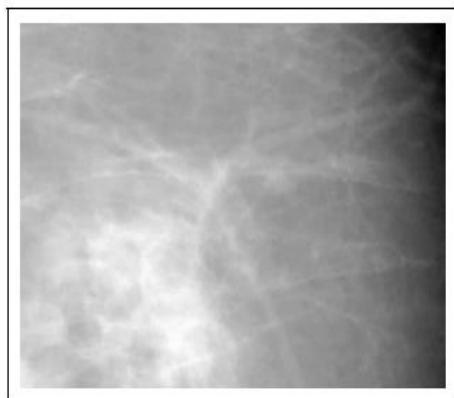
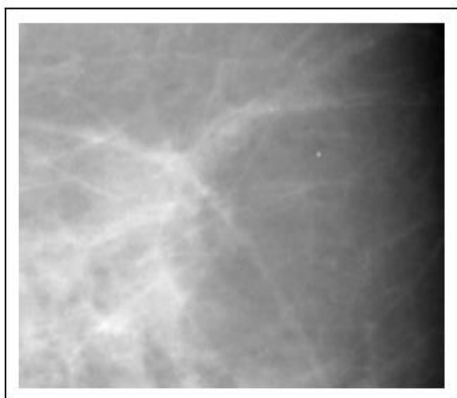
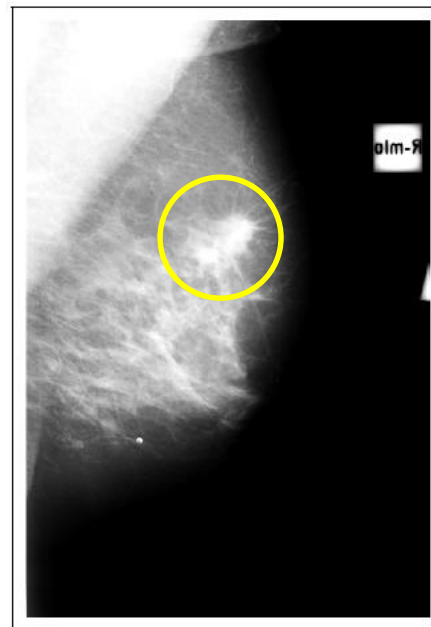
1992



1995



2000

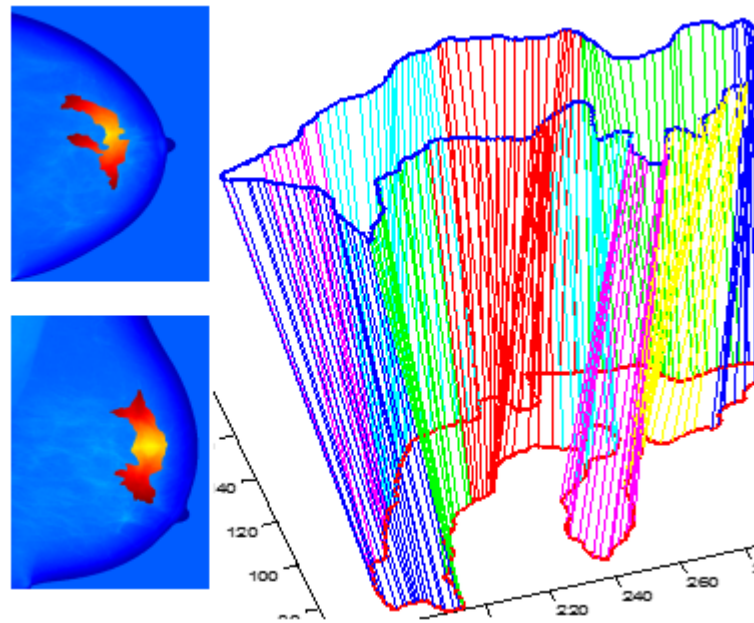
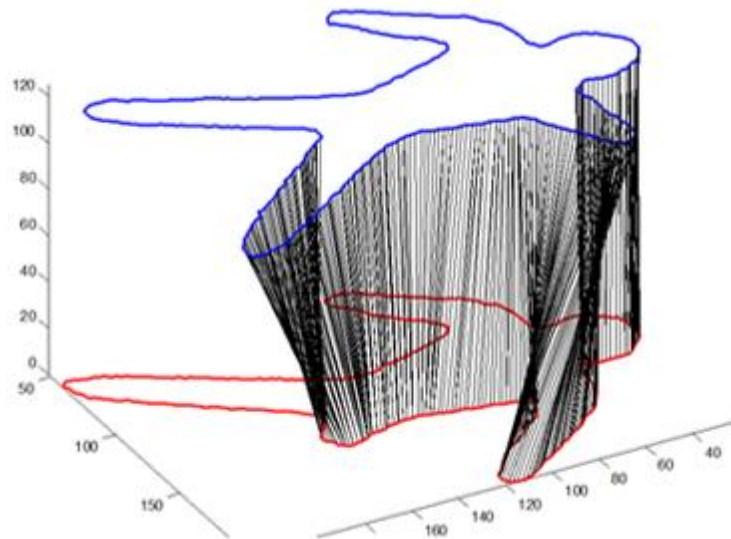


# Shape matching

- Task: match shapes, noting significant difference
  - Disease progression; response to therapy; imaging conditions..
- Shape descriptors
  - Boundary & interior contain complementary information – use both
- Boundary
  - Robust to noise, errors in segmentation, ..
  - Need to align “key” points: scale space
  - Invariant to articulations
- Interior
  - Geodesics between points
- Fast marching algorithm
  - Fusion of boundary and interior

# Shape matching

Two of Kimia's dude shapes



Left: a CC/MLO pair of density maps output from Volpara

Right: match of the contours using integral invariants and fast-marching algorithm

Robustness to articulation differences rules out projective\* & algebraic invariants

\*Except if combined with pictorial structures

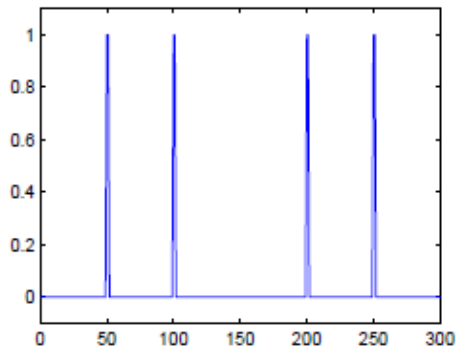
# Differential invariants?



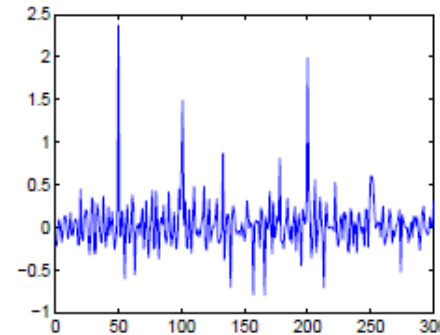
(a) A rectangular shape.



(b) A rectangular shape with noise.



(c) Curvature of (a).

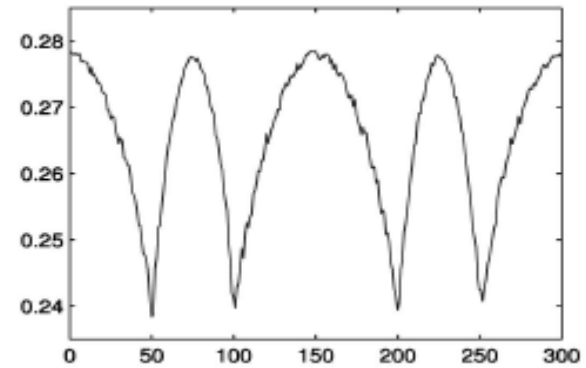
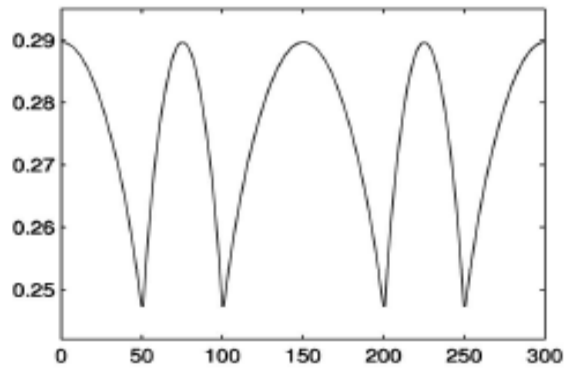


(d) Curvature of (b).

- Differential invariants are based on 2<sup>nd</sup> plus order derivatives, so VERY prone to noise...
- Less well known are *integral* invariants ... but they have substantial advantages, and they are fast to compute

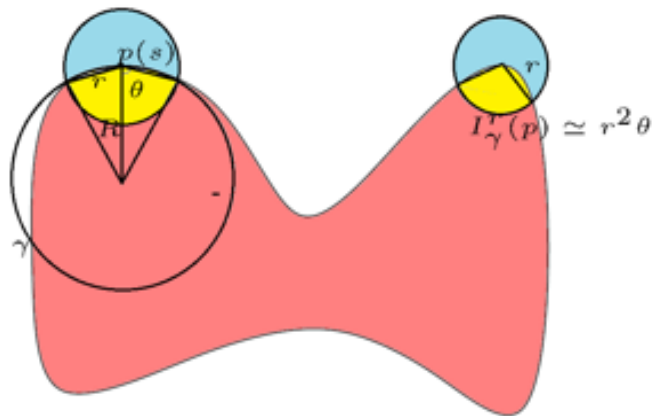


# Integral invariants



Integral invariants are resistant to noise

# Integral Invariants



The value at each point along the curve is the intersection of the circle with the shape

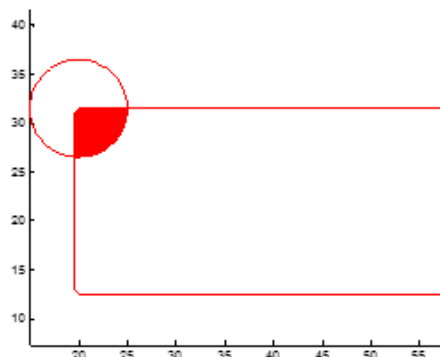
Increasing the radius of the shape defines a scale space

Curve  $C$ , point  $p \in C$ . Integral invariant at scale  $r$  is

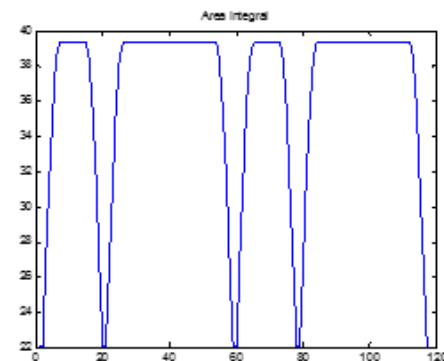
$$I_r(p) = \int_{\Omega} \chi(B_r(p), C)(x) dx$$

where  $\Omega$  is domain( $C$ ), and

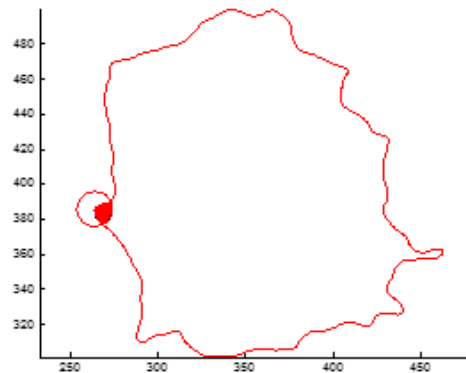
$$\chi(B_r(p), C)(x) = \begin{cases} 1 & x \in B_r(p) \cap \text{Int}(C) \\ 0 & \text{otherwise} \end{cases}$$



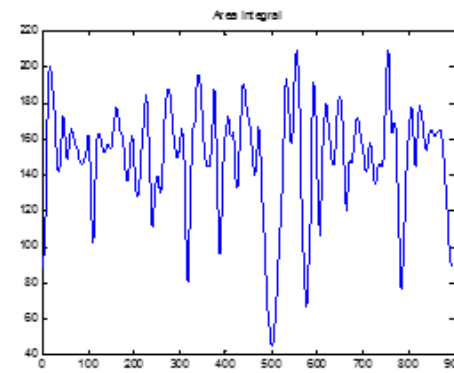
Simple shape



Integral invariant

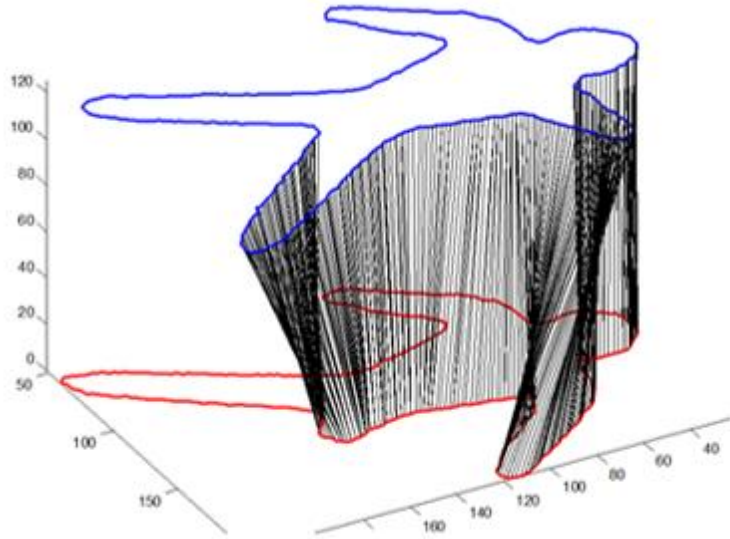


Outline of a spiculated mass



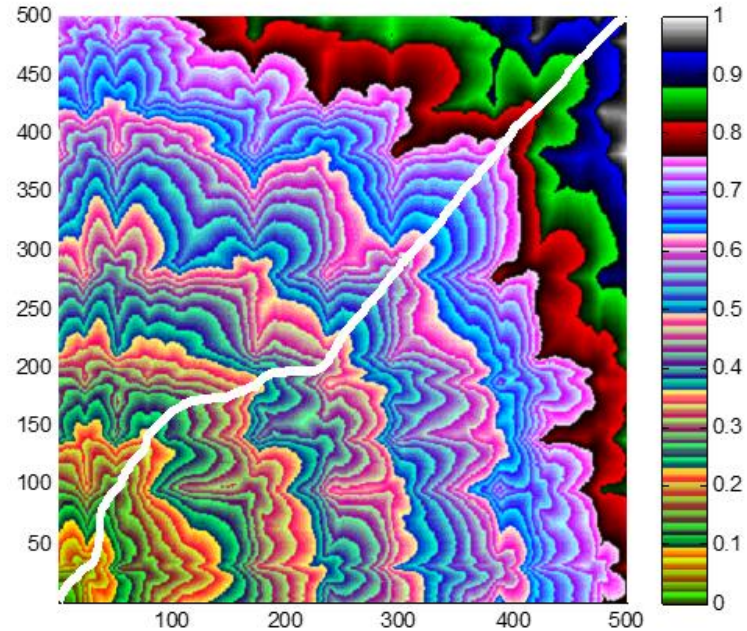
Integral invariant – a signature

# Example

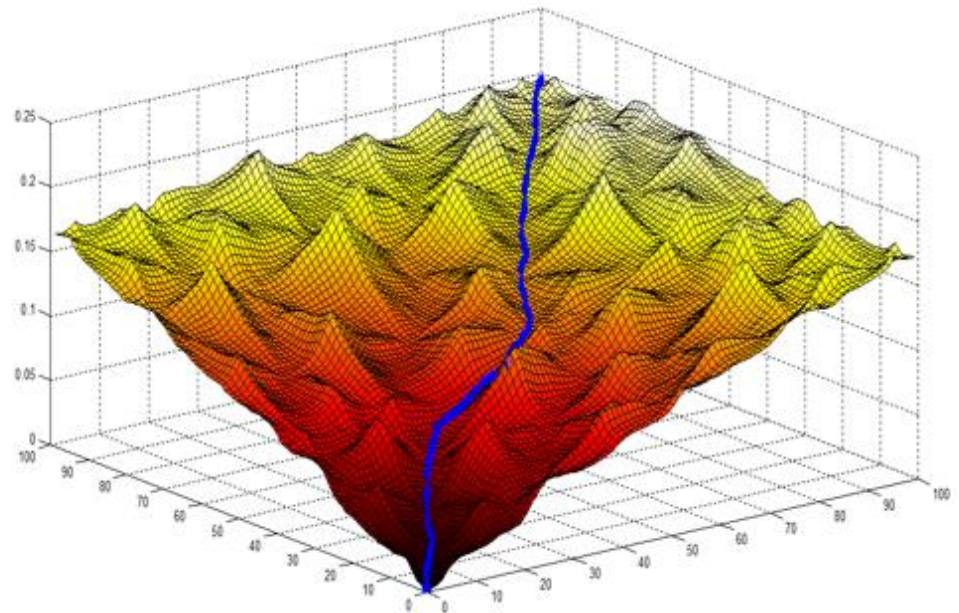


Two shapes; the red one has an occlusion (not an amputation)

Correspondences shown as black lines













Geodesic distance map computed by Fast Marching Algorithm

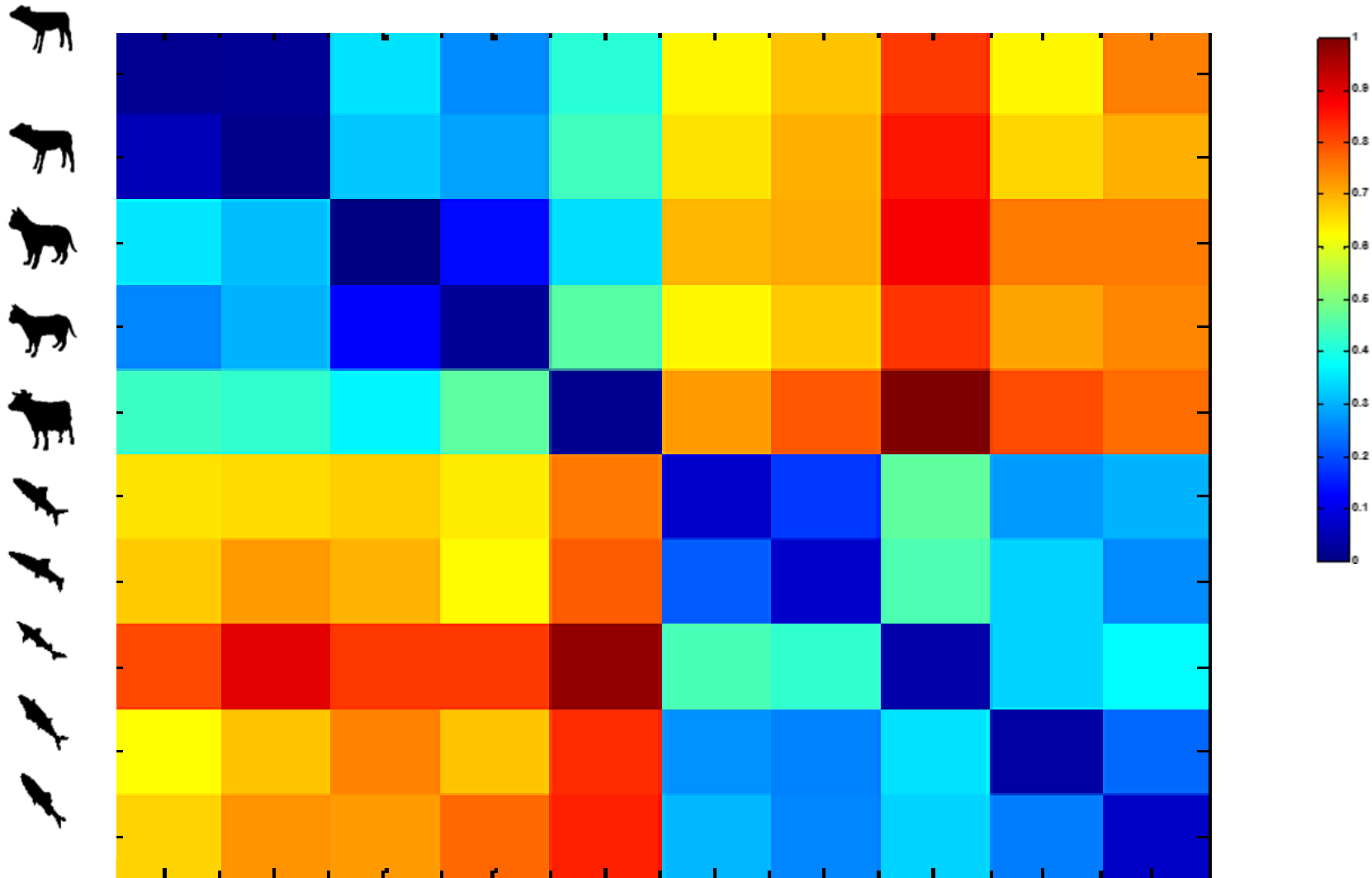


## Results for Kimia's database of shapes



|  |      |      |      |      |      |      |      |      |      |      |
|--|------|------|------|------|------|------|------|------|------|------|
|    | 0.29 | 0.49 | 2.41 | 1.81 | 2.66 | 3.34 | 4.07 | 4.41 | 4.10 | 3.59 |
|    | 0.49 | 0.24 | 2.16 | 2.03 | 2.28 | 3.67 | 4.15 | 4.24 | 3.95 | 3.91 |
|    | 1.98 | 1.88 | 0.00 | 1.10 | 2.11 | 3.42 | 3.70 | 4.08 | 3.82 | 4.05 |
|    | 1.96 | 1.72 | 0.91 | 0.35 | 2.51 | 3.26 | 3.98 | 4.00 | 3.93 | 3.81 |
|    | 2.82 | 2.40 | 2.24 | 2.64 | 0.31 | 3.91 | 4.11 | 4.88 | 4.42 | 5.00 |
|    | 3.71 | 3.65 | 3.17 | 3.24 | 3.85 | 0.17 | 0.88 | 2.61 | 1.97 | 1.90 |
|  | 3.82 | 3.81 | 3.87 | 3.66 | 3.84 | 0.90 | 0.52 | 1.97 | 1.77 | 1.60 |
|  | 4.30 | 4.01 | 4.10 | 3.62 | 4.93 | 2.47 | 1.38 | 0.39 | 1.98 | 2.74 |
|  | 3.67 | 3.47 | 3.78 | 3.58 | 4.45 | 1.53 | 1.90 | 2.15 | 0.79 | 0.99 |
|  | 3.98 | 4.11 | 4.38 | 3.48 | 4.63 | 1.85 | 1.32 | 2.05 | 1.25 | 0.61 |

# Results for Kimia's database of shapes



Good news!!! Fish do not resemble mammals

# Encoding the shape interior depends on geodesic distance

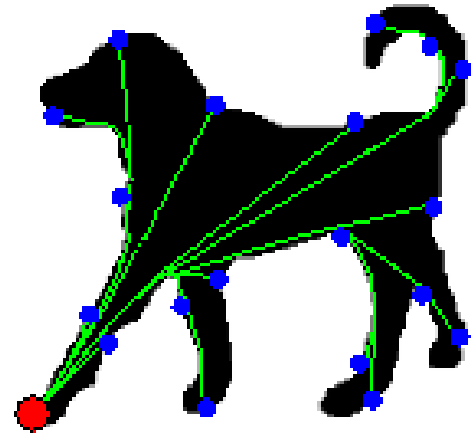
Geodesic distance tells how far two points in a shape are, in particular how far apart two points on the boundary  $\partial C$  are – enabling combination with the integral invariants



Euclidean distance



Geodesic  
distances from  
Fast Marching  
Algorithm



Example  
geodesic  
paths

# Eccentricity transform

Let  $x, y$  be points on a curve  $C$ . The eccentricity transform

$$Ecc_C(x) = \max_{y \in \partial C} d_C(x, y)$$

where  $d_C(x, y) \stackrel{\text{def}}{=} U(x)$  is computed from the solution to the

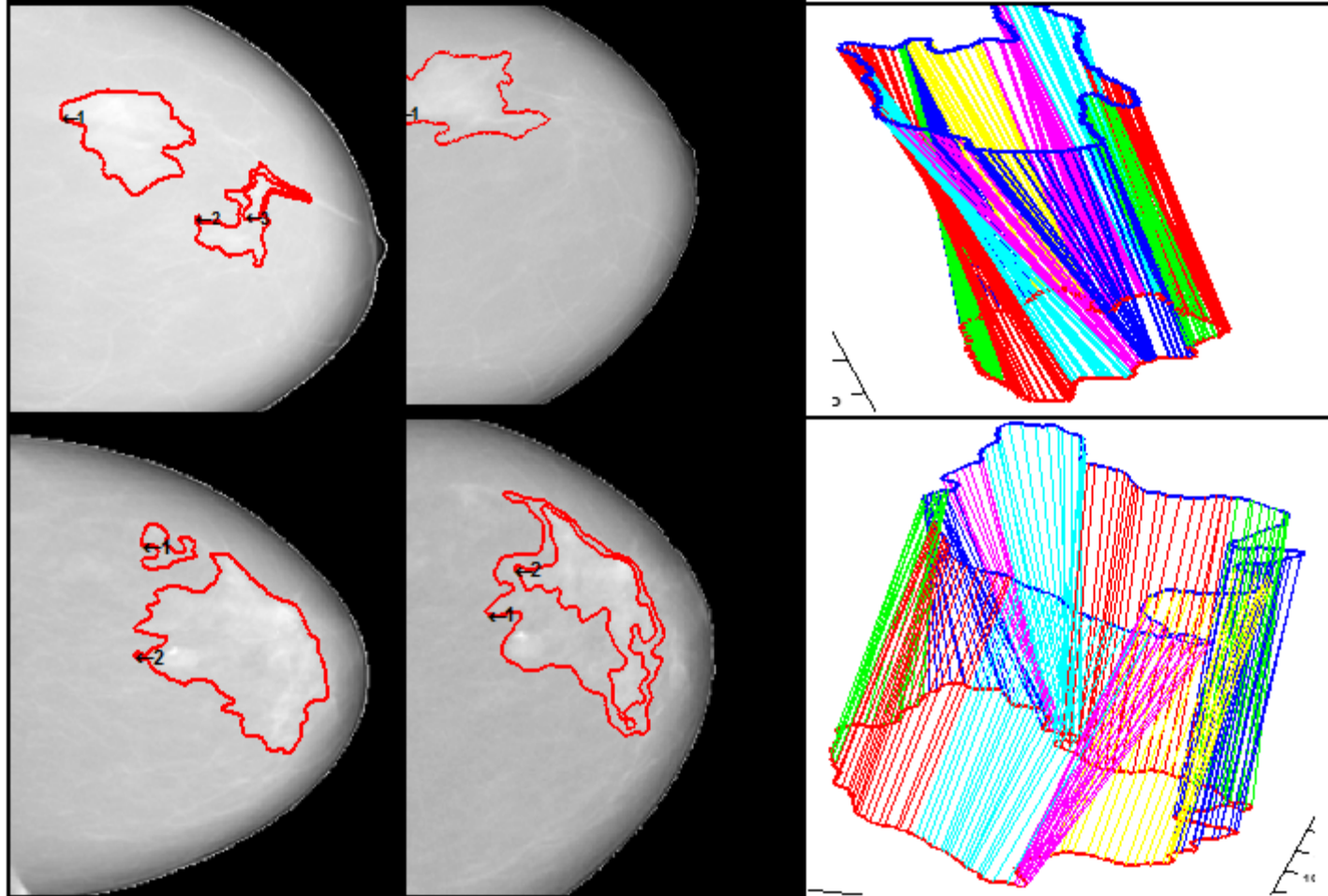
Eikonal equation:  $\forall x \in C, |\nabla U(x)| = 1; U(0) = 0$

The Fast Marching Algorithm can be used to compute this solution



Temporal evolution of the FMA

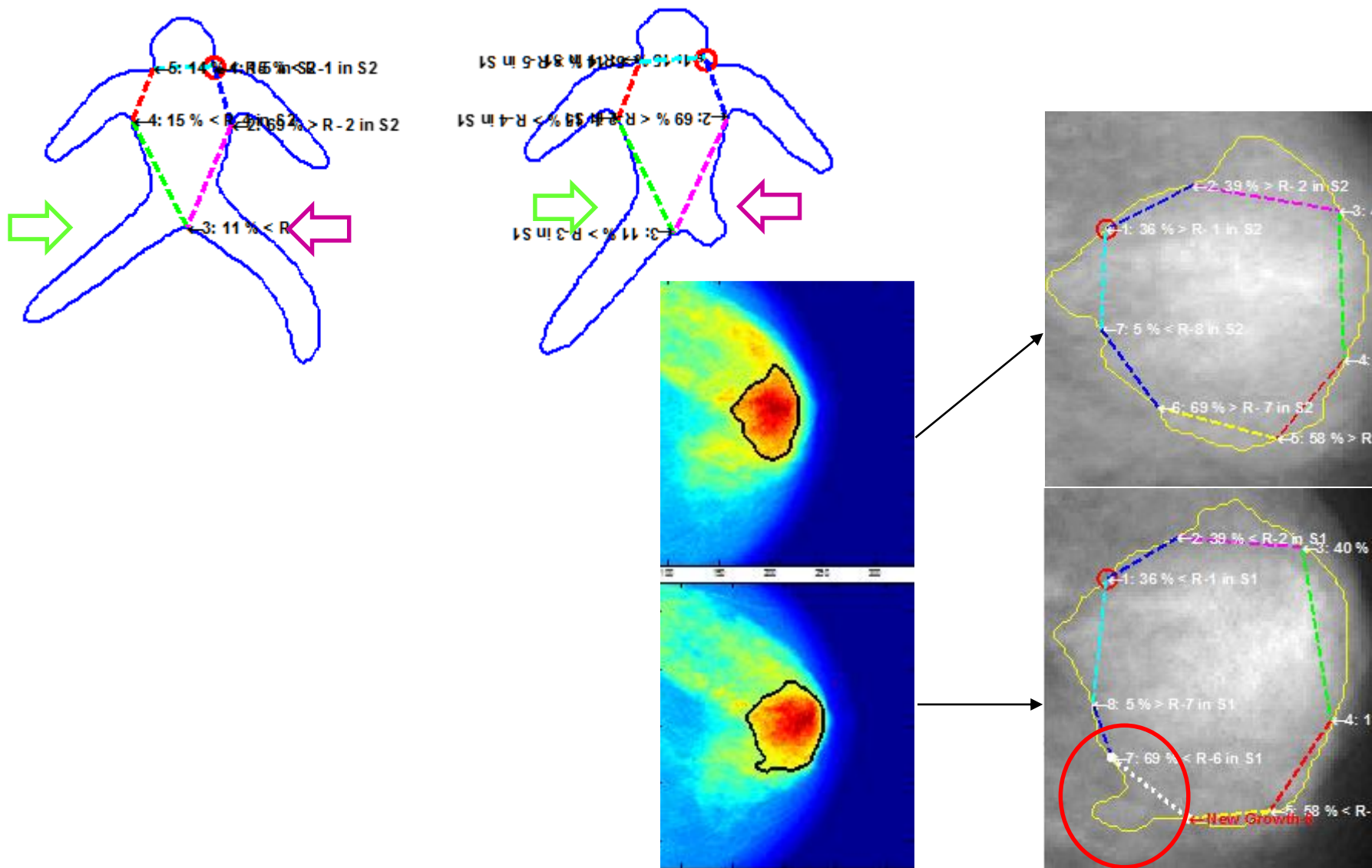
# Matching temporal mammograms



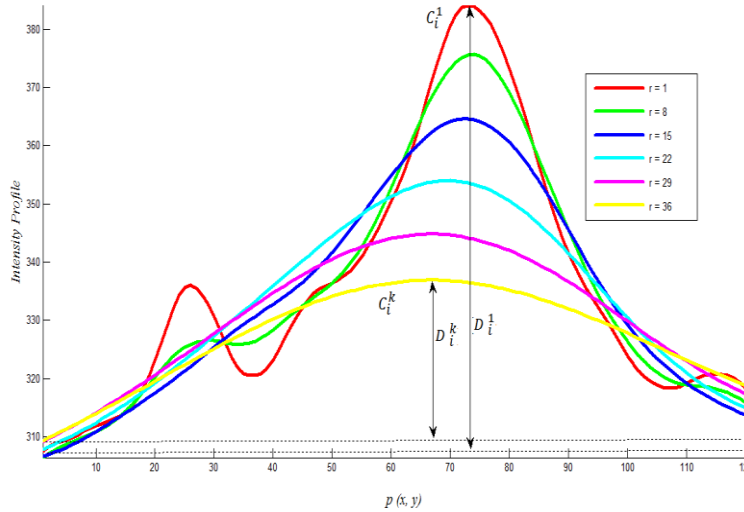
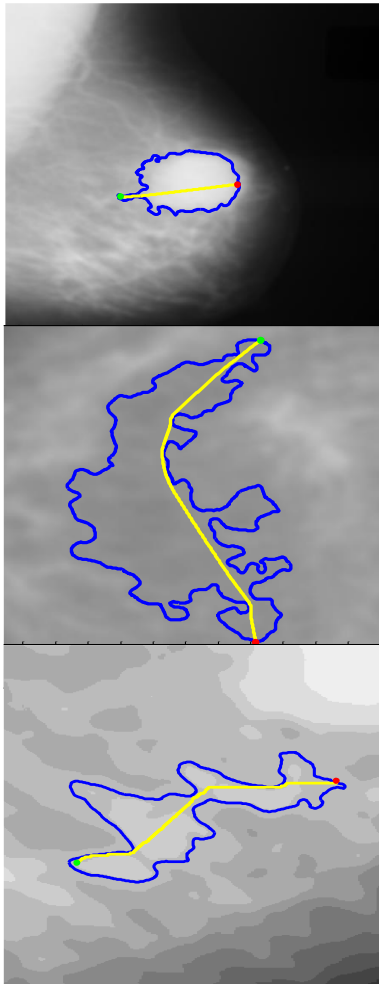
Temporal pairs from the Elizabeth Wende clinic, NY



# Detecting mismatched portions of the shape occlusions and new growths



# False positive reduction in mass segmentation

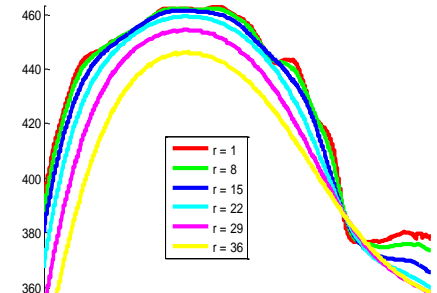


Intensity profile scale space of a certain region

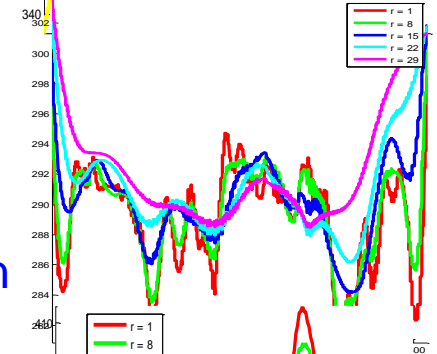
$$T_i = \left( \sum_{p=1}^l \left( \frac{C_i^1(p) - C_i^k(p)}{\text{length of } C_i^1} \right) \right) * \frac{\bar{D}_i}{D_B} * (D_i^1 - D_i^k)$$

where  $D_i^r = \text{abs}(\max(C_i^r)) -$

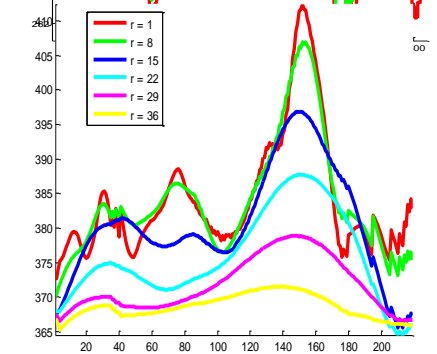
TP



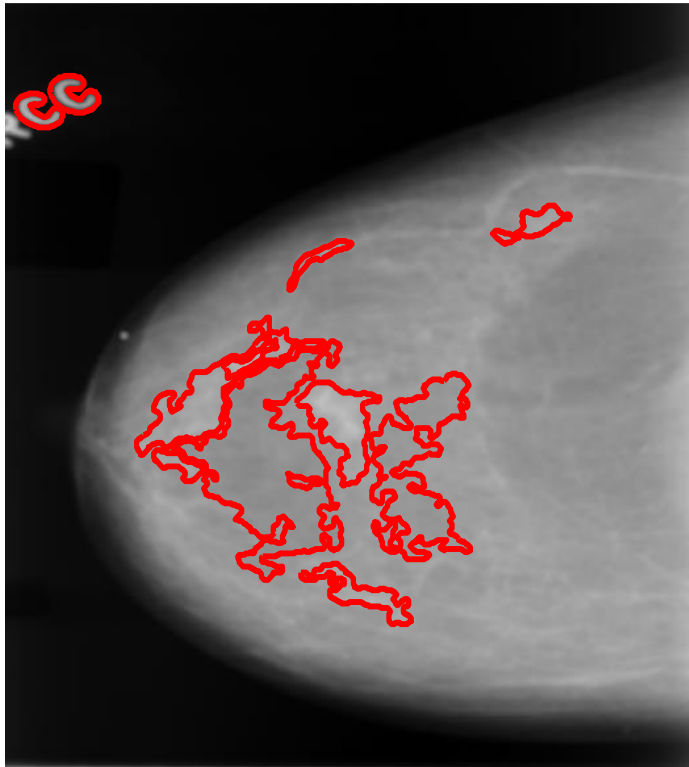
FP



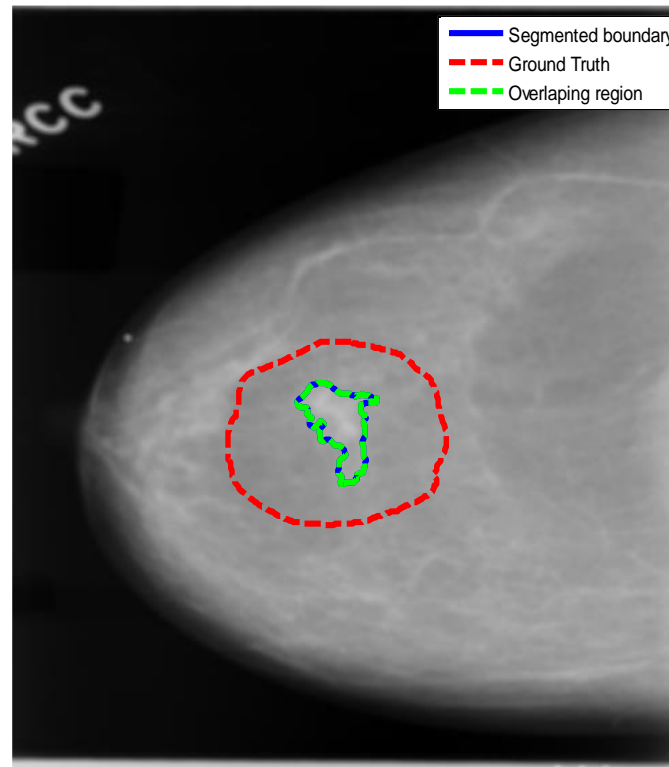
FP



## False positive reduction



Automated segmentation of a mammogram, no FP reduction



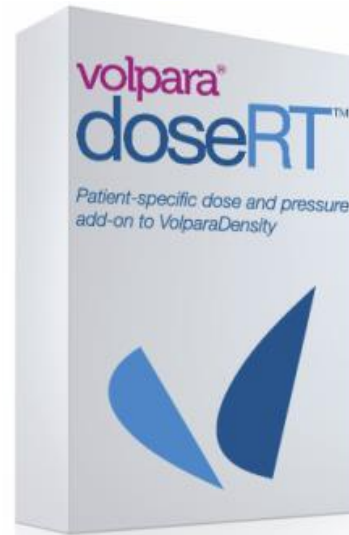
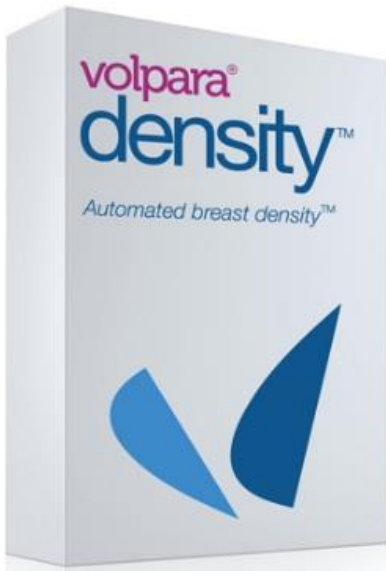
“ground truth” and the ROI boundary after FP reduction

# Conclusions



... but allow me add a postscript

# ... commercial exploitation



MIRADA™  
SOLUTIONS



cti  
The path to molecular medicine



SIEMENS



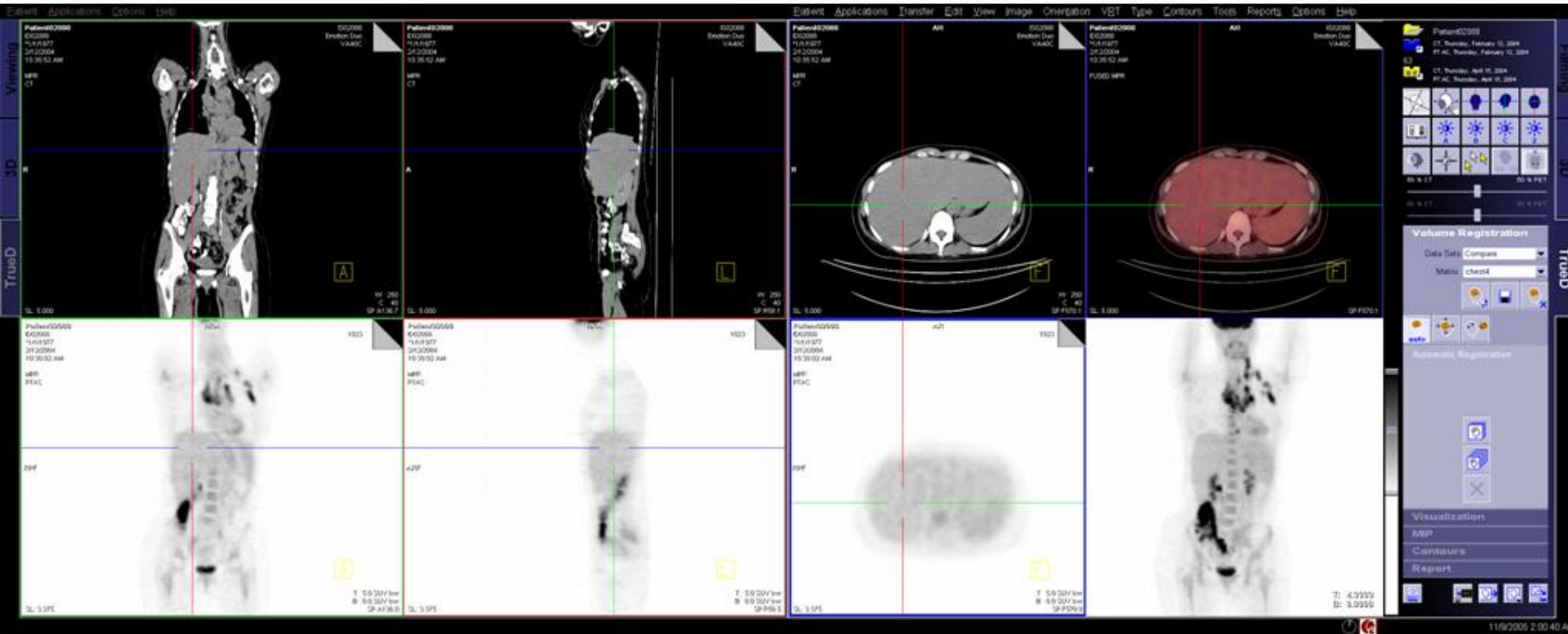
MIRADA  
medical

Fusion7D

MiraView

TrueD

XD

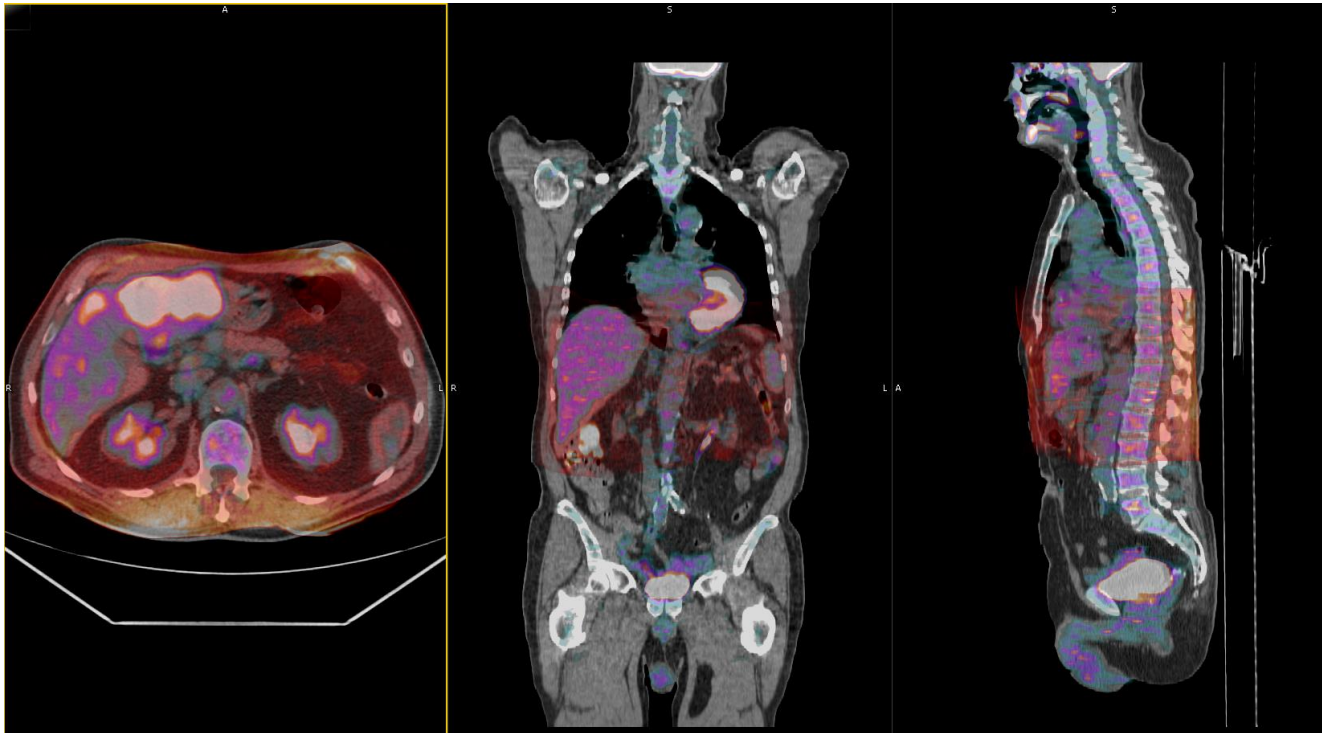


PET-CT image fusion. Upper left: CT; lower left FDG-PET; upper right PET fused with CT by non-rigidly registering the PET data to the coordinate frame of the CT. This snapshot is from the Siemens TrueD workstation, courtesy Dr. Jérôme Declerck, Chief Scientist, Siemens Molecular Imaging, Advanced Applications Laboratory, Oxford.

All told, installed in over 2,000 hospitals world-wide

Oxford Eng Science + Siemens

# Tri-modal fusion: PET, CT, MRI

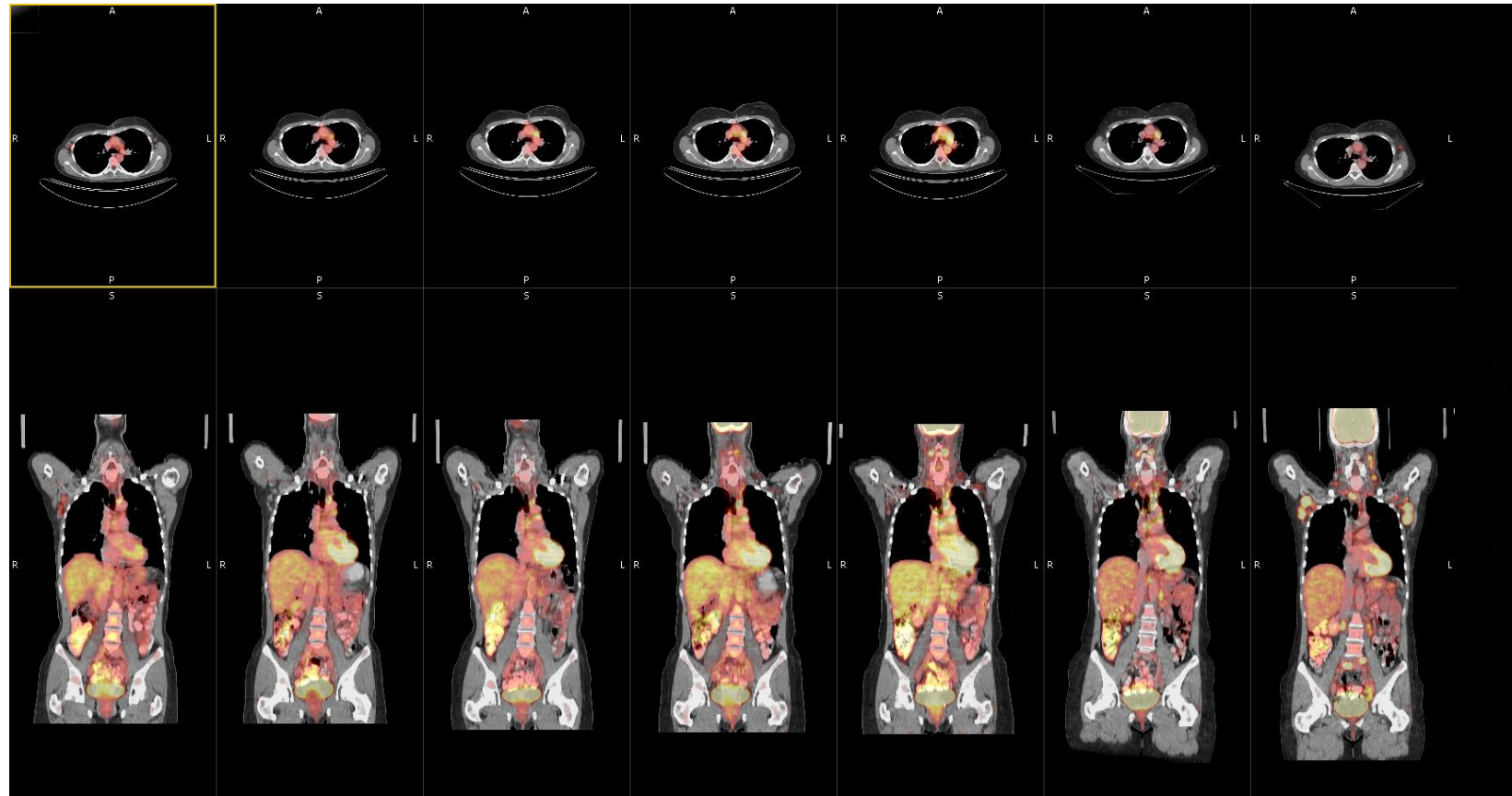


## Key

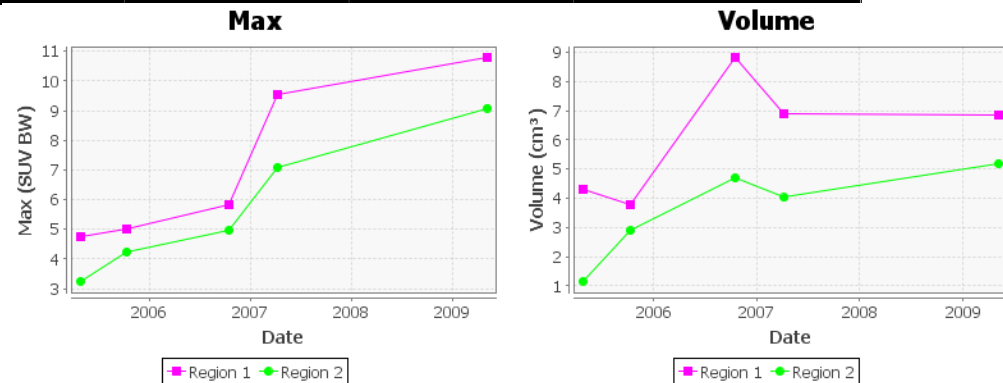
CT in Grayscale  
PET in Purple/White  
MR in Red/Brown

- Software based PET-MR fusion
- Data from hybrid PET/CT and stand-alone MR scanners
- Doesn't require new hardware

# Quantifying disease/therapy progression

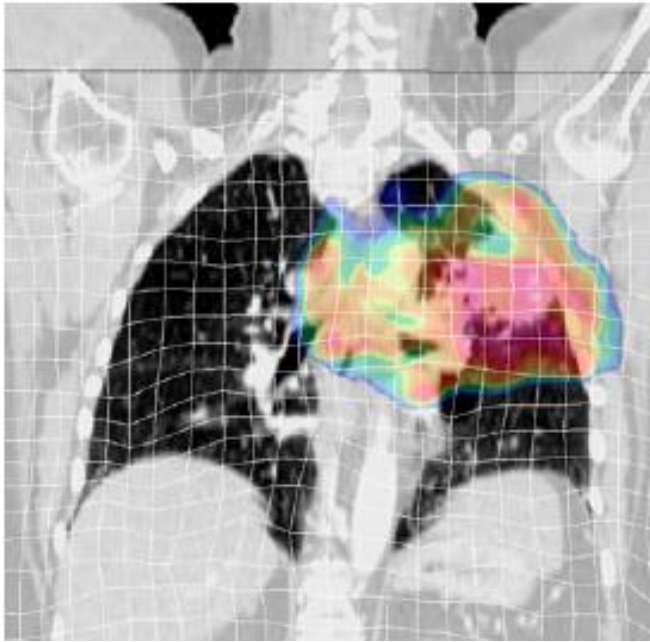


7 time-point PET/CT of the same patient

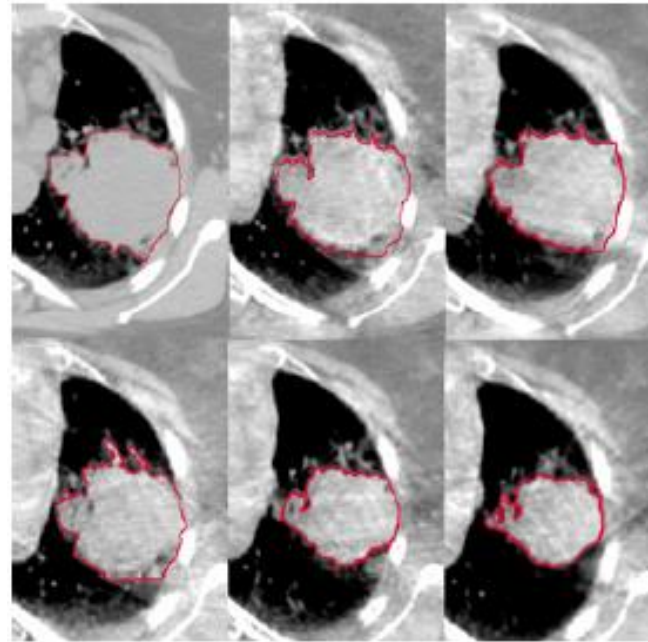




# Radiotherapy planning/monitoring



Dose deformation and summation...



Adaptive re-planning

# The looming pandemic



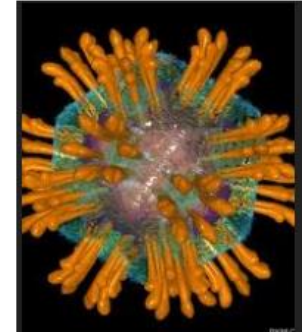
36% of US population is obese  
24% UK population



In 2008, 170 million of the world's children were obese  
20% EU kids and rising fast

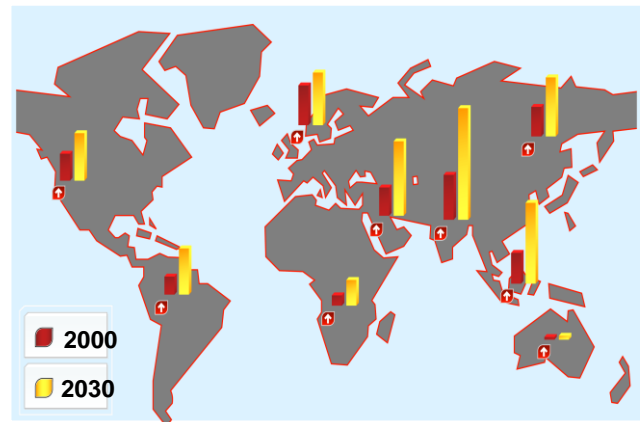


The world's favourite foods



Hepatitis C

- Cirrhosis, hepatocellular carcinoma, ... metabolic syndrome, ....
- Surge in (non-alcoholic) fatty liver disease and NASH
- 30% Western population has liver disease – ill defined
- Dame Sally Davies: liver disease is THE main priority
- Leading cause of liver transplant by 2020
- Desperate need for (imaging) biomarkers for drug trials



Fatty liver disease in numbers

2000: 155 million  
2030: 357 million

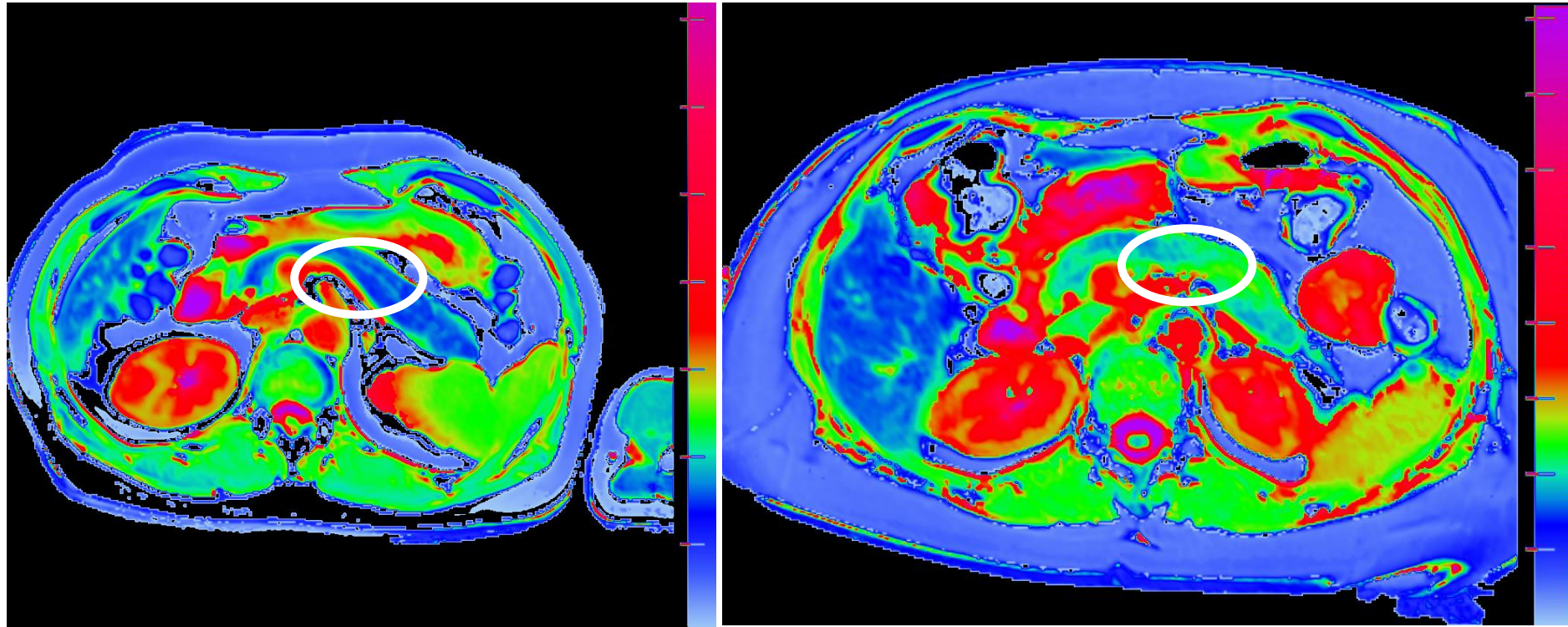
Massive growth in BRIC countries

# What happens if liver disease is suspected?



- Biopsy with a 20cm needle
  - ... is painful, costly (\$1K – rising to \$4K in cases of complications)
  - ... has a 1-2% risk of significant bleeding and 0.1% risk of death
  - ... and samples 0.02% of the 2.5Kg liver

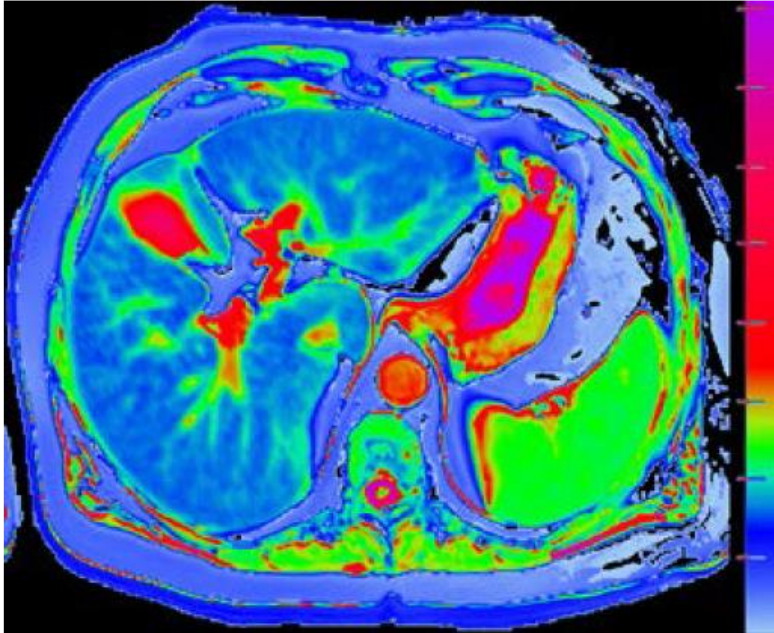
## Normal and post-pancreatitis patients



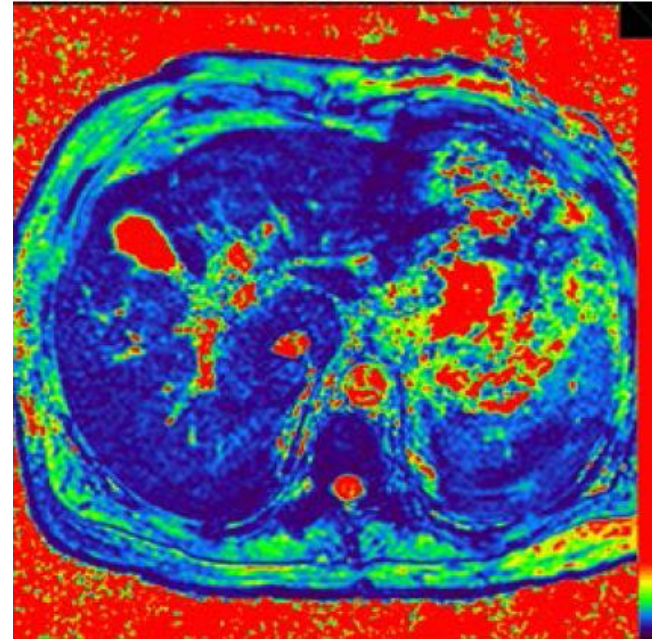
In liver, normal T1 is <810 milliseconds. Both patients here have normal liver T1.

Patient on **left** has presumed normal pancreas, with low T1 (blue = normal). Patient on **right** is being investigated for suspected gallstone pancreatitis (2 admissions in last 6/52), and has **much higher pancreatic T1**, approx 1050 milliseconds (green suggests ↑extracellular fluid). **Need for physics-based fusion: T1, T2\*, Dixon**

# Why image fusion?



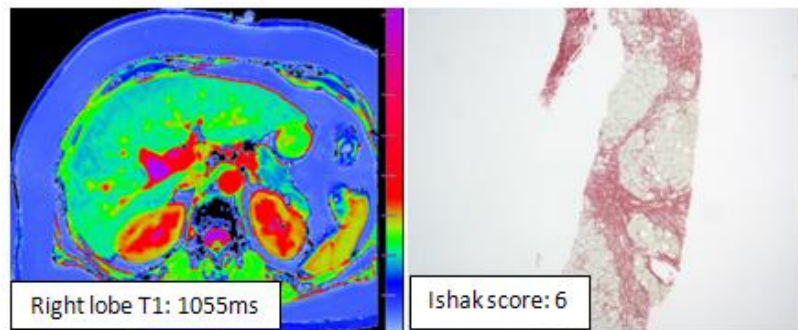
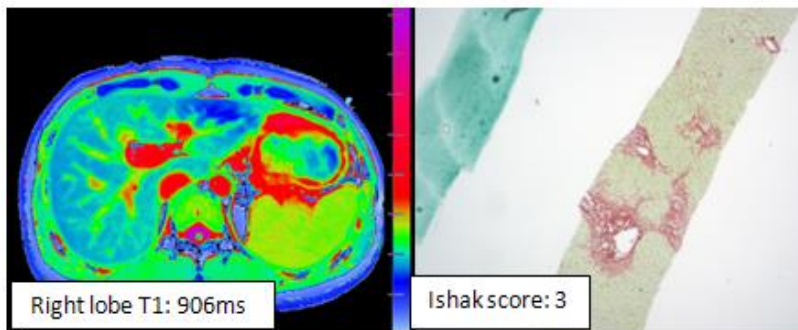
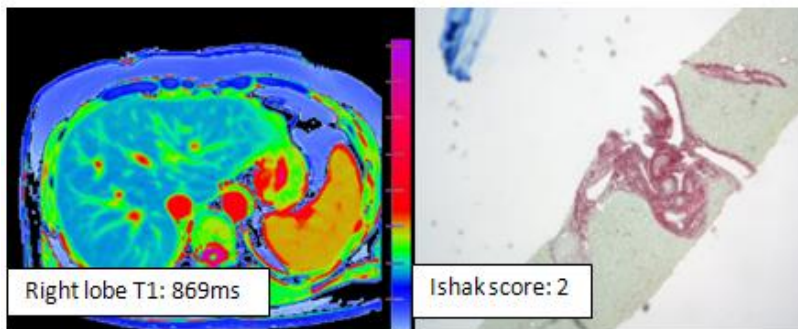
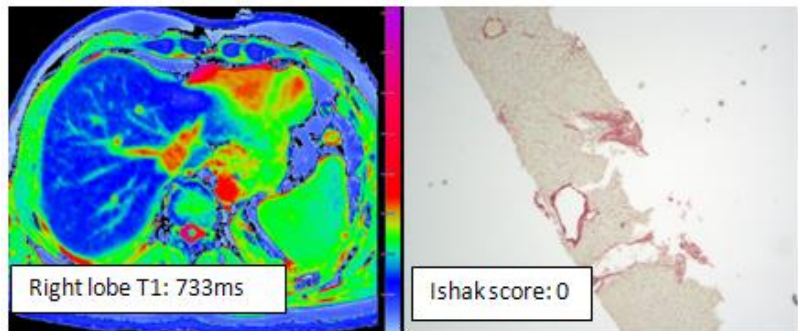
Average T1 is 817ms – which is reassuringly normal



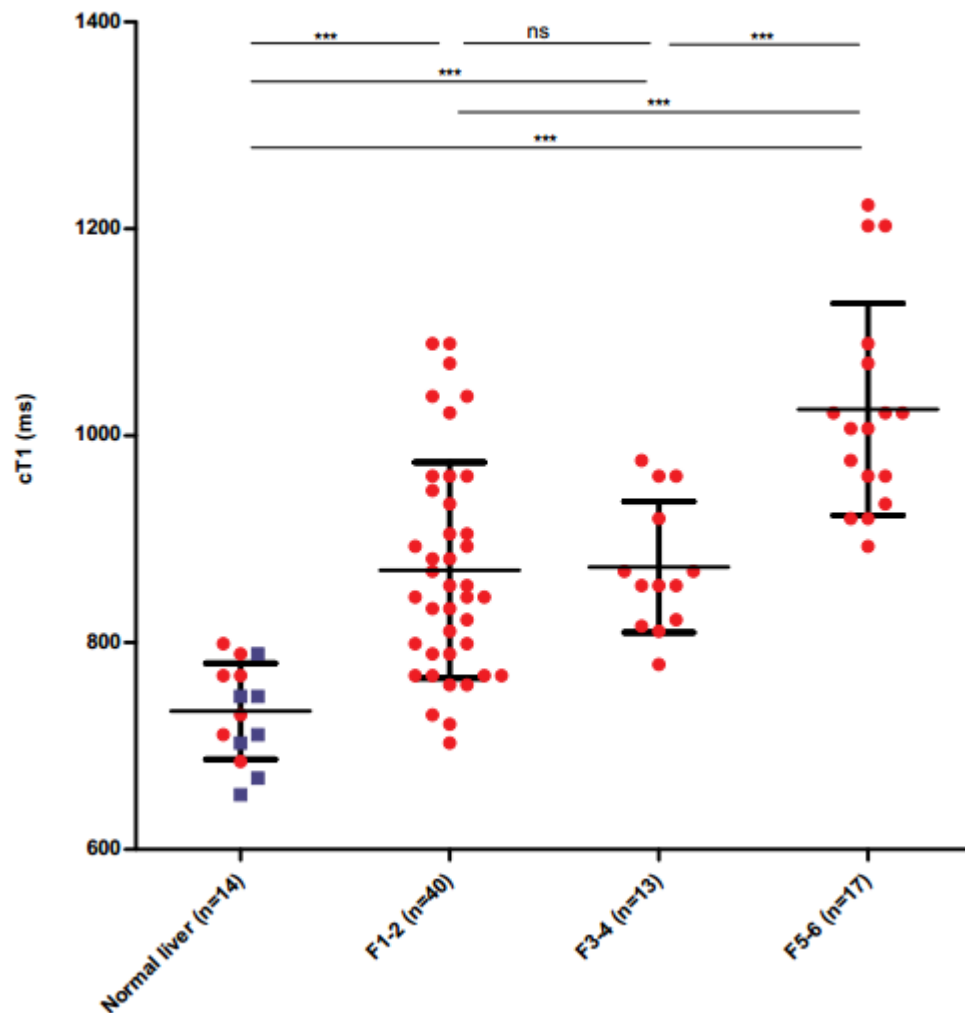
... but the T2\* image shows massive iron content (too much red wine)

... after image fusion of T1, T2\*, Dixon, the **corrected** T1 is 959ms, indicative of severe disease – confirmed on biopsy.

## Staging patients with chronic disease

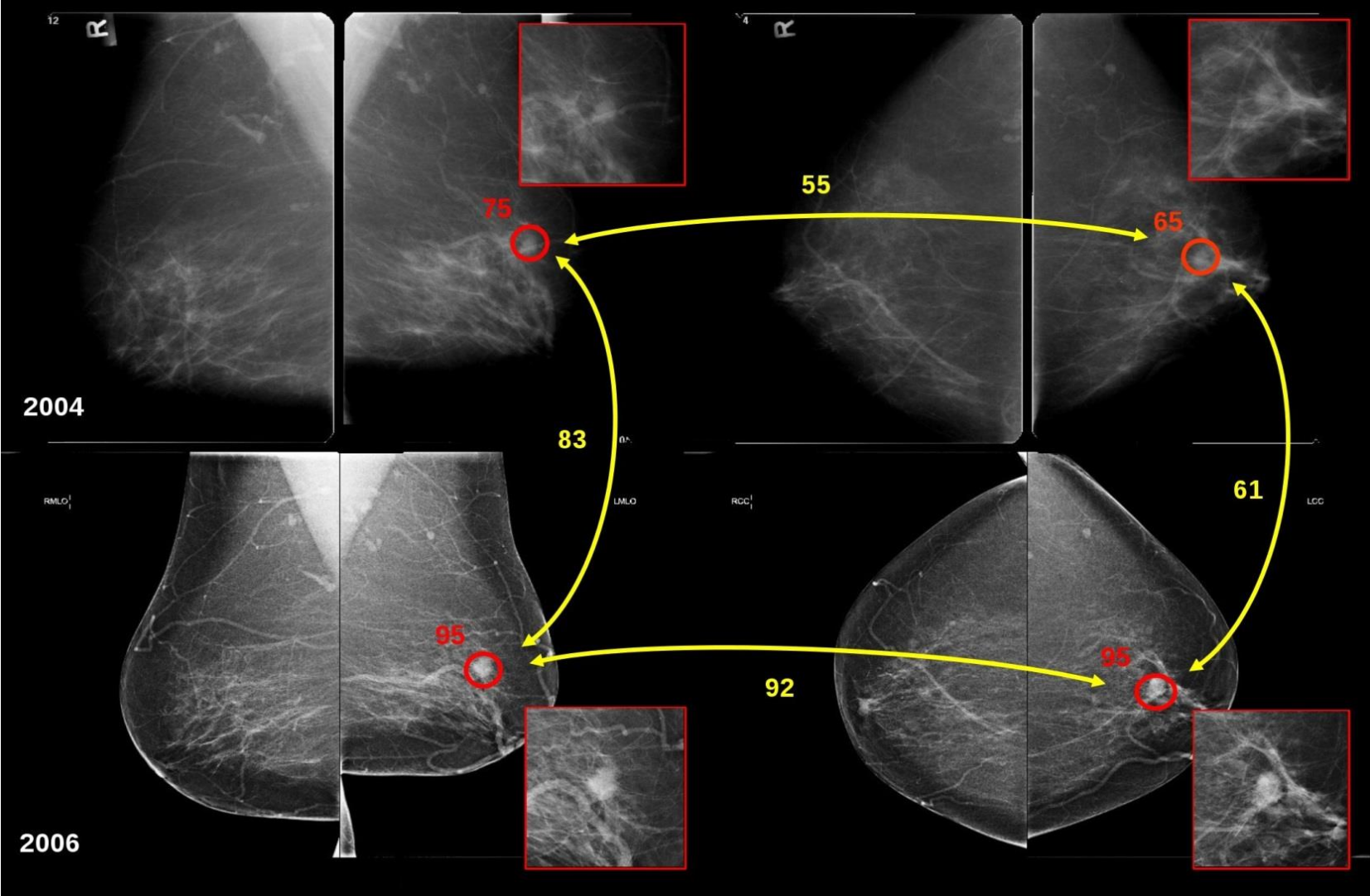


cT1 vs Ishak stage for all subjects (n=84)



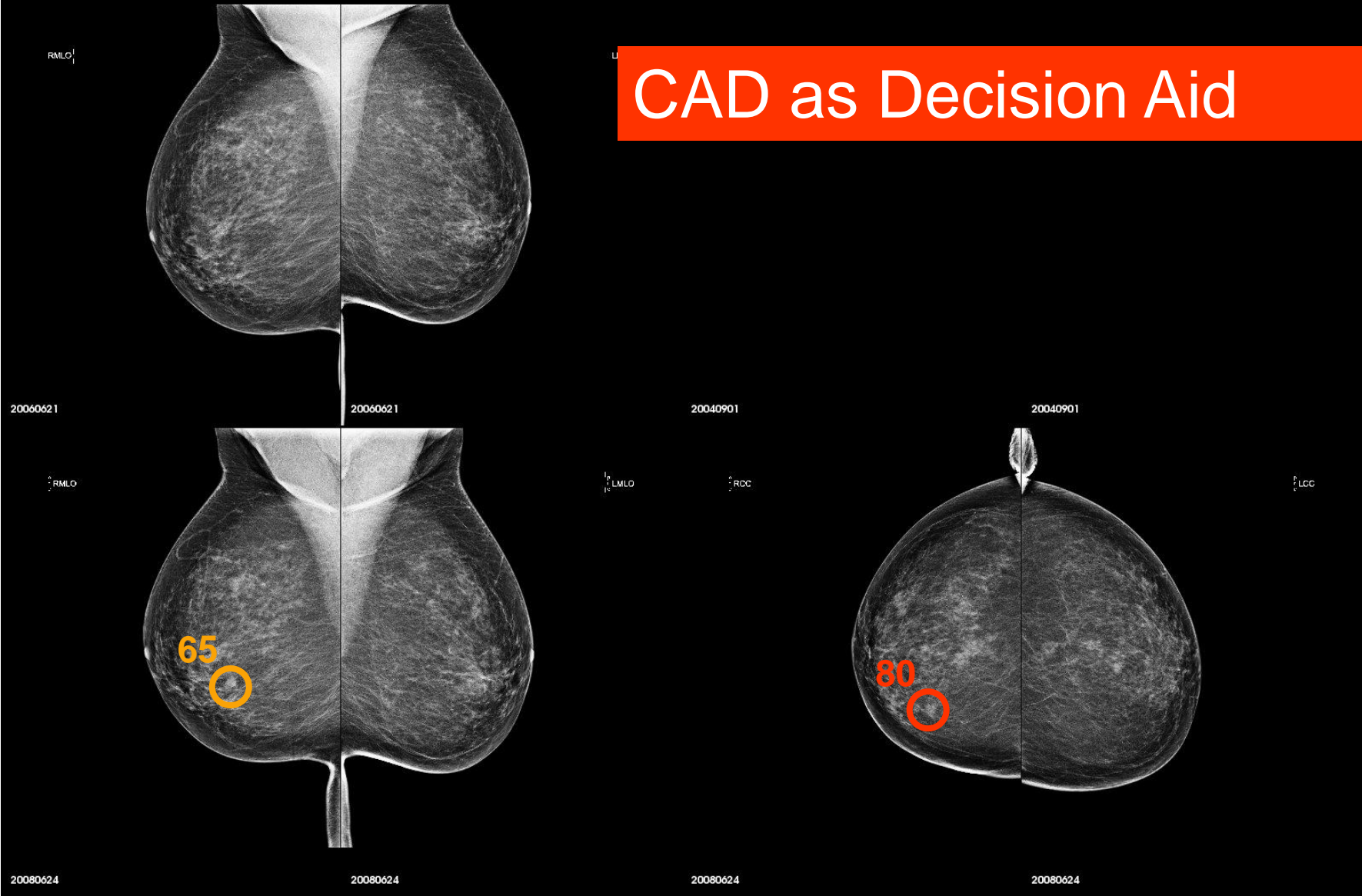
Multiparametric Magnetic Resonance for the non-invasive diagnosis of liver disease. *Banerjee R et al, J Hepatol. 2013*

# Superior algorithms using multi-view context



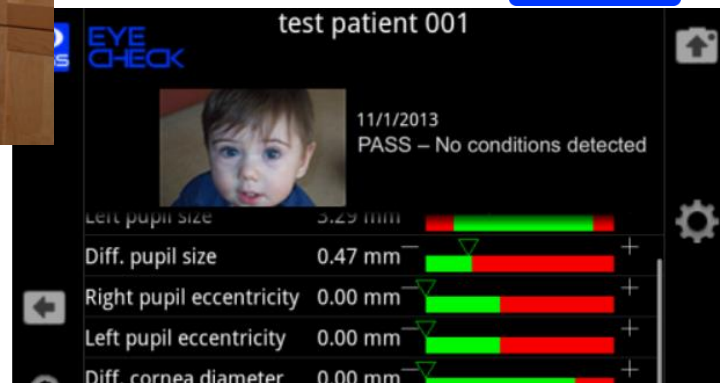
Breast CAD company, jointly with Nico Karssemeijer, based largely on his work over the past 20 years...

# CAD as Decision Aid



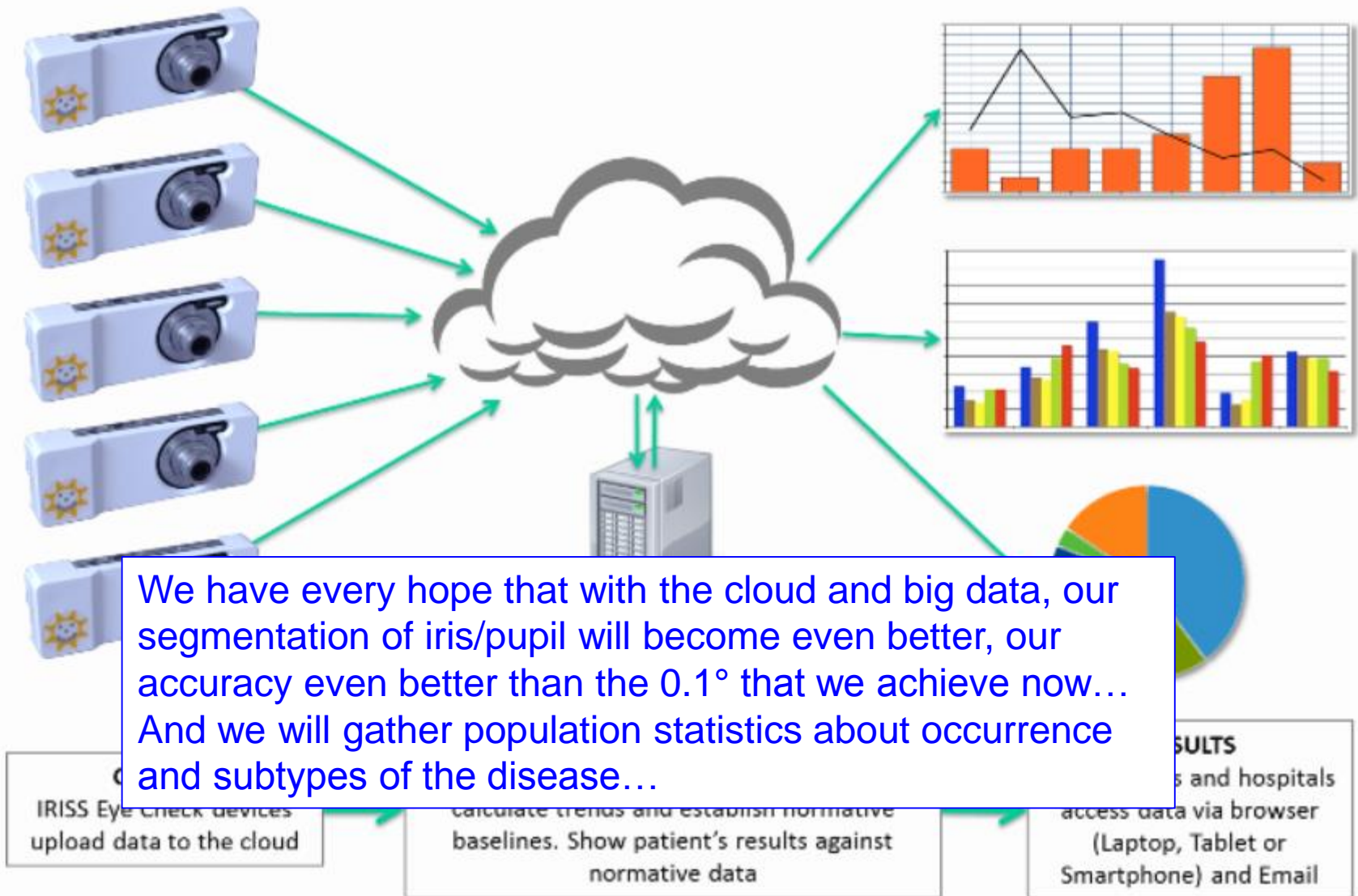


# Detecting strabismus (squint)

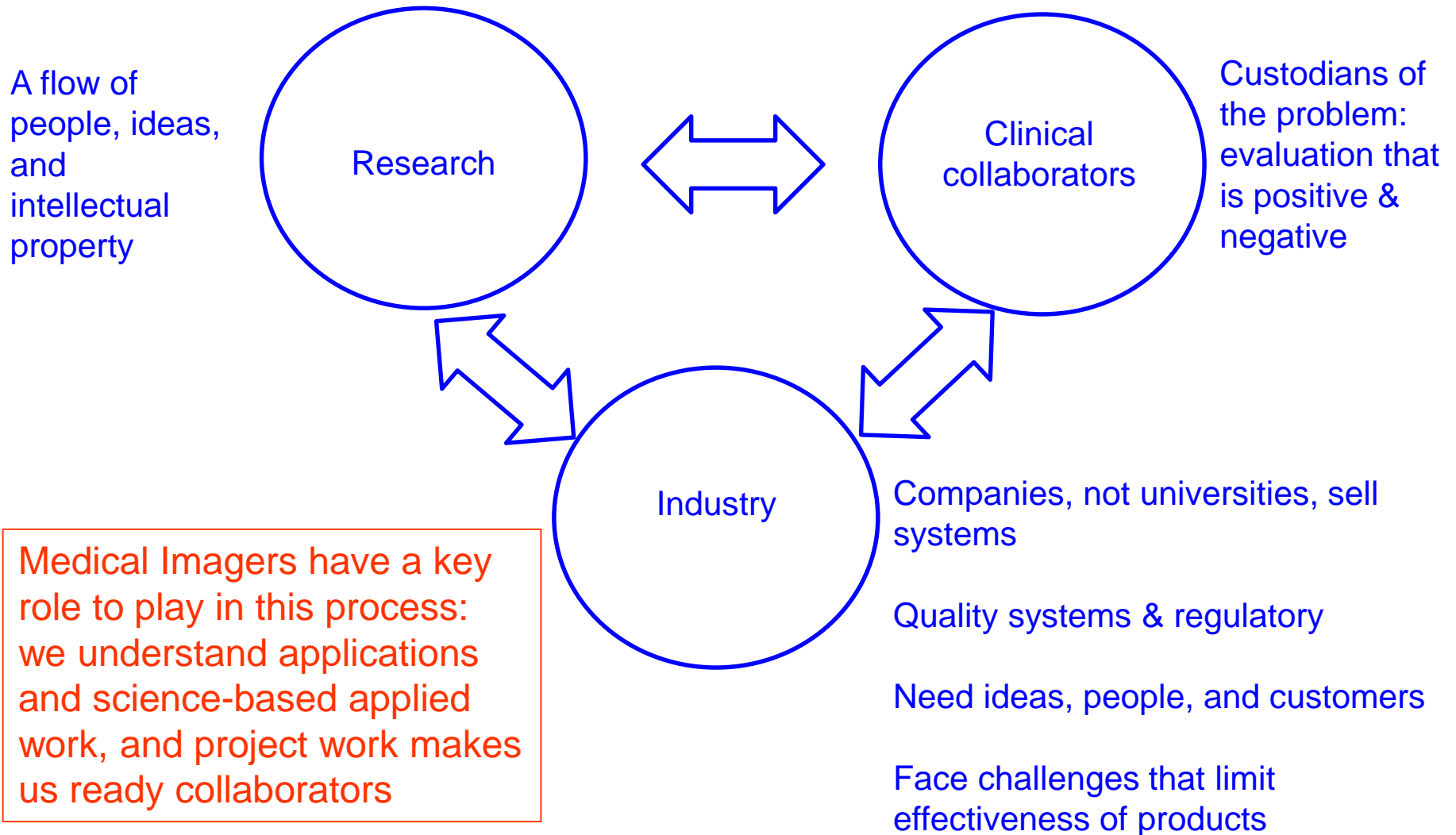


Strabismus affects 4% of children throughout the world – incidence is essentially same everywhere – that means millions of children who could benefit from screening....

# From data to information ...via the cloud



# 3-way collaboration



# The messages of MISS

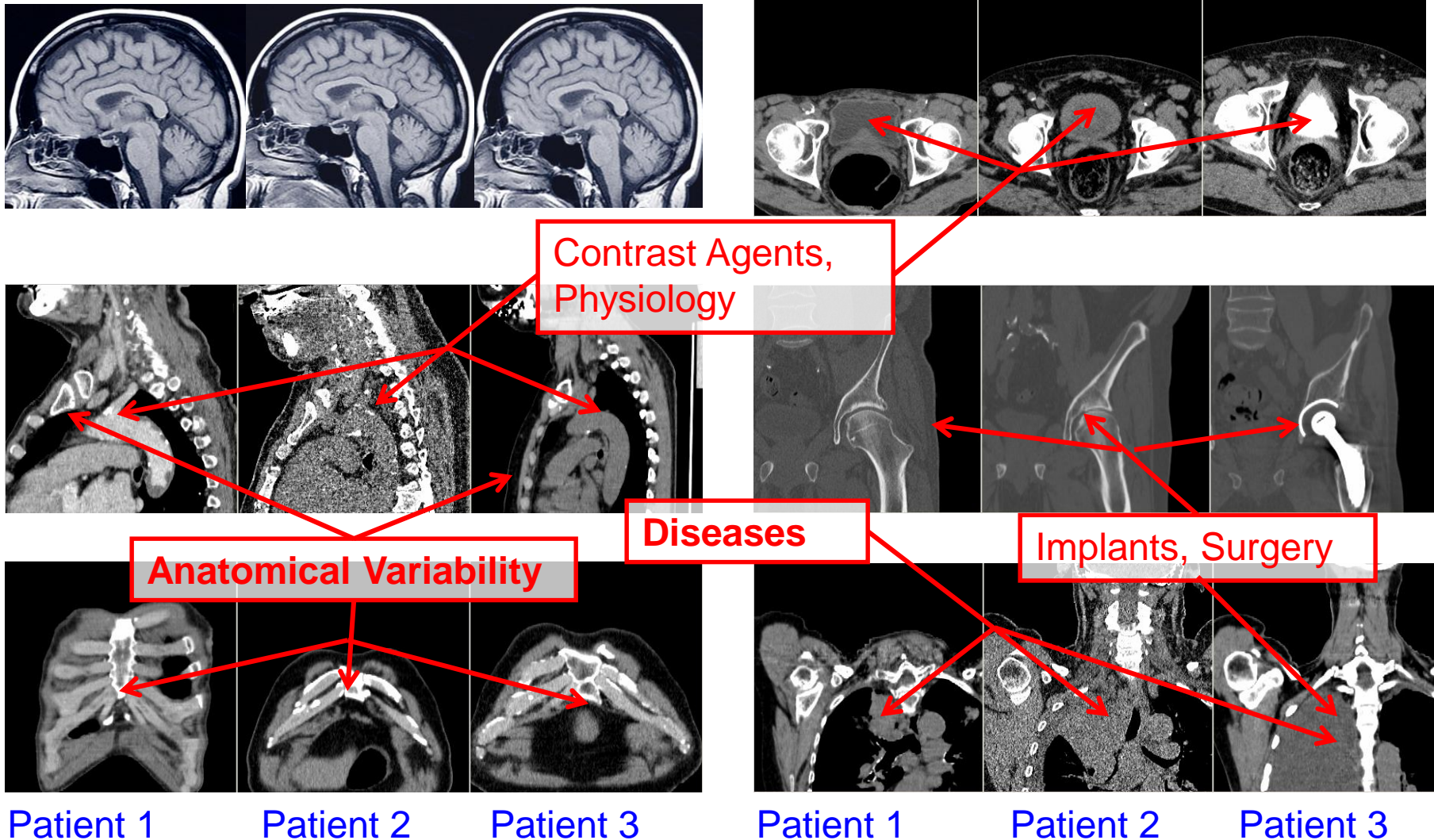
- There is lots of wonderful science to work on
- There are many clinical problems that need addressing
- There is too much about disease that we do not understand
- There can be a symbiotic relationship between academia and industry
- Progress demands the commitment of brilliant young scientists ...

# 20 things to work on\*

1. Estimate if fat is a biomarker for cancer
2. Develop a method for the combination of mammo, breast MRI and US
3. Use 2 to develop a decision support system to integrate into the tumour board's workflow
4. Develop a model-based framework for the fusion of dPET and dceMRI
5. Apply 4 to colorectal and liver cancer
6. Determine how to uncover masked tumours in mammography
7. From CT and PET develop a method for mesothelioma
8. Develop an MRI based method to support clinical assessment of endometriosis
9. Develop spatiotemporally regularised dynamic PET
10. Combine non-rigid registration and pictorial structure matching in a robust, accurate non-rigid registration algorithm for jointed structures (spine, ribcage, ...)
11. Develop existing hypoxia model to incorporate additional up-stream pathways, eg RAS
12. Extend the hypoxia & glycolysis models to incorporate angiogenesis
13. Develop a model of the effect of chemotherapy on the tumour microenvironment & implications for image analysis
14. Develop a model like 3 for radiotherapy, and combine with 3 to model their fruitful combination
15. Explore further the Pancreatic Stellate Cell conjecture
16. Model mathematically and computationally micrometastases, relate to Muschel's recent expt work
17. Explore further the tumour growth model described in the lecture
18. Show that microcalcifications and masses can be assigned malignant/benign on the basis of spectroscopic data
19. Extend current techniques for hyperpolarised MRI to detect mesothelioma
20. Extend Hoffman's work on MR-based attenuation correction to dPET & dceMRI

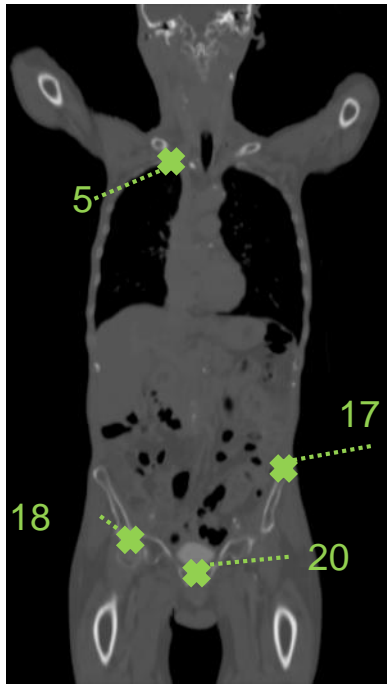
\* We are, and there are lots more too.....

# Whole Body Oncology More Challenging Than Single Organs



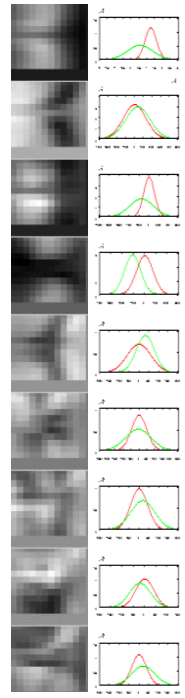
# Landmark Localization Using Parts-Based Graphical Models

Database

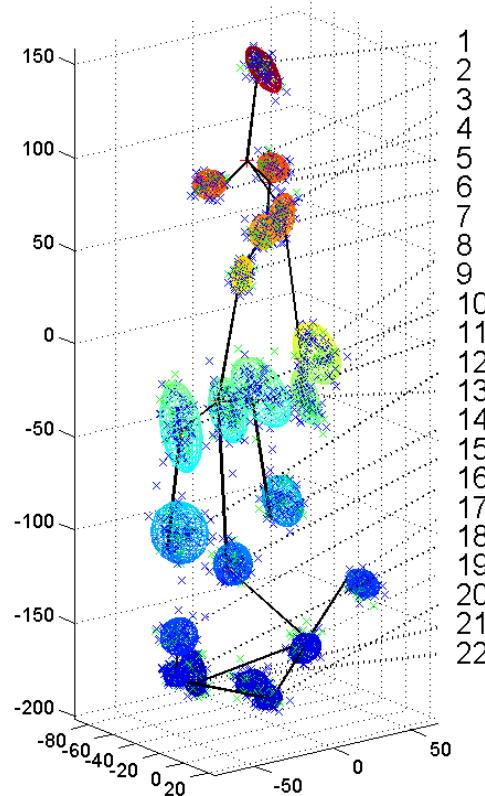


Learning

Parts-Based Model



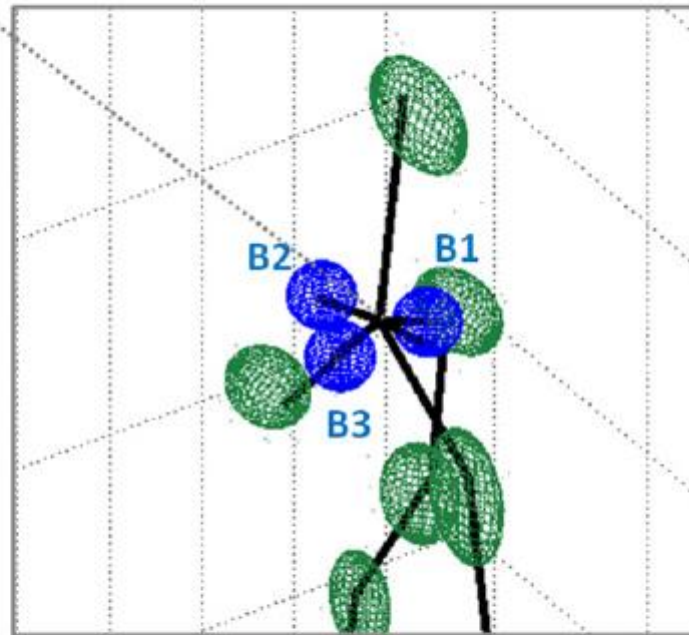
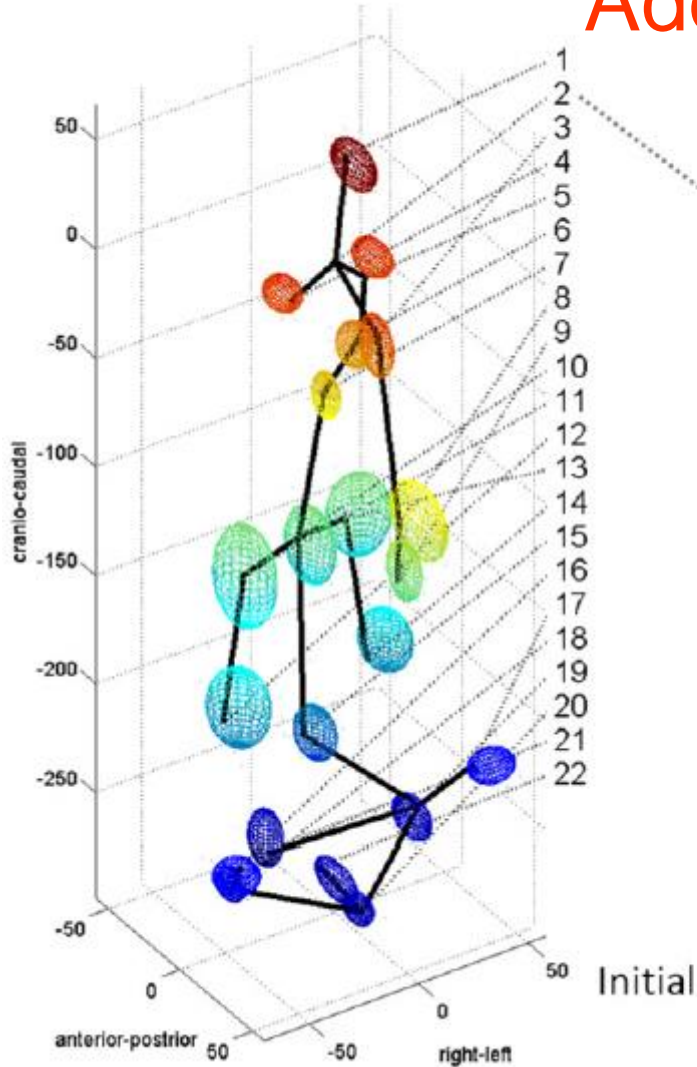
Local Tissue  
Appearance



Anatomical  
Relations

|    |                                      |
|----|--------------------------------------|
| 1  | C2 vertebra                          |
| 2  | C7 vertebra                          |
| 3  | top of the sternum                   |
| 4  | top right lung                       |
| 5  | top left lung                        |
| 6  | aortic arch                          |
| 7  | carina                               |
| 8  | lowest point of sternum (ribs)       |
| 9  | lowest point of sternum (tip)        |
| 10 | Th12 vertebra                        |
| 11 | top right kidney                     |
| 12 | bottom right kidney                  |
| 13 | top left kidney                      |
| 14 | bottom left kidney                   |
| 15 | L5 vertebra                          |
| 16 | right spina iliaca anterior superior |
| 17 | left spina iliaca anterior superior  |
| 18 | right head of femur                  |
| 19 | left head of femur                   |
| 20 | symphysis                            |
| 21 | os coccygeum                         |
| 22 | center of bladder                    |

# Adding landmarks

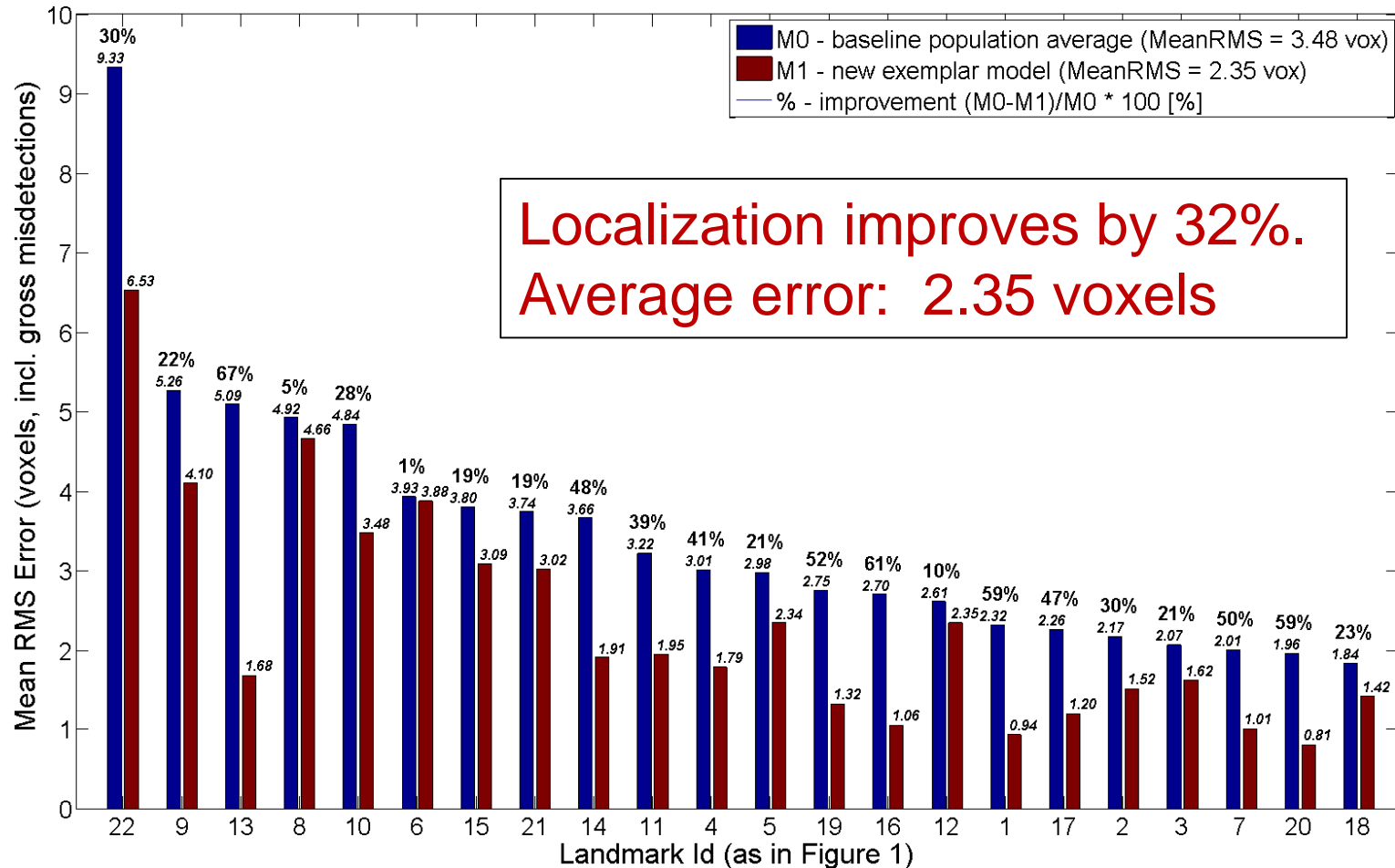


Initial (green) enriched with  
B-Landmarks (blue)

Initially, the additional landmarks (Beacons) were inferred from the population average, more recently *personalised* by selecting only the most relevant patient exemplars



# Personalized PS outperforms standard GMs



... 2-5x more repeatable than clinician

| Good              | Clinician Error | Algorithm Error<br>(2mm voxels) |
|-------------------|-----------------|---------------------------------|
| Vertebraes        | 6-10mm          | 2-6mm                           |
| Top lung          | 10mm            | 3-4mm                           |
| Kidney tips       | 10mm            | 3-4mm                           |
| Aortic arch       | 10-20mm         | 7mm                             |
| Carina            | 6mm             | 2mm                             |
| Sternum (top-low) | 10-20mm         | 3mm – 8mm                       |
| Spina illiaca     | 10mm            | 2mm                             |
| Femur heads       | 6-8mm           | 3mm                             |
| Bladder           | 20-30mm         | 10mm                            |
| Coccygeum         | 10mm            | 6mm                             |
| Symphisis         | 10mm            | 2mm                             |